2021

Investigation of novel mitoNEET ligand NL-1 as a therapeutic for cerebral ischemia and reperfusion injury

Pushkar Saralkar
West Virginia University, pas0020@mix.wvu.edu

Graduate Theses, Dissertations, and Problem Reports

2021

Investigation of novel mitoNEET ligand NL-1 as a therapeutic for cerebral ischemia and reperfusion injury

Pushkar Saralkar

Investigation of novel mitoNEET ligand NL-1 as a therapeutic for cerebral ischemia and reperfusion injury

Pushkar Atul Saralkar, M.S.

Dissertation submitted to

School of Pharmacy at

West Virginia University

in partial fulfillment of the requirements for the degree of

Doctor of Philosophy in Pharmaceutical and Pharmacological Sciences

Werner J. Geldenhuys, Ph.D., Chair

Paul R. Lockman, Ph.D.

Yon Rojanasakul, Ph.D,

James W. Simpkins, Ph.D.

Candice M. Brown, Ph.D.

Department of Pharmaceutical and Pharmacological Sciences

Robert C. Byrd Health Sciences Center

Morgantown, West Virginia 2020

Keywords: Cerebral ischemia reperfusion injury, mitoNEET, NL-1, nanoparticles, pharmacokinetics

ABSTRACT Investigation of novel mitoNEET ligand NL-1 as a therapeutic for Cerebral Ischemia and Reperfusion Injury

Pushkar Atul Saralkar, M.S.

Cerebral ischemia reperfusion injury, a common type of stroke, is a neurodegenerative disorder which is the leading cause of permanent disability in the United States. The underlying pathophysiology of ischemic stroke involves an occlusion in the vasculature supplying oxygen and glucose to the brain tissue, leading to infarction and eventual necrosis in the brain. MitoNEET is an outer mitochondrial protein that plays a role in the cellular bioenergetics and its redox physiology. Although its endogenous ligands are under investigation, mitoNEET binds molecules with a thiazolidinedione moiety, such as NL-1. This dissertation investigates NL-1 as a potential cytoprotective agent, and its possible use as a stroke therapeutic. After establishing the binding of NL-1 to mitoNEET, the effects of the drug on cellular bioenergetics as well as the mitochondrial function were studied. Upon the successful preliminary studies, NL-1 was formulated into a polymeric nanoparticle system and its efficacy evaluated in an *in vitro* stroke model on endothelial cells. The NL-1 loaded nanoparticles were found to reduce the generation of cell damaging peroxide, which is an important component of the oxidative stress causing milieu. The NL-1 nanoparticles also helped improve cell survival by decreasing the apoptotic cell population, one of the principal modes of cell damage following stroke. To evaluate promising *in vitro* results *in vivo*, a two-hour transient middle cerebral artery occlusion model was utilized. Analysis of brain sections after 24 hours showed a significantly reduced infarct volume and hemispheric swelling following treatment with NL-1 and NL-1 nanoparticles. Reduced levels of IgG extravasation were seen in treated animals compared to controls, after a 72-hour period following treatment. Qualitative analysis also revealed decreased staining area and intensity for GFAP, nitrotyrosine and 4-hydroxynonenal. Future studies need to be focused on determining the exact mechanism of action of NL-1 in the mitochondrial axis, which could help improve its dosing. A long-term study with focus on cognitive and motor neurological outcomes, following treatment with NL-1 would be the primary translational future aim. In summary, this dissertation establishes the preliminary basis for use of NL-1 as a stroke therapeutic which could compliment the current therapy in alleviating the effects of reperfusion injury.

ACKNOWLEDGEMENTS

for their support and help in my vivo studies. Your contribution helped me bring this project to fruition. Thank you to School of Pharmacy and Dr. William Petros for the excellent support to graduate students. Dr. Grazyna Szklarz, you've always been cheerful and helpful everytime!

I would like to thank my labmates Dr. Afroz Mohammad, Dr. Neal Shah and Samuel Sprowls for making my lab experience wonderful. Afroz, you have always been a great source of guidance and I hope we can play out a match of tennis soon. Neal, thanks for reminding me why I can't stand death metal and introducing me to your hot sauce collection. Sam, it was great to have the 'guy at my interview who likes soccer' become a labmate and a friend. It is always fun bantering with you! Thank you to Jacob Boos and your calming presence, our little lab chats have always been fun. Thank you to Shannon Brunzo-Hager and Gina Miller for your help in brain slicing and staining.

A big thanks to Dr. Akash Patil, Dr. Ajinkya Bhagurkar and Tanvee Thakur for being great friends and their support throughout this journey. Thank you to Trupti Dhumal for making my final year at WVU memorable. I would like to thank Tasneem Arsiwala for her constant support through thick and thin, you've been truly amazing!

I would like to thank my entire family, especially Abhishek Potnis, Priyanka Potnis, Tushar Pradhan, Anuja Pradhan, Rohan Kapkar and Mamta Iyer for always being supportive. Finally, and most importantly, I would like to thank my parents, Mrs. Amita Saralkar and Mr. Atul Saralkar to whom I owe everything and all my success!

TABLE OF CONTENTS

CHAPTER 3

Evaluation of the mitochondrial mitoNEET ligand NL-1 as a protective agent in

CHAPTER 4

Formulation, characterization and *in vitro* evaluation of NL-1 polymeric nanoparticle

CHAPTER 5

CHAPTER 6

LIST OF TABLES

LIST OF FIGURES

LIST OF ABBREVIATIONS

AMPA: α-Amino-3-hydroxy-5-methyl-4-isoxazolepropionic acid

ANOVA: Analysis of Variance

APAF-1: Apoptotic Protease Activating Factor 1

ATCC: American Type Cell Culture

ATP: Adenosine triphosphate

AUC: Area Under the Curve

BBB: Blood Brain Barrier

BSA: Bovine Serum Albumin

CH: Contralateral Hemisphere

CIV: Corrected Infarct Volume

CNS: Central Nervous System

DAB: 3,3'-Diaminobenzidine

DAPI: 4',6-Diamidino-2-phenylindole

DMEM: Dulbecco's Modified Eagle Medium

DMSO: Dimethyl Sulfoxide

ECAR: Extracellular Acidification Rate

ETC: Electron Transport Chain

FAD: Flavin Adenine Dinucleotide

FCCP: Carbonyl cyanide-p-trifluoromethoxyphenylhydrazone

FITC: Fluorescein Isothiocyanate

FMN: Flavin Mononucleotide

GDH: Glutamate Dehydrogenase

GFAP: Glial Fibrillary Acidic Protein

GTT: Glucose tolerance Test

HBSS: Hank's Balanced Salt Solution

HIF-1α: Hypoxia Inducible Factor-1α

4-HNE: 4-Hydroxy Nonenal

Iba-1: Ionized calcium binding adaptor molecule 1

ICAM1: Intracellular Cell Adhesion Molecule 1

IH: Ipsilateral Hemisphere

IL-1β: Interleukin 1β

IR: Ischemia-Reperfusion

IRP-1: Iron Regulatory Protein 1

LC-MS/MS: Liquid Chromatography-Mass Spectrometry

MMP: Matrix Metalloproteinase mNSS: Modified

Neurological Severity Score

MTT: 3-(4,5-dimethylthiazol-2-yl)-2,5-diphenyltetrazolium bromide

NADPH: Nicotinamide Adenine Dinucleotide Phosphate

NAF-1: Nuclear Associated Factor 1

NL-1: NEET Ligand 1

NMDA: N-methyl-D-aspartic acid

NO: Nitric Oxide

NOX: NADPH Oxidase

NT: Nitrotyrosine

OCR: Oxygen Consumption Rate

OGDR: Oxygen and Glucose Deprivation and Reperfusion

PBS: Phosphate Buffer Saline

PCET: Proton Coupled Electron Transfer

PDGFβ: Platelet Derived Growth Factor β

PDK: Pyruvate Dehydrogenase Kinase PLGA:

Poly(lactic-co-glycolic acid)

PPARγ: Peroxisome Proliferator Activated Receptor γ

PVA: Polyvinyl Alcohol

RIPA: Radio Immunoprecipitation Assay

RNS: Reactive Nitrogen Species

ROS: Reactive Oxygen Species

SEM: Scanning electron Microscopy

TBARS: Thiobarbituric Acid Reactive substances

TBI: Traumatic Brain Injury TLR:

Toll-like Receptor

tMCAO: Transient Middle Cerebral Artery Occlusion

TMRM: Tetramethyl   rhodamine

TNF-α: Tumor Necrosis Factor α t-

PA: Tissue Plasminogen Activator

TTC: 2,3,5-Triphenyltetrazolium chloride

TZD: Thiazolidinedione

VCAM1: Vascular Cell Adhesion Molecule 1

VDAC1: Voltage Dependent Anion Channel 1

VEGF: Vascular Endothelial Growth Factor

WNK: Lysine deficient protein kinase

XRD: X-ray Diffraction

CHAPTER 1

INTRODUCTION

Stroke is a common neurodegenerative pathology that leads to a gradual loss of cerebral functions. It is among the leading causes of deaths and the leading cause of permanent disability in the United States. About 800,000 Americans suffer from stroke each year, which results in 150,000 deaths, and the financial burden on the health care system is over $33 billion USD[1]. About 80% of the strokes are ischemic in origin, wherein, an occlusion in the blood vessels leads to inadequate supply of oxygen and essential nutrients such as glucose to the brain tissue.

The only FDA approved treatment for ischemic stroke is the administration of tissue plasminogen activator (tPA), which is a thrombolytic agent. Treatment with tPA and other investigational thrombolytic agents is aimed at dissolving the clot that is occluding blood flow. Although seemingly counterintuitive, a resumption in blood flow has the potential to cause greater damage in most patients. This event, called reperfusion, triggers multiple downstream cascade of events that can exacerbate the toxic effects on the components of the neurovascular unit. The 'reperfusion injury' can increase the size of infarct and is the principal reason for the hemorrhagic edema which can often be fatal[2]. The consequences of stroke such as long-term disability often go unmitigated due to the lack of effective neuroprotective strategies addressing the issue of reperfusion injury[3]. Although the literature is replete with over 1000 candidate compounds tested with the hopes of eventual clinical use, not a single compound has been successfully translated into a viable clinically useful drug[4].

MitoNEET is a fairly recently discovered protein present in the outer mitochondrial membrane. This 14 kD protein was identified in 2003 by Colca et al., as the mitochondrial target

for the anti-diabetic drug pioglitazone[5]. Pioglitazone is a drug from the thiazolidinedione category, whose target for diabetic therapy is the PPARγ receptor. Thus mitoNEET is an off-target binding partner of this class of drugs. Subsequent investigations revealed the crystal structure of mitoNEET, and the protein was found to contain two iron-sulfur clusters, which are involved in electron transfer and redox processes[6]. MitoNEET has been implicated to play a role in numerous pathologies, including the neurodegenerative CNS disorders such as Alzheimer's and Parkinson's Disease[7,8]. The efforts to develop a mitoNEET ligand that lacked PPARγ activity, led our group to synthesize thiazolidinedione analog, NL-1[9]. This ligand has been shown to have a cytoprotective effect on cardiac stem cells by combating oxidative stress induced cell death[10]. Together, the role of mitoNEET and the potential of NL-1 lays the premise for its use in the neurodegenerative disease of stroke, wherein the mitochondria play a pivotal role in the pathophysiology. NL-1 is a ligand for an unexplored stroke target, and we hypothesize that by improving on cellular bioenergetics and mitigating cell death, NL-1 could provide an effective and improved therapy for stroke.

In this dissertation, we investigate the role of the mitoNEET ligand NL-1 as a potential therapeutic agent in treatment of stroke, mainly the consequences arising from reperfusion injury. We start with the basis establishing NL-1 as a cytoprotective agent, acting on cellular bioenergetics. We then propose a polymeric nanoparticle system for effective NL-1 delivery, and explore the efficacy of the drug and nanoparticles on *in vitro* stoke models. Further, we determine if the *in vitro* success could be translated *in vivo*, in a rat stroke model.

Chapter 2 reviews the pathophysiology of stroke. We discuss the multiple facets of cell damage associated with stroke such as oxidative stress, apoptosis, inflammation, edema and BBB disruption. With the research in understanding the protein mitoNEET still in a nascent stage, we

also discuss the progress made so far with the structural features of mitoNEET, its role in general cellular physiology as well as its potential role in pathophysiology.

Chapter 3 focuses on preliminary studies on NL-1 as a candidate drug. We establish the binding of NL-1 to mitoNEET, without the extraneous PPARγ effects. Further, we test the effect of NL-1 on mitochondrial membrane potential during oxidative stress, and its effect on cellular respiration as function of oxidative phosphorylation and pH.

The development, characterization and efficacy studies for PLGA nanoparticles for NL-1 have been described in Chapter 4. We discuss the formulation and optimization of NL-1 loaded PLGA nanoparticles. We further highlight the characterization of this formulation for particle size, surface charge, physical state and drug release. The two primary mechanisms of cell death following stroke and reperfusion injury with a mitochondrial dimension include the generation of ROS and induction of the apoptosis cascade[11]. The efficacy of the formulation is determined using an *in vitro* hypoxia-reperfusion model, and its effect on peroxide generation and apoptosis is studied. Finally, we address the safety of the formulation in this chapter.

In Chapter 5, we aim to evaluate the NL-1 nanoparticle formulation to a pre-clinical level. We determine the efficacy of NL-1 nanoparticles in a rat transient middle cerebral artery occlusion model of stroke. The effect of the treatment is studied on infarct size as well as the brain edema, which is a hallmark feature of the reperfusion injury. We also evaluate the outcome of these effects, and check if they are translated at a behavioral level. The impact of NL-1 therapy on the mediators of cell damage in stroke is explored by performing immunohistochemistry on brain slices.

In summary, this dissertation explores a new treatment strategy for cerebral ischemia and reperfusion injury, a common form of stroke. We aim to establish NL-1, a first in class mitoNEET ligand as a therapeutic agent for stroke. Overall, this would be the first study targeting the protein

mitoNEET to achieve improved cell survival and neurological outcomes at an *in vitro* and preclinical level, respectively, following stroke. It lays the groundwork for future investigation of a possible synergy between thrombolytic agents and mitoNEET ligands for improved mitigation of this dreadful condition.

References:

1.   Stroke Facts | cdc.gov. https://www.cdc.gov/stroke/facts.htm. Accessed April 13, 2020.

2.   Raslan A, Bhardwaj A. Medical management of cerebral edema. *Neurosurg Focus*. 2007;22(5). doi:10.3171/foc.2007.22.5.13

3.   Reis C, Akyol O, Ho WM, et al. Phase I and Phase II Therapies for Acute Ischemic Stroke: An Update on Currently Studied Drugs in Clinical Research. *Biomed Res Int*. 2017;2017:4863079. doi:10.1155/2017/4863079

4.   Green AR. Pharmacological approaches to acute ischaemic stroke: reperfusion certainly, neuroprotection possibly. *Br J Pharmacol*. 2009;153(S1):S325-S338. doi:10.1038/sj.bjp.0707594

5.   Colca JR, McDonald WG, Waldon DJ, et al. Identification of a novel mitochondrial protein ("mitoNEET") cross-linked specifically by a thiazolidinedione photoprobe. *Am J Physiol - Endocrinol Metab*. 2003;286(2). http://ajpendo.physiology.org/content/286/2/E252.long. Accessed June 10, 2017.

6.   Wiley SE, Paddock ML, Abresch EC, et al. The Outer Mitochondrial Membrane Protein mitoNEET Contains a Novel Redox-active 2Fe-2S Cluster. *J Biol Chem*. 2007;282(33):23745-23749. doi:10.1074/jbc.C700107200

7.   Sauerbeck A, Gao J, Readnower R, et al. Pioglitazone attenuates mitochondrial dysfunction, cognitive impairment, cortical tissue loss, and inflammation following traumatic brain injury. *Exp Neurol*. 2011;227(1):128-135. doi:10.1016/j.expneurol.2010.10.003

8.   Geldenhuys WJ, Benkovic SA, Lin L, et al. MitoNEET (CISD1) Knockout Mice Show Signs of Striatal Mitochondrial Dysfunction and a Parkinson's Disease Phenotype. *ACS Chem Neurosci*. 2017;8(12):2759-2765. doi:10.1021/acschemneuro.7b00287

9.   Geldenhuys WJ, Funk MO, Barnes KF, Carroll RT. Structure-based design of a thiazolidinedione which targets the mitochondrial protein mitoNEET. *Bioorganic Med Chem Lett*. 2010;20(3):819-823. doi:10.1016/j.bmcl.2009.12.088

10. Logan SJ, Yin L, Geldenhuys WJ, et al. Novel thiazolidinedione mitoNEET ligand-1 acutely improves cardiac stem cell survival under oxidative stress. *Basic Res Cardiol*. 2015;110(2):19. doi:10.1007/s00395-015-0471-z

11. Liu F, Lu J, Manaenko A, Tang J, Hu Q. Mitochondria in Ischemic Stroke: New Insight and Implications. *Aging Dis*. 2018;9(5):924. doi:10.14336/AD.2017.1126

CHAPTER 2

Cerebral ischemia-reperfusion injury and the mitoNEET protein

<u>**Chapter included in the following manuscript:**</u>

Medicinal chemistry of the novel mitochondrial MitoNEET drug target

Pushkar Saralkar, Brandon Richter, Alayna Mickoloff, Jacob Boos, Michael Menze, Mary E. Konkle and Werner J. Geldenhuys

2.1. Ischemic Stroke

Cerebral ischemia is a consequence of occlusion of the blood flow to the brain, leading to depleted supply of glucose and oxygen to the cerebral tissue. Ischemic stroke, which accounts for about 80% of stroke cases, can be either focal or global[1]. The focal cerebral ischemia occurs in a specific

region of the brain, and is characterized by an ischemic core and an ischemic penumbra surrounding the core. Global ischemic event begins in the arteries of lower regions such as the head and neck region. Global cerebral ischemia leads to widespread brain damage and is often fatal. Cerebral ischemia in the brain can be divided into two regions, that vary in blood flow occlusion and hence the pathophysiology. The central area that has the highest reduction in blood flow and undergoes irreversible damage is called the ischemic core. The area surrounding the core is called the penumbra which has a reduced blood flow, but can be salvaged with timely intervention[2].

2.2. The energy crisis and excitotoxicity

A dearth of essential nutrients leads to a dysfunctional electron transport chain, which eventually affects the generation of ATP. As a result, cellular respiration begins to shift from aerobic to anaerobic. Decreased ATP production also affects the functioning of energy-dependent transport pumps such as the Na+/K+, Na+/H+ and calcium pumps. The sodium ion concentration inside the cells increases, while the potassium ion import is reduced. Calcium reuptake in the endoplasmic reticulum is inhibited leading to a rise in the cytoplasmic calcium ion levels. High cation levels subsequently increase the osmolarity of the cell, leading to water influx in the cells and their swelling. Accumulation of hydrogen ions lowers the cellular pH leading to lower enzyme activity and clumping of nuclear chromatin. Protein synthesis is also affected as a result of ribosomal detachment[3]. ATP imbalance also affects the functioning of reuptake pumps of neurotransmitters such as glutamate, leading to their prolonged presence in the synapses. Glutamate is an excitatory neurotransmitter that acts on the NMDA and AMPA receptors, and cell damage due to glutamate excitotoxicity is often seen in stroke. The permeability of these receptors to calcium ions is increased. A build-up of intracellular calcium activates the mediators of apoptosis and necrosis.

Excess calcium in mitochondria leads to the loss of membrane potential and enhanced permeability of the mitochondrial membranes, promoting apoptosis. A disturbed calcium homeostasis loosens the BBB tight junctions, increasing permeability[4,5].

While most of the manifestations of stroke are a result of neuronal damage, the factors contributing to the pathophysiology of stroke are not limited to neurons. These encompass a complex interplay between the components of the neurovascular unit that forms the BBB such as the endothelial cells, astrocytes, pericytes, microglia and the physiological markers emanating from these cells.

2.3. Oxidative stress in stroke

The reactive oxygen species (ROS) and reactive nitrogen species (RNS) mediate the cell damage associated with oxidative stress. The ROS and RNS generation in ischemic and reperfusion phase is very heterogeneous, due to the variable blood flow in the stroke core and the penumbra. Mitochondria are the predominant intracellular source as well as the target of oxidative stress. Indeed, a post-stroke upregulation in mitophagy to rid the neurons of damaged mitochondria has been reported[6]. Their sources are primarily enzymatic, involving the enzymes such as the xanthine oxidase system, NADPH oxidase system, nitric oxide (NO) system and the electron transport chain. The electron transport chain (ETC) generates ATP, using oxygen during the process. Most of the oxygen used is converted to water molecules, however, a small amount is reduced to form superoxide radicals. Superoxide radicals ($O_2^{\cdot-}$) are converted to hydrogen peroxide by the enzyme superoxide dismutase. The primary enzymes of xanthine oxidase system include xanthine dehydrogenase and xanthine oxidase. During ischemia, both are shifted to xanthine oxidoreductase. Upon reperfusion, this enzyme system initiates the metabolism of hypoxanthine to xanthine and further to uric acid. In this process, oxygen acts as the final electron acceptor, and ROS such as superoxide and hydrogen peroxide are released, causing oxidative stress and

downstream inflammatory events[3]. The expression of NADPH oxidases (NOX enzymes) has been reported to be upregulated after an ischemic event[7]. The increased activity of NOX enzymes leads to the production of superoxide radicals, that eventually forms hydrogen peroxide[8].

Superoxide also contributes to RNS formation and turns cell organelles alkaline, whereas, hydrogen peroxide affects the functioning of tyrosine and serine-threonine phosphatases. Hypoxic environment induces the hypoxia inhibitory factor 1α (HIF-1α) to promote NOX enzyme activation, and a positive feedback loop is established with increased oxidative stress, HIF-1α production and NOX enzyme activation. NOX activity is also enhanced by cytokines during the reperfusion process. NO is a free radical generated by the enzyme nitric oxide synthase (NOS). The subtypes of NOS involved depends on the cell type. Neurons use neuronal NOS, glial cells use inducible NOS, while endothelial NOS generates NO from endothelial cells. While NO from endothelial cells promotes vasodilation and has protective tendency, neuronal and glial NO contributes to cerebral damage[9]. NO reacts with superoxide radicals to form peroxynitrite (ONOO), a powerful oxidant. Peroxynitrite has about 400-fold faster membrane permeability as compared to superoxide radical, providing it an easy access to its intracellular biological targets[10]. One of the reactions peroxynitrite is involved in is the tyrosine nitration to form nitrotyrosine (NT), which is used as a marker for peroxynitrite[11]. Under ROS-RNS influence and in conjunction with plateletderived growth factor (PDGF)-β, pericytes undergo contraction which leads to capillary constriction and further impedes blood flow in the cerebral vasculature[12]. The constriction of pericytes is more prominently seen during the reperfusion phase, and is a contributing factor to reperfusion injury[12,13].

2.4. Apoptosis induced cell death in stroke

Cell damage and death in stroke is bimodal, and can occur due to the consequences of both ischemia or reperfusion. Ischemic event can result in build-up of metabolites and cellular acidosis, whereas reperfusion usually triggers ROS generation and recruitment of inflammatory mediators, all of which are responsible for cytotoxicity. Apoptosis, the process of programmed cell death, is initiated during both phases. Both, hypoxic events during ischemia and ROS generation during reperfusion can initiate cell apoptosis[14]. An overload of ROS tends to exhaust the scavengers such as superoxide dismutase[15]. This could in turn promote apoptosis, as superoxide dismutase has been reported to prevent the early release of cytochrome c from the mitochondria after transient focal cerebral ischemia[16]. Mitochondrial damage varies in transient ischemia compared to permanent ischemia, indicating the effect of reperfusion. The primary difference reported shows that reperfusion injury can cause disintegration of mitochondria after 24 hours, while permanent ischemia leaves mitochondrial shapes intact, albeit swollen[17]. Intracellular calcium ion build up has been shown cause mitochondrial swelling in neurons to an extent, and subsequently causing a moderate release of cytochrome c[18]. Calcium induced mitochondrial swelling has been shown to be calcium ion concentration dependent. The loss of membrane potential worsens with reperfusion period, reaching an ebb at 24 hours[19].

Apoptosis occurs via two pathways: extrinsic and intrinsic. The extrinsic pathway is activated by external receptors and ligands, the prominent among which is the Fas-ligand. This pathway activates the initiator caspases 8 and 10 that mediate the cell death. The intrinsic pathway of apoptosis is initiated at the mitochondrial level, and is more likely to be involved in stroke as it is activated by hypoxia, cellular toxins and damage to mitochondrial membrane. Ischemia reperfusion injury enhances the activity of pro-apoptotic members of the Bcl-2 protein family.

Cytoplasmic pro-apoptotic Bad binds the anti-apoptotic Bcl-2 and Bcl-XL proteins attenuating their activity. Moreover, the formation of mitochondrial channel involving cytoplasmic Bax and mitochondrial membrane protein Bak is promoted. The Bax-Bak channel allows the release of cytochrome c from mitochondria. The protein Bid that promotes this channel formation has been reported to be regulated by ROS levels[20]. Cytochrome c binds apoptotic protease activation factor1 (Apaf-1) to then form the apoptosome, which activates the initiator caspase-9. Caspase-9 finally activates the effector caspases such as caspase-3 and 7. Caspase-3 mRNA expression was found to be upregulated in neuronal cells in ischemia models[21]. A second form of cell death that has been reported following ischemia and reperfusion injury is necroptosis, showing a death pattern similar to necrosis which is characterized by plasma membrane permeation and organelle swelling, and is a result of excess external stress. Ischemia-reperfusion also induces cell autophagy.

2.5. Stroke and inflammation

Inflammatory events are initiated soon after the onset of focal cerebral ischemia, and subsequently worsened following reperfusion. Inflammatory events are mediated by the components of neurovascular unit as well as neutrophils, leukocytes and dendritic cells[22]. The BBB serves as a barrier to the brain entry of leukocytes. However, under inflammatory conditions, this barrier function is compromised. The pro-inflammatory mediators released during the early acute phase of ischemia induce the endothelial expression of adhesion molecules such as ICAM-1 and selectins, promoting leukocyte infiltration and adhesion. Over the course of time in the subacute phase, the infiltrating leukocytes amplify the inflammatory and ROS population. Amongst the infiltrating leukocytes, neutrophils dominate the early phase of up to a few hours after ischemia[23]. Mast cells secrete vasoactive substances and gelatinase granules and contribute to the overall BBB disruption[24]. In a rat stroke model, mast cells have been shown to regulate brain swelling and

neutrophil accumulation in the early phase[25]. There are reports of infiltration of dendritic cells in the brain after an ischemia, which could worsen stroke outcomes by heightening a CNS T-cell immune response, and an overall immunodepression in the body due to a decrease in dendritic cell population in the systemic circulation[26]. Ischemic events lead to activation of the cerebral immune system, most notably the activation of the microglial cells. Microglia represent the predominant population amongst the macrophage-like cells, and have a heightened activity during the first few days after ischemia[23]. While activated microglia can eliminate the harmful excitotoxins, they also display enhanced phagocytosis, release of pro-inflammatory cytokines via Toll-like receptor (TLR2 and TLR4) activation, TNFα, IL-1β, Iba-1, CD40 among others, which cause damage. Apart from microglia, reactive astrocytes also contribute to the pro-inflammatory milieu. Astrocytes in an ischemic environment show an upregulation of glial fibrillary acidic protein (GFAP) denoting an inflamed state. The glial scar formed by inflamed astrocytes often demarcates the healthy brain tissue from the ischemic zone[22,27].

CD4+ and CD8+ T-lymphocytes also contribute to the inflammatory disequilibrium in stroke by releasing pro-inflammatory cytokines[28].

2.6. Edema in stroke

A hallmark feature of cerebral ischemia and reperfusion injury is the damage resulting from brain swelling, or edema. The CNS cells have higher intracellular concentrations of potassium ions, and low concentrations of sodium and calcium ions. Under normal physiologic conditions, the osmotic concentrations of intracellular and extracellular fluids are maintained. However, in the case of an imbalance of solute concentrations, a transmembrane osmotic gradient is generated, and because the cell membrane is freely permeable to water, this gradient causes a flow of water into or out of the cell to attain an osmotic balance. This leads to swelling or shrinkage of the cell, depending on

the directions of water flow. Lack of energy in ischemia leads to the dysfunction of ion pumps, and cell swelling occurs due to the electrolyte imbalance with excess buildup of intracellular sodium ions, and extracellular potassium ions, and subsequent water influx from the extracellular space.

Ischemia-induced edema can be broadly classified in having cytotoxic, vasogenic and ionic origins[29]. The primary component of the neurovascular unit that accounts for cytotoxic edema are the astrocytes, due to their larger populations. Cytotoxic edema leads to an alteration of ionic gradient, mainly via secondary active transport (co-transporters) or passive transport of ions. Glutamate excitotoxicity at NMDA and AMPA receptors also contributes to the abnormal influx of extracellular ions. The influx of sodium ions, followed by chloride ions accumulate in the intracellular space. This triggers an influx of water through the aquaporin channels to maintain the osmotic balance. Aquaporin channels are key mediators of the water influx. Astrocytic AQP4 channel activity, which is upregulated by excess glutamate is known to facilitate increased water influx[27]. AQP4 overexpression leads to swelling of astrocytes and activates microglia, leading to inflammatory consequences[30]. AQP4 can thus contribute to the transition of cytotoxic edema to vasogenic edema[31].

The cytotoxic edema occurs within the boundaries of the CNS, and thus, only redistributes the ionic and water within. It does not alter the total brain volume, which is seen in stroke. The increase in brain volume is primarily mediated by endothelial cells, which contribute to the ionic and vasogenic edema. Ionic edema, which precedes the vasogenic edema is facilitated by changes in the BBB. Due to the events surrounding the cytotoxic edema, the extracellular space of the brain suffers a shortage of water and ions. The resulting gradient triggers the movement of ions and water from the vasculature into the brain extracellular space. Ionic edema occurs early during

ischemia when the BBB tight junctions are intact, and thus, the ionic edema fluid lacks plasma proteins. The toxic mediators of ischemia also enhance the endothelial cell permeability by increasing the expression of ion transporters.

The secondary phase of endothelial cell mediated edema is the vasogenic edema, which is a delayed phase occurring a few hours after the onset of ionic edema[32]. The primary difference between the two phases is that the vasogenic edema begins when the BBB tight junctions suffer a breakdown[33]. Vasogenic edema predominates during the reperfusion phase, does not lead to cell swelling and the edema fluid is plasma protein rich[34]. It is caused by a multiple factors acting simultaneously to breakdown the BBB and include the likes of VEGF, MMPs, metabolites of arachidonic acid and inflammatory cytokines among others[29,35,36].

Cerebral edema during ischemia and reperfusion leads to increased brain swelling and an elevated intracranial pressure. It is a leading consequence of the reperfusion injury and an important factor contributing to fatalities related to stroke[37].

2.7. The BBB in stroke

The complex interplay between oxidative and inflammatory stress has a deleterious effect on the integrity of the BBB and causes barrier opening. The BBB disruption is known to be more severe in transient ischemia compared to permanent occlusion[38]. This is indicative of the damage reperfusion can cause. The opening of BBB after transient ischemia has been demonstrated to be biphasic, with peaks occurring around 3 and 48 hours post-reperfusion commencement[39,40]. The BBB in the ischemic core is prone to irreversible damage, whereas the BBB in the penumbra region is known to be mildly damaged and can be salvaged[41,42]. The BBB permeability in stroke was studied using an MRI contrast agent such as Gd-DTPA by applying Patlak plot analysis to the

influx of the agent, wherein elevated influx rate constant (K_{in}) values were observed for Gd-DTPA and sucrose, which is normally impermeable.[43]. MRI imaging in stroke patients has revealed that the BBB is most permeable during 6-48-hour period after the onset of ischemia, and the leakage was seen for up to 90 hours after the ischemic onset[44]. Permeability surface area product was also found to be increased in patients with delayed infarction seen in subarachnoid hemorrhage[45]. Raja et al. compiled a comparative review focusing on the patient BBB permeability in disease states, measured by different groups using dynamic contrast enhanced magnetic resonance imaging[46]. The permeability coefficient K^{trans} for the imaging agent, calculated based on the Patlak model, was used as a measure of BBB permeability. The K^{trans} values indicated an almost four-fold higher permeability in stroke as compared to early AD in normal appearing white matter.

Enhanced BBB permeability and tight junction disruption after stroke occurs through the mediation of multiple factors which include immune cells, cytokines, chemokines, micro-RNAs and the mitochondria[47]. Inflammatory mediators such as IL-6 and TNF-α downregulate ZO-1 expression and its association with occludin, thereby reducing the transendothelial electrical resistance. They also cause phosphorylation of tight junction proteins such as claudin-5 and ZO1, affecting their functioning[48]. Pericytes secrete mediators such as matrix metalloproteases that loosen the BBB tight junctions, aiding in infiltration of leukocytes in the cerebral vessels. The BBB disruption by MMPs occurs as a biphasic event[49]. MMP-2, in conjunction with HIF-1α, participates during the initial hypoxic phase. The later phase, which occurs about 24-48 hours post the initial ischemic event, is primarily regulated by MMP-3 and MMP-9. Overall, the proteases such as MMPs lead to a dysfunctional BBB, and are responsible for the hemorrhagic events following a stroke. Peroxynitrite is known to cause BBB disruption in stroke[50]. Another major source of MMPs are neutrophils and thus, neutrophil infiltration following stroke aggravates BBB damage[51,52].

Microglia upregulate the cell adhesion molecules such as ICAM-1, P-selectin, VCAM, thereby promoting leukocyte infiltration[53].

The breakdown of BBB is often attributed to be the reason of transformation of ischemic stroke to a hemorrhagic one, especially after t-PA administration[54]. The highest risk of hemorrhagic transformation exists between 24-48 hours after onset of ischemia, when the BBB exists in a highly permeable state[55]. Thus, a BBB dysfunction of a heterogeneous nature is seen in stroke and facilitates the eventual grave consequences of stroke such as edema and hemorrhage.

2.8. The mitoNEET protein

As the powerhouse of the cell, mitochondria play a vital role of ATP synthesis and nucleotide production. During this process and beyond, the mitochondrial constituent elements contribute to a host of biochemical and physiological processes that could impact the cellular microenvironment, as well as the organ systems. One such mitochondrial protein that has drawn attention in recent years in mitoNEET. The efforts into investigation of the off-target actions of thiazolidinedione category of drugs used to treat diabetes led to the discovery of mitoNEET. These drugs, such as pioglitazone, were found to demonstrate effects that were not downstream of their intended target, the PPARγ receptor. Colca et al., used tritiated pioglitazone and a photoaffinity cross-linker, and identified a binding site for the drug in mitochondria[56]. Using size exclusion chromatography, the protein was isolated and identified by a combination of mass spectrometry and amino terminal sequencing. This protein, with a molecular weight of under 17kDa, was found to contain a characteristic Asn-Glu-Glu-Thr (NEET) sequence. Since it was isolated from mitochondrial fractions it was subsequently named mitoNEET. The binding of pioglitazone to mitoNEET was speculated to be responsible for its actions, such as increased lowering of lipid levels as compared

to rosiglitazone, which happens to be a more potent agonist of the PPARγ receptor. In the years following its discovery, mitoNEET has been the subject of study by various research groups.

2.9. MitoNEET structure and the iron-sulfur cluster

The structural features of mitoNEET started to be elucidated soon after its discovery. Wiley et al., used bioinformatics analysis and found that mitoNEET belonged to a family of proteins containing the CDGSH-type zinc finger[57]. The protein, when expressed by the recombinant technology, was found to be red in color. Further metal analysis revealed that, although it contained the zinc finger, zinc was present only in trace amounts. Instead, mitoNEET was found to have a presence of iron as the predominant metal, which was 1.6 mole per mole of the His-tagged mitoNEET. The mitochondrial localization of mitoNEET was confirmed by generation of an analog that lacked the first 32 amino acids from the N-terminal. The lack of mitochondrial presence of the analog indicated that mitoNEET was localized to mitochondria by its N-terminal. Further studies established the localization in the outer mitochondrial membrane and cytoplasmic orientation of mitoNEET. The same group also found that iron was present as a 2Fe-2S iron sulfur cluster[58]. Although the cluster is found in other proteins such as ferredoxin, the combination of amino acids that bind this cluster make mitoNEET and its family members unique. In mitoNEET, the 2Fe-2S cluster is bound by three cysteines and one histidine residue. It was also found that the cluster is labile to be released at pH of 6 or lower. The reason for this lability has been attributed to the protonation of His-87 that in turn, leads to cluster release. The pH sensitivity of the cluster and the contribution of His-87 was further established using resonance Raman spectral analysis of mitoNEET at varying pH values[59]. Binding of pioglitazone leads to stabilization of the 2Fe-2S cluster and prevents its release[60].

Around the same time, the crystal structure of mitoNEET was studied by Lin et al. and Paddock et al., revealing a homodimeric structure with superimposable subunits[60,61]. Hydrophobic interactions and water molecule mediated hydrogen bonding contribute to the dimerization of the monomers[62]. Lys-55 was found to be one of the conserved residues in eukaryotic mitoNEET contributing to the hydrogen bonding network[63]. Each monomer of mitoNEET binds one 2Fe-2S cluster, and thus mitoNEET as a whole contains two such clusters, separated by a distance of 16 Å. The cluster binding region was found to contain an amino acid sequence which was unique to this family of proteins: (hb)-C-X1-C-X2-(S/T)-X3-P-(hb)-C-D-X2-H. The cluster is bound between the amino acid residues 71 through 87. MitoNEET is a vase shaped protein with a narrow central region. Hydrophobic residues predominate the central region, whereas charged residues are present around the cluster binding region (bottom), and the β-cap domain at the top. Thus, mitoNEET is polar at the top and the bottom with a hydrophobic region in between. MitoNEET exhibits evolutionary conservation in its structure across species of mammals, plants and thermophilic bacteria[64], showing a possible important physiological role. The cytoplasmic tethering arms of mitoNEET were found to be flexible in nature, allowing the cytoplasmic portion of the protein to attain two different conformations[65]. Most of the studies geared toward crystal structure have centered on the structure of mitoNEET in its native form. However, a recent study by Geldenhuys et al., has revealed the crystal structure of mitoNEET bound to a ligand[66]. The ligand used in this study was furosemide, which has a benzoic-sulfonamide-furan structure. This could potentially help in future design of novel mitoNEET ligands that can be used as therapeutic agents.

An EPR analysis of the protein suggests that the two clusters might be involved in intramolecular electron transfer[67]. A redox analysis of the iron-sulfur cluster was performed using protein film voltammetry, with and without thiazolidinedione binding[68]. In the wild type protein, the binding

of pioglitazone and rosiglitazone reduces the midpoint potential of the cluster from around 0 mV to -100 mV, near neutral pH. However, when mutant form of mitoNEET was used wherein the His-87 was replaced by a cysteine, no change in the midpoint potential was observed, indicating the importance of the His-87 residue in thiazolidinedione drug binding to mitoNEET. The effect of replacing the His-87 with a cysteine on the cluster properties was studied by Conlan et al[69]. Cluster co-ordination by four Cys residues imparts greater stability to the cluster within the protein. However, the pH sensitivity of the cluster is not altered in the mutant as compared to the wild type protein. This finding contradicts the prior theory that protonation of His-87 is responsible for cluster release at an acidic pH. It was concluded that the unique co-ordination pattern seen in wild type protein could be a possible evolutionary effect, as four Cys ligands would hinder the transfer of electrons to partners in the cytosol. Subsequently, it was found that His-87 was not the sole contributing factor to pH dependence of cluster stability, with other residues namely Lys-55, Ser77, and Asp-84 also known to play a role[63]. This shows that it is not just the cluster coordinating residues but also the residues from the hydrogen bonding network that contribute to the stability of the 2Fe-2S cluster.

The stability of the cluster is also influenced by its oxidation state, with the reduced form being more stable as compared to the oxidized form[63]. The polarity and strength of the His-87 and iron co-ordinate bond also influences cluster stability in mitoNEET[70]. Higher polarity and lower bond strength contribute to cluster lability. When His-87 is protonated, the bond between the histidine and iron is more polar and weaker. The hydration of histidine promotes its protonation, indirectly affecting the cluster lability. In the protonated state, mitoNEET forms hydrogen bonds with water; whereas in the deprotonated state, it hydrogen bonds with Lys-55. This lysine residue has an orientation state that favors hydration of His-87. The presence or absence of the cluster can also

affect the overall structure of mitoNEET. Removal of cluster from one monomer not only leads to unfolding of the α-helix of that monomer, but also affects the other monomer[70]. Loss of both clusters could lead to a loss of secondary structure folding. This could lead to a loss of mitoNEET function and could potentially be a factor in cancer and neurodegenerative diseases. MitoNEET can alternate between an unstructured apo-form without the cluster, and a cluster-bound folded form[71]. MitoNEET receives the cluster from the mitochondria. The efficient functioning of the iron-sulfur cluster assembly enzymes and its export mechanisms from the mitochondria are inevitable to keep mitoNEET in a structured form and prevent its eventual proteasomal degradation.

A model of mitoNEET 2Fe-2S cluster was shown to mediate proton coupled electron transfer (PCET), and the His-87, which undergoes protonation at acidic pH, has been thought to play an important functional role in the PCET process[72]. The exposure of nitrogen of the histidine imidazole on the protein surface facilitates an easy protonation of the residue. MitoNEET displays a difference in colorimetric absorption maxima depending on its oxidation state. When mitoNEET exists in an oxidized state, an absorption maximum is observed at 458 nm wavelength, and a minimum is seen at this wavelength when the cluster is in a reduced state[73].

2.10. Role of mitoNEET in physiology
MitoNEET has been found to play a vital role in regulation of cellular bioenergetics. The cardiac cells of mitoNEET knockout mice were found to have a significantly lower respiration rate as compared to the wild-type[57]. It was found that the redox potential of mitoNEET 2Fe-2S cluster could be manipulated over a wide range for the wild type and the His-87, Lys-55, and Asp-44 mutants[74]. The range encompasses about 700 mV (from -360 mV to +305 mV) which happens to

span the cellular redox range. This indicated the potential for use of mitoNEET and its mutant forms as externally administered redox agents.

The cluster transfer from mitoNEET to cytosolic proteins is one of the primary physiological functions of mitoNEET. Unlike other iron-sulfur cluster containing proteins, mitoNEET can transfer its iron-sulfur cluster under aerobic conditions as well[75]. The activity of cytosolic aconitase was found to be lower upon knockdown of mitoNEET. Further investigation revealed that the significant reduction in the iron-sulfur cluster transfer to cytosolic aconitase caused the depletion in activity, which was promptly rescued upon mitoNEET transfection. Transfection with a His-87 mutant did not show similar rescue, once again showing the involvement of the critical residue in cluster transfer. Coupled with the fact that loss of mitoNEET did not affect aconitase expression, this study outlined the importance of mitoNEET in function and maturation of cytosolic proteins[76]. MitoNEET also plays a role in repairing the cytosolic iron-sulfur cluster of Iron Regulatory Protein-1 (IRP-1)[71], and is a key regulator of cellular iron homeostasis. MitoNEET has been reported to interact with 1,4-Alpha-Glucan Branching Enzyme (AGBE) in a *Drosophila* model[77]. The Drosophila AGBE assists mitoNEET in IRP-1 repair, keeping it viable for nuclear entry. Using NMR and UV-visible spectroscopy, it has been determined that mitoNEET transfers the iron-sulfur cluster to cytosolic recipients in an oxidized form. Upon transfer, the protein changes from a well-folded holo-form to an unfolded apo-form. The reduced state of mitoNEET has thus been termed as the dormant state, whereas the oxidized transfer-ready state has been termed as the active state[78]. Upon completion of the repair of IRP-1, mitoNEET needs to be brought back to its 'dormant' reduced form. This is achieved by an interaction of mitoNEET with a complex of two proteins. These two proteins are anamorsin and NADPH-dependent diflavin oxidoreductase 1 (Ndor1).

Anamorsin-Ndor1 complex thus reduces mitoNEET and halts the repair process that mitoNEET is involved in[79].

The cluster transfer details were further studied using apo-ferredoxin, wherein it was found that only one of the two clusters of mitoNEET are transferred to the apo-protein in a direct manner; while the second cluster undergoes degradation[80]. MitoNEET and the acceptor protein form a transient, unstable complex during the process of cluster transfer. This study also demonstrated that pH dictates the cluster stability only under anaerobic conditions. The iron-sulfur cluster is rendered stable under anaerobic conditions, at acidic pH. The cluster transfer to an apo-protein is also dependent on the pH, and likely allows mitoNEET to act as a pH sensor while transferring the iron-sulfur cluster. Low pH not only affects the cluster stability, but also lowers the stability of the holo-mitoNEET dimer. The iron-sulfur cluster was also found to be stable to hydrogen peroxide exposure *in vitro*, indicating its role in cell response to oxidative stress.

Apart from its direct interactions with cytosolic proteins, mitoNEET can influence the interactions of mitochondrion with cytosolic proteins through the regulation of voltage-dependent anion channel 1 (VDAC1). MitoNEET, in an oxidized form, has been found to bind and gate the VDAC1[81]. VDAC1 controls mitochondrial respiration, regulates apoptosis, transport of ions and metabolites between the mitochondrial intermembrane space and the cytosol. The interactions if mitoNEET and VDAC1 were confirmed using an irreversibly binding inhibitor of VDAC1. The regulation of VDAC1 by mitoNEET can prove to be vital for mitochondrial homeostasis.

Studies have been performed to determine the effect of binding of endogenous molecules, especially the ones involved in redox processes, on mitoNEET and the iron-sulfur cluster. Zhou et al., determined the that upon binding mitoNEET at an acidic pH, NADPH caused the

destabilization of the cluster and its eventual release from the protein[82]. Following cluster release, mitoNEET loses its three dimensional structure. NADPH is thought to interact with the residues in mitoNEET that in turn interact with the cluster binding residues. Upon loss of these interactions, destabilization of the cluster occurs. These events have been speculated to be contributing factors in pathophysiology of metabolic diseases, wherein mitoNEET might act as an NADPH sensor. Subsequently, Zuris et al., studied the effect of NADPH binding on the ability of mitoNEET to transfer the cluster[83]. It was found that NADPH binding at a K_i of 200 μM inhibited the transfer of the cluster to an apo-acceptor protein. The primary residue mediating the NADPH actions of cluster transfer was found to be the cluster interacting residue Asp-84. NAPDH also shifts the redox potential of the cluster. These findings give more substance to the role of mitoNEET as a sensor of NADPH, the levels of which could be altered in disease states. Lowered NADPH levels in a pathophysiological condition would then lead to cluster release from mitoNEET. Thus NADPH can modulate the cluster levels in mitoNEET and cytoplasm, as well as the mitoNEET structure. Apart from NADPH, Flavin nucleotides have also been shown to display specific interactions with mitoNEET[84]. Reduced flavin mononucleotide (FMN) was found to reduce mitoNEET cluster under aerobic and anaerobic conditions. A combination of EPR and molecular docking studies showed that FMN, and not flavin adenine dinucleotide (FAD) has the reducing ability; and FMN binds mitoNEET between the transmembrane portion and the iron-sulfur cluster. This was deemed ideal for electron transfer between the biomolecule and the cluster. This is yet another example of mitoNEET acting as a metabolic regulator.

MitoNEET also has a stimulatory effect on cellular glycolysis[85]. During the reduction reaction of $FMNH_2$, catalyzed by flavin reductase, mitoNEET also undergoes reduction upon binding of cytosolic NADH, which in turn gets oxidized. Oxidation of NADH is necessary for sustenance of

glycolytic process. Thus mitoNEET is thought to contribute to enhance glycolysis. Ubiquinone-2, which is an important biochemical constituent of the respiratory cycle milieu, was found to oxidize the reduced clusters of mitoNEET under aerobic and anaerobic conditions. Ubiquinone-2 has a strong presence in inner and outer mitochondrial membranes, and due to its superior efficiency in oxidizing clusters, it has been proposed to be an intrinsic electron acceptor of mitoNEET clusters. The oxidation of mitoNEET by ubiquinone-2 under anaerobic conditions is 500 times faster than oxygen, with a rate constant of 3000 $M^{-1}s^{-1}$ as compared to 6 $M^{-1}s^{-1}$ for oxygen[86]. Under aerobic conditions, ubiquinone-2 causes rapid oxidation of mitoNEET clusters, preventing their reduction by $FMNH_2$.

The importance of mitoNEET in the formation of mitochondrial network has also been studied[87]. Mitochondria often assemble into groups of two or three. Using electron microscopy, it was seen that when mitoNEET was knocked down, the formation of intermitochondrial junctions was significantly lowered as compared to wild type cells. Upon overexpression of mitoNEET, an increase in the intermitochondrial junction formation and mitochondrial clustering was observed, confirming the necessity of mitoNEET in their formation. The mechanism for mitochondrial tethering has been suggested to be linkage of two mitoNEET proteins from separate mitochondria. The respiratory capacity of the cells was found to be reduced due to decrease in the mitochondrial numbers. However, mitochondrial size was not seen to be affected by mitoNEET knockdown. MitoNEET was also not found to be relevant in establishment of contact between mitochondria and endoplasmic reticulum.

Landry et al., studied the redox effects of biological thiols and hydrogen peroxide on mitoNEET[88]. MitoNEET cluster can be partially reduced by monothiols such as glutathione and L-cysteine, whereas dithiothreitol and E. coli thioredoxin-1 cause complete reduction. The cluster reduction is

reversible, and they can be oxidized by hydrogen peroxide. This is suggestive of mitoNEET's role as a sensor for the levels of redox compounds and ROS. Upon binding mitoNEET, pioglitazone inhibits the thiol mediated reduction of the iron-sulfur clusters. Subsequently, the same group showed that human glutathione reductase had the ability to reduce mitoNEET clusters, in a similar reversible manner[89]. Their studies with N-ethylmaleimide, which inhibits the activity of the enzyme on mitoNEET clusters, showed that the redox active disulfide present in the catalytic center of glutathione reductase was involved in the reduction of the iron-sulfur cluster.

MitoNEET belongs to the family of NEET proteins wherein the 2Fe-2S cluster is coordinated by three cysteine and one histidine residues. Another member of this family happens to be NAF-1, which is encoded by the CISD2 gene. The interactions between the two proteins have been studied by Karmi et al., and it gives us an understanding of the dependence and independence of these members of the NEET family of proteins[90]. Using *in vivo* biomolecular fluorescence complementation analysis, it was found that mitoNEET and NAF-1 interacted in endoplasmic reticulum and mitochondria. This interaction was mainly in the form of cluster transfer from an oxidized form of mitoNEET to a pre-reduced apo-form of NAF-1. It was further stated that mitoNEET and NAF-1 work complimentarily in the same biochemical pathway, and control the levels of iron and ROS in the cells. This helps in cell survival and prevention of cellular apoptosis, having favorable effects in cell survival in neurodegenerative diseases and pro-survival effects in cancer cells. A possibility of mitoNEET and NAF-1 being a part of cluster transfer relay has also been proposed. Thus, along with their independent functions, mitoNEET and NAF-1 also work in a cooperative manner as part of common biochemical processes.

The role of cisd-1 gene in physiological germline apoptosis has been elucidated in a *Caenorhabditis elegans* (*C. elegans*) model[91]. In C. elegans, this gene encodes for a protein which

is homologous to mitoNEET (CISD1) and NAF-1 (CISD2) in vertebrates, and retains the 2Fe-2S cluster. A *C. elegans* mutant with deletion in cisd-1 coding region displayed germline defects including reduction in number of differentiated oocytes and distal tip cell migration defects. Increased numbers of cell corpses within the germline were also observed. The mechanism for cell death was attributed to apoptotic pathway dependent on CED-13 (pro-apoptotic protein in C. elegans) function. Thus, CISD family members, mitoNEET and NAF-1, were found to have prosurvival effects in this model. They are said to work in a co-operative manner.

2.11. MitoNEET in neurodegenerative diseases

The unravelling of the physiological contributions of mitoNEET lead to investigations into its role in disease conditions. Due to its functional importance at a cellular level, any disruption in its normal function can potentially be a causative factor in a wide variety of anomalies. We have seen that the presence of iron – sulfur cluster in mitochondrial proteins is found to be critical to many cellular functions and disease development. It was found that zinc and iron-sulfur cluster share a binding site on mitoNEET and excess zinc ions compete with the cluster on that binding site in mitoNEET, thus prohibiting the assembly of these essential clusters[92]. Zinc toxicity is known to be the cause of neurodegenerative conditions such as Alzheimer's disease and neuronal death following a stroke[93,94,95]. High zinc levels were previously found to disrupt iron homeostasis[96], and a likely reason can be narrowed down to its mitoNEET binding.

MitoNEET also plays an important role following spinal cord transection, possibly revealing mitoNEET as a target for treatment and repair of a spinal cord injury. MicroRNA-127 was shown to induce neuronal loss via apoptosis, axonal degradation, sensory and motor dysfunction following spinal cord transection. Such effects of microRNA-127 were also seen on spinal cord cells *in vitro*. In these events, a target of microRNA-127 was mitoNEET. Knockdown of

mitoNEET *in vitro* lead to similar neurodegenerative effects showing that mitoNEET and microRNA-127 can be used as therapeutic targets to prevent the exacerbation of neuronal loss[97]. MitoNEET has also been identified as a potential target for treating Parkinson's disease. MitoNEET knockout mice exhibit mitochondrial dysfunction in their brain. Loss of mitoNEET decreases striatal tyrosine hydroxylase and dopamine, as a result of which the mice display motor deficits with shortened strides and lack of balance. Increased iron accumulation is also observed in striatum in knockout mice, which is a possible precedent for increased ROS levels that contribute to the Parkinson's pathology. This shows that mitoNEET has an impact on the neurons that control movement, similar to the phenotype of Parkinson's disease, making it a promising target[98]. The mitoNEET agonist TT01001 was recently shown to prevent mitochondrial dysfunction by mitigation of oxidative stress and apoptosis in rats with subarachnoid hemorrhage[99].

The role of mitoNEET in postnatal brain development has recently been elucidated[100]. Quantitative proteomics on presynaptic mitochondria in postnatal mice found elevated levels of mitoNEET. Overexpressing mitoNEET displayed a neuronal cell-type specific enhanced mitochondrial membrane potential, fragment generation, and further increased ATP levels. These changes are characteristic of mitochondria working at their full potential to fulfill the increased energy demand, which occurs during brain development at the postnatal stage. Due to its role as a bioenergetics regulator, and its ROS-protective effects in the developing brain, mitoNEET can be used as a target for neurodevelopmental disorders.

2.12. The NEET ligand 1 (NL-1)

MitoNEET has binding sites that have been determined to bind thiazolidinedione (TZD or glitazone) compounds and stabilize the 2Fe-2S cluster. Aided by a combination of molecular

docking studies and radiolabeled ligands, a novel glitazone analog, the NEET ligand 1 or NL-1 was synthesized[101]. As mentioned, the glitazones (2, 4-thiazolidiendiones; TZD) have been used to treat type II diabetes, to lower blood glucose levels. Several of the marketed glitazones were removed from the market, including troglitazone, due to liver toxicity, and rosiglitazone (BRL49653C, (±)-5-[[4-[2-methyl-2-(pyridinylamino)ethoxy]phenyl]methyl]methyl]-2,4-thiazolidinedione), due to cardiac toxicity. Pioglitazone, AD-4833, (Actos) was first discovered by Takeda Pharmaceuticals by exploration of substitution patterns on the cyclohexyl ring of ciglitazone, the prototypical thiazolidinedione in the pharmacological class. The glucose lowering and amelioration of insulin resistance led to the successful development and FDA approval of pioglitazone in July of 1999. Pioglitazone was found to be a PPAR-gamma agonist, as its primary mechanism of action.

The synthesis of NL-1 (5-[3,5-Bis(1,1-dimethylethyl)-4-hydroxyphenyl]methyl-2,4thiazolidinedione) was based on a Knoevenagel condensation reaction as shown in **Figure 2.2**. Due to the steric hindering of the tert-butyl groups, the reduction of the unsaturated bond requires LiBH4 and a week reduction to allow for sufficient generation of product. This compound retained the thiazolidinedione pharmacophore of glitazones, which was thought to be the essential structural feature for binding mitoNEET. The hydrogen bonding and acceptor groups on the thiazolidinedione moiety contribute to the drug binding to mitoNEET. NL-1, selectively binds mitoNEET, without any activity at the peroxisome proliferator-activated gamma (PPAR-γ) receptor, to which glitazones typically bind.

NL-1 has been successful in reducing rotenone induced cell death by almost 40%. It was also able to cause uncoupling of mitochondrial respiration, and reduced state III respiration rate by 45%. The ability of NL-1 to reduce the capacity of mitochondrial complex I has implications in treatment

of neurodegenerative diseases such as Parkinson's disease as complex I is shown to generate the noxious reactive oxygen species (ROS)[101]. Other applications of NL-1 have been investigated such as its use in increasing viability of cardiac stem cells introduced in regenerative therapy for ischemic heart disease. NL-1 was seen to have a short-term cytoprotective effect as an increased cardiac stem cell survival under oxidative stress was observed. However, this result was not exhibited by chronic exposure in *in vivo* studies. Due to the oxidative environment associated with heart disease, NL-1 is thought to interact with mitoNEET to reduce mitochondrial function showing lower oxygen consumption rates (OCR) which has been established to reduce ROS. The specificity of NL-1 toward mitoNEET was confirmed when no significant difference in cell survival was observed in mitoNEET knockdown cells with NL-1 and vehicle treatments. In general, NL-1 was able to reduce cardiac stem cell death when exposed to an oxidative environment[102]. Due to NL-1's affinity for mitoNEET, novel drugs targeting mitoNEET may prove to be beneficial in stem cell therapy. NL-1 has also been tested as a potential drug candidate in relapsed acute lymphoblastic leukemia[103]. NL-1 was found to have a dose-dependent cytotoxic effect in cytarabine-resistant leukemic cell line. The anti-cancer activity of NL-1 was seen in six different acute lymphoblastic leukemia cell lines, and through hemosphere assay as spheroid disruption. The mechanism of action of NL-1 has been suggested to be prevention of cancer cell migration, and induction of autophagy in the cancer cells. NL-1 also showed anti-leukemic activity in a preliminary *in vivo* study using a mouse model of acute lymphoblastic leukemia. NL-1 has been found to be cytotoxic against MCF-7 breast cancer cells with an IC_{50} value of 7.1 μM, when the cells were subjected to oxidative phosphorylation using galactose containing growth medium[104].

For a quantitative approach, a liquid chromatography/tandem mass spectrometry (LC-MS/MS) assay has been developed to accurately quantify NL-1 levels[105]. The application of this method was also demonstrated in a pharmacokinetic analysis of NL-1 levels in serum samples from mice after a single intraperitoneal dose. The drug was found to reach a maximal serum level within 30 minutes of administration. The NL-1 levels were found to be within the mitoNEET binding activity range. NL-1 is shown to have similar binding affinity to mitoNEET compared to known neuroprotectant, pioglitazone[106]. This fact and the LC-MS/MS technique served useful in a preliminary pharmacokinetic study of NL-1 that is applicable to a human model of drug delivery. Using NL-1 as a starting point, many new compounds are being investigated for protective effects in oxidative environments.

2.13. References

1.   Sarkar S, Chakraborty D, Bhowmik A, Ghosh MK. Cerebral ischemic stroke: Cellular fate and therapeutic opportunities. *Front Biosci - Landmark*. 2019;24(3):435-450. doi:10.2741/4727

2.   Shi H, Liu KJ. Cerebral tissue oxygenation and oxidative brain injury during ischemia and reperfusion. *Front Biosci*. 2007;12(4):1318-1328. doi:10.2741/2150

3.   Meng-Yu Wu, Giou-Teng Yiang, Wan-Ting Liao, Andy Po-Yi Tsai, Yeung-Leung Cheng, Pei-Wen Cheng, Chia-Ying Li C-JL. Current Mechanistic Concepts in Ischemia and Reperfusion Injury. *Cell Physiol Biochem*. 2018;46(4):1650-1667. doi:10.1159/000489241

4.   Nagy Z, Nardai S. Cerebral ischemia/repefusion injury: From bench space to bedside. *Brain Res Bull*. 2017;134:30-37. doi:10.1016/j.brainresbull.2017.06.011

5.   Nagy Z, Goehlert UG, Wolfe LS, Hüttner I. Ca2+ depletion-induced disconnection of tight junctions in isolated rat brain microvessels. *Acta Neuropathol*. 1985;68(1):48-52. doi:10.1007/BF00688955

6.   Liu K, Sun Y, Gu Z, Shi N, Zhang T, Sun X. Mitophagy in ischaemia/reperfusion induced cerebral injury. *Neurochem Res*. 2013;38(7):1295-1300. doi:10.1007/s11064-013-1033-0

7.   Miller AA, Dusting GJ, Roulston CL SC. NADPH-oxidase activity is elevated in penumbral and non-ischemic cerebral arteries following stroke. *Brain Res*. 2006;1111(1):111-116. doi:10.1016/j.brainres.2006.06.082

8. Ma MW, Wang J, Zhang Q, Wang R, Dhandapani KM, Vadlamudi RK BD. NADPH oxidase in brain injury and neurodegenerative disorders. *Mol Neurodegener*. 2017;12(1).

9. Moro MA, Cárdenas A, Hurtado O, Leza JC, Lizasoain I. Role of nitric oxide after brain ischaemia. *Cell Calcium*. 2004;36(3-4):265-275. doi:10.1016/j.ceca.2004.02.011

10. Groves JT. Peroxynitrite: Reactive, invasive and enigmatic. *Curr Opin Chem Biol*. 1999;3(2):226-235. doi:10.1016/S1367-5931(99)80036-2

11. Kuhn DM, Sakowski SA, Sadidi M, Geddes TJ. Nitrotyrosine as a marker for peroxynitrite-induced neurotoxicity: The beginning or the end of the end of dopamine neurons? *J Neurochem*. 2004;89(3):529-536. doi:10.1111/j.1471-4159.2004.02346.x

12. Yemisci M, Gursoy-Ozdemir Y, Vural A, Can A, Topalkara K, Dalkara T. Pericyte contraction induced by oxidative-nitrative stress impairs capillary reflow despite successful opening of an occluded cerebral artery. *Nat Med*. 2009;15(9):1031-1037. doi:10.1038/nm.2022

13. Cai W, Liu H, Zhao J, et al. Pericytes in Brain Injury and Repair After Ischemic Stroke. *Transl Stroke Res*. 2017;8(2):107-121. doi:10.1007/s12975-016-0504-4

14. Lopez-Neblina F, Toledo AH, Toledo-Pereyra LH. Molecular biology of apoptosis in ischemia and reperfusion. *J Investig Surg*. 2005;18(6):335-350. doi:10.1080/08941930500328862

15. Bai J, Lyden PD. Revisiting cerebral postischemic reperfusion injury: New insights in understanding reperfusion failure, hemorrhage, and edema. *Int J Stroke*. 2015;10(2):143152. doi:10.1111/ijs.12434

16. Fujimura M, Morita-Fujimura Y, Noshita N, Sugawara T, Kawase M, Chan PH. The cytosolic antioxidant copper/zinc-superoxide dismutase prevents the early release of mitochondrial cytochrome c in ischemic brain after transient focal cerebral ischemia in mice. *J Neurosci*. 2000;20(8):2817-2824. doi:10.1523/jneurosci.20-08-02817.2000

17. Solenski NJ, DiPierro CG, Trimmer PA, Kwan A-L, and Gregory A. Helms. Ultrastructural Changes of Neuronal Mitochondria After Transient and Permanent Cerebral Ischemia. *Stroke*. 2002;33(3):816-824. doi:10.1161/hs0302.104541

18. Tohru Kobayashi, Satoshi Kuroda, Mitsuhiro Tada, Kiyohiro Houkin, Yoshinobu Iwasaki HA. Calcium-induced mitochondrial swelling and cytochrome c release in the brain: its biochemical characteristics and implication in ischemic neuronal injury. *Brain Res*. 2003;960(1-2):62-70. doi:10.1016/s0006-8993(02)03767-8

19. Li J, Ma X, Yu W, et al. Reperfusion Promotes Mitochondrial Dysfunction following Focal Cerebral Ischemia in Rats. *PLoS One*. 2012;7(9). doi:10.1371/journal.pone.0046498

20. Niizuma K, Endo H, Chan PH. Oxidative stress and mitochondrial dysfunction as determinants of ischemic neuronal death and survival. *J Neurochem*. 2009;109(SUPPL. 1):133-138. doi:10.1111/j.1471-4159.2009.05897.x

21. Ni B, Wu X, Su Y, et al. Transient global forebrain ischemia induces a prolonged expression of the caspase-3 mRNA in rat hippocampal CA1 pyramidal neurons. *J Cereb Blood Flow Metab*. 1998;18(3):248-256. doi:10.1097/00004647-199803000-00003

22. Petrovic-Djergovic D, Goonewardena SN, Pinsky DJ. Inflammatory disequilibrium in stroke. *Circ Res*. 2016;119(1):142-158. doi:10.1161/CIRCRESAHA.116.308022

23. Jin R, Yang G LG. Inflammatory mechanisms in ischemic stroke: role of inflammatory cells. *J Leukoc Biol*. 2010;87(5):779-789. doi:10.1189/jlb.1109766.

24. Mattila OS, Strbian D, Saksi J, et al. Cerebral mast cells mediate blood-brain barrier disruption in acute experimental ischemic stroke through perivascular gelatinase activation. *Stroke*. 2011;42(12):3600-3605. doi:10.1161/STROKEAHA.111.632224

25. Strbian D, Karjalainen-Lindsberg M-L, Tatlisumak T, Lindsberg PJ. Rapid Communication Cerebral mast cells regulate early ischemic brain swelling and neutrophil accumulation. *J Cereb Blood Flow Metab*. 2006;26:605-612. doi:10.1038/sj.jcbfm.9600228

26. Yilmaz A, Fuchs T, Dietel B, et al. Transient decrease in circulating dendritic cell precursors after acute stroke: Potential recruitment into the brain. *Clin Sci*. 2010;118(2):147-157. doi:10.1042/CS20090154

27. Panickar KS, Noremberg MD. Astrocytes in cerebral ischemic injury: Morphological and general considerations. *Glia*. 2005;50(4):287-298. doi:10.1002/glia.20181

28. Yilmaz G, Arumugam T V, Stokes KY, Granger DN. Role of T lymphocytes and interferon-γ in ischemic stroke. Circulation. *Stroke*. 2006;113:2105-2112. doi:10.1161/CIRCULATIONAHA.105.593046

29. Kahle KT, Marc Simard J, Staley KJ, Nahed B V., Jones PS, Sun D. Molecular mechanisms of ischemic cerebral edema: Role of electroneutral ion transport. *Physiology*. 2009;24(4):257-265. doi:10.1152/physiol.00015.2009

30. Zador Z, Stiver S, Wang V, Manley GT. Role of Aquaporin-4 in Cerebral Edema and Stroke. In: *Aquaporins*. Vol 190. Berlin, Heidelberg: Springer Berlin Heidelberg; 2009:159-170. doi:10.1007/978-3-540-79885-9_7

31. Tang G, Yang GY. Aquaporin-4: A potential therapeutic target for cerebral edema. *Int J Mol Sci*. 2016;17(10). doi:10.3390/ijms17101413

32. A L Betz, F Iannotti JTH. Brain edema: a classification based on blood-brain barrier integrity. *Cerebrovasc Brain Metab Rev*. 1989;1(2):133-154.

33. Jha SK. Cerebral edema and its management. *Med J Armed Forces India*. 2003;59(4):326331. doi:10.1016/S0377-1237(03)80147-8

34. Unterberg AW, Stover J, Kress B, Kiening KL. Edema and brain trauma. *Neuroscience*. 2004;129(4):1019-1027. doi:10.1016/j.neuroscience.2004.06.046

35. Sara M. Nehring, Prasanna Tadi ST. Cerebral Edema. In: *Treasure Island (FL): StatPearls Publishing*. ; 2020.

36. Rosenberg GA, Yang Y. Vasogenic edema due to tight junction disruption by matrix metalloproteinases in cerebral ischemia. *Neurosurg Focus*. 2007;22(5). doi:10.3171/foc.2007.22.5.5

37. Raslan A, Bhardwaj A. Medical management of cerebral edema. *Neurosurg Focus*. 2007;22(5):1-12. doi:10.3171/foc.2007.22.5.13

38. Yang GY, Betz AL. Reperfusion-induced injury to the blood-brain barrier after middle cerebral artery occlusion in rats. *Stroke*. 1994;25(8):1658-1664. doi:10.1161/01.STR.25.8.1658

39. Kuroiwa T, Ting P, Martinez H, Klatzo I. The biphasic opening of the blood-brain barrier to proteins following temporary middle cerebral artery occlusion. *Acta Neuropathol*. 1985;68(2):122-129. doi:10.1007/BF00688633

40. Belayev L, Busto R, Zhao W, Ginsberg MD. Quantitative evaluation of blood-brain barrier permeability following middle cerebral artery occlusion in rats. *Brain Res*. 1996;739(1-2):88-96. doi:10.1016/S0006-8993(96)00815-3

41. Nagaraja TN, Karki K, Ewing JR, Croxen RL, Knight RA. Identification of variations in blood-brain barrier opening after cerebral ischemia by dual contrast-enhanced magnetic resonance imaging and T1sat measurements. *Stroke*. 2008;39(2):427-432. doi:10.1161/STROKEAHA.107.496059

42. Simpkins AN, Dias C, Leigh R. Identification of Reversible Disruption of the Human Blood-Brain Barrier Following Acute Ischemia. *Stroke*. 2016;47(9):2405-2408. doi:10.1161/STROKEAHA.116.013805

43. Ewing JR, Knight RA, Nagaraja TN, et al. Patlak plots of Gd-DTPA MRI data yield blood-brain transfer constants concordant with those of14C-sucrose in areas of bloodbrain opening. *Magn Reson Med*. 2003;50(2):283-292. doi:10.1002/mrm.10524

44. Merali Z, Huang K, Mikulis D, Silver F, Kassner A. Evolution of blood-brain-barrier permeability after acute ischemic stroke. Deli MA, ed. *PLoS One*. 2017;12(2):e0171558. doi:10.1371/journal.pone.0171558

45. Ivanidze J, Kesavabhotla K, Kallas ON, et al. Evaluating blood-brain barrier permeability in delayed cerebral infarction after aneurysmal subarachnoid hemorrhage. *AJNR Am J Neuroradiol*. 2015;36(5):850-854. doi:10.3174/ajnr.A4207

46. Raja R, Rosenberg GA, Caprihan A. MRI measurements of Blood-Brain Barrier function in dementia: A review of recent studies. *Neuropharmacology*. 2018;134(Pt B):259-271. doi:10.1016/j.neuropharm.2017.10.034

47. Sarvari S, Moakedi F, Hone E, Simpkins JW, Ren X. Mechanisms in blood-brain barrier opening and metabolism-challenged cerebrovascular ischemia with emphasis on ischemic stroke. *Metab Brain Dis*. 2020;35(6):851-868. doi:10.1007/s11011-020-00573-8

48. Jiang X, Andjelkovic A V., Zhu L, et al. Blood-brain barrier dysfunction and recovery after ischemic stroke. *Prog Neurobiol*. 2018;163-164:144-171. doi:10.1016/j.pneurobio.2017.10.001

49. Yang Y, Rosenberg GA. Blood-brain barrier breakdown in acute and chronic cerebrovascular disease. *Stroke*. 2011;42(11):3323-3328. doi:10.1161/STROKEAHA.110.608257

50. Chen H, Guan B, Chen X, et al. Baicalin Attenuates Blood-Brain Barrier Disruption and Hemorrhagic Transformation and Improves Neurological Outcome in Ischemic Stroke Rats with Delayed t-PA Treatment: Involvement of ONOO−-MMP-9 Pathway. *Transl Stroke Res*. 2018;9(5):515-529. doi:10.1007/s12975-017-0598-3

51. Gidday JM, Gasche YG, Copin JC, et al. Leukocyte-derived matrix metalloproteinase-9 mediates blood-brain barrier breakdown and is proinflammatory after transient focal cerebral ischemia. *Am J Physiol - Hear Circ Physiol*. 2005;289(2 58-2). doi:10.1152/ajpheart.01275.2004

52. Justicia C, Panés J, Solé S, et al. Neutrophil Infiltration Increases Matrix Metalloproteinase-9 in the Ischemic Brain after Occlusion/Reperfusion of the Middle Cerebral Artery in Rats. *J Cereb Blood Flow Metab*. 2003;23(12):1430-1440. doi:10.1097/01.WCB.0000090680.07515.C8

53. da Fonseca ACC, Matias D, Garcia C, et al. The impact of microglial activation on bloodbrain barrier in brain diseases. *Front Cell Neurosci*. 2014;8(November):1-13. doi:10.3389/fncel.2014.00362

54. Jickling GC, Liu D, Stamova B, et al. Hemorrhagic transformation after ischemic stroke in animals and humans. *J Cereb Blood Flow Metab*. 2014;34(2):185-199. doi:10.1038/jcbfm.2013.203

55. Abdullahi W, Tripathi D, Ronaldson PT. Blood-brain barrier dysfunction in ischemic stroke: Targeting tight junctions and transporters for vascular protection. *Am J Physiol - Cell Physiol*. 2018;315(3):C343-C356. doi:10.1152/ajpcell.00095.2018

56. Colca JR, McDonald WG, Waldon DJ, et al. Identification of a novel mitochondrial protein ("mitoNEET") cross-linked specifically by a thiazolidinedione photoprobe. *Am J Physiol - Endocrinol Metab*. 2003;286(2). http://ajpendo.physiology.org/content/286/2/E252.long. Accessed June 10, 2017.

57. Wiley SE, Murphy AN, Ross SA, van der Geer P, Dixon JE. MitoNEET is an ironcontaining outer mitochondrial membrane protein that regulates oxidative capacity. *Proc Natl Acad Sci U S A*. 2007;104(13):5318-5323. doi:10.1073/pnas.0701078104

58. Sandra E. Wiley, Mark L. Paddock ECA, Larry Gross, Peter van der Geer RN, Anne N. Murphy, Patricia A. Jennings and JED. The Outer Mitochondrial Membrane Protein mitoNEET Contains a Novel Redox-active 2Fe-2S Cluster. *J Biol Chem*. 282(33):2374523749. doi:10.1074/jbc.C700107200

59. Timothy F. Tirrell, Mark L. Paddock, Andrea R. Conlan, Eric J. Smoll, Jr. RN, Patricia A. Jennings and JEK. Resonance Raman Studies of the (His)(Cys)3 2Fe-2S Cluster of

MitoNEET: Comparison to the (Cys)4 Mutant and Implications of the Effects of pH on the Labile Metal Center. *Biochemistry2*. 2009;48(22):4747-4752. doi:10.1021/bi900028r

60. Paddock ML, Wiley SE, Axelrod HL, Cohen AE, Roy M, Abresch EC, Capraro D, Murphy AN, Nechushtai R, Dixon JE JP. MitoNEET is a uniquely folded 2Fe–2S outer mitochondrial membrane protein stabilized by pioglitazone. *Proc Natl Acad Sci U S A*. 104(36):14342-14347. doi:10.1073/pnas.0707189104

61. Lin J, Zhou T, Ye K, Wang J. Crystal structure of human mitoNEET reveals distinct groups of iron-sulfur proteins. *Proc Natl Acad Sci U S A*. 2007;104(37):14640-14645. doi:10.1073/pnas.0702426104

62. Xiaowei Hou, Rujuan Liu, Stuart Ross EJS, Haining Zhu and WG. Crystallographic Studies of Human MitoNEET. *J Biol Chem*. 282(46):33242-33246. doi:10.1074/jbc.C700172200

63. Elliott DWB and SJ. Conserved Hydrogen Bonding Networks of MitoNEET Tune Fe-S Cluster Binding and Structural Stability. *Biochemistry*. 52(27):4687-4696. doi:10.1021/bi400540m

64. Asako Kounosu T, Iwasaki, Seiki Baba Y, Hayashi-Iwasaki, Tairo Oshima T, Kumasaka. Crystallization and preliminary X-ray diffraction studies of the prototypal homologue of mitoNEET (Tth-NEET0026) from the extreme thermophile Thermus thermophilus HB8. *Struct Biol Cryst Commun*. 2008;64(12):1146–1148. doi:10.1107/S1744309108035975

65. Conlan AR, Paddock ML, Axelrod HL, et al. The novel 2Fe-2S outer mitochondrial protein mitoNEET displays conformational flexibility in its N-terminal cytoplasmic tethering domain. *Acta Crystallogr Sect F Struct Biol Cryst Commun*. 2009;65(7):554559. doi:10.1107/S1744309109019605

66. Geldenhuys WJ, Long TE, Saralkar P, et al. Crystal structure of the mitochondrial protein mitoNEET bound to a benze-sulfonide ligand. doi:10.1038/s42004-019-0172-x

67. Iwasaki T, Samoilova RI, Kounosu A, Ohmori D DS. Continuous-Wave and Pulsed EPR Characterization of the [2Fe-2S](Cys)3(His)1 Cluster in Rat MitoNEET. *J Am Chem Soc*. 131(38):13659-13667. doi:10.1021/ja903228w.

68. Bak DW, Zuris JA, Paddock ML, Jennings PA ES. Redox characterization of the FeS protein MitoNEET and impact of thiazolidinedione drug binding. *Biochemistry*. 48(43):10193-10195. doi:10.1021/bi9016445

69. Conlan AR, Paddock ML, Homer C, Axelrod HL, Cohen AE, Abresch EC, Zuris JA, Nechushtai R JP. Mutation of the His ligand in mitoNEET stabilizes the 2Fe–2S cluster despite conformational heterogeneity in the ligand environment. *Acta Crystallogr Sect D Biol Crystallogr*. 67(6):516-523. doi:10.1107/S0907444911011577

70. Pesce L, Calandrini V, Marjault HB, Lipper CH, Rossetti G, Mittler R, Jennings PA, Bauer A, Nechushtai R CP. Molecular Dynamics Simulations of the [2Fe-2S] Cluster-Binding Domain of NEET Proteins Reveal Key Molecular Determinants That Induce Their Cluster Transfer/Release. *J Phys Chem B*. 121(47):10648-10656.

doi:10.1021/acs.jpcb.7b10584

71. Ferecatu I, Gonçalves S, Golinelli-Cohen MP, Clémancey M, Martelli A, Riquier S, Guittet E, Latour JM, Puccio H, Drapier JC, Lescop E BC. The Diabetes Drug Target MitoNEET Governs a Novel Trafficking Pathway to Rebuild an Fe-S Cluster into Cytosolic Aconitase/Iron Regulatory Protein 1. *J Biol Chem*. 289(41):28070-28086. doi:10.1074/jbc.M114.548438

72. Marie Bergner, Sebastian Dechert, Serhiy Demeshko, Claudia Kupper JMM, Meyer and F. Model of the MitoNEET [2Fe−2S] Cluster Shows Proton Coupled Electron Transfer. *J Am Chem Soc*. 2017;139(2):701-707. doi:10.1021/jacs.6b09180

73. Sandra E. Wiley, Matthew J. Rardin and JED. Localization and Function of the 2Fe-2S Outer Mitochondrial Membrane Protein mitoNEET. In: *Methods in Enzymology*. ; 2009:233-246. doi:10.1016/S0076-6879(08)04413-3

74. John A. Zuris, Danny A. Halim, Andrea R. Conlan, Edward C. Abresch, Rachel Nechushtai, Mark L. Paddock and PAJ. Engineering the Redox Potential over a Wide Range within a New Class of FeS Proteins. *J Am Chem Soc*. 2010;132(38):13120-13122. doi:10.1021/ja103920k

75. Mons C, Ferecatu I, Riquier S, Lescop E, Bouton C G-CM. Combined Biochemical, Biophysical, and Cellular Methods to Study Fe–S Cluster Transfer and Cytosolic Aconitase Repair by MitoNEET. *Methods Enzymol*. 2017;595:83-106. doi:10.1016/bs.mie.2017.07.010

76. Tan G, Liu D, Pan F, Zhao J, Li T, Ma Y, Shen B LJ. His-87 ligand in mitoNEET is crucial for the transfer of iron sulfur clusters from mitochondria to cytosolic aconitase. *Biochem Biophys Res Commun*. 470(1):226-232. doi:10.1016/j.bbrc.2016.01.040

77. Huynh N, Ou Q, Cox P, Lill R, King-Jones K. Glycogen branching enzyme controls cellular iron homeostasis via Iron Regulatory Protein 1 and mitoNEET. *Nat Commun*. 2019;10(1):5463. doi:10.1038/s41467-019-13237-8

78. Golinelli-Cohen MP, Lescop E, Mons C, Gonçalves S, Clémancey M, Santolini J, Guittet E, Blondin G, Latour JM BC. Redox Control of the Human Iron-Sulfur Repair Protein MitoNEET Activity via Its Iron-Sulfur Cluster. 291(14):7583-7593. doi:10.1074/jbc.M115.711218

79. Francesca Camponeschi, Simone Ciofi-Baffoni and LB. Anamorsin/Ndor1 Complex Reduces [2Fe−2S]-MitoNEET via a Transient Protein−Protein Interaction. *J Am Chem Soc*. 139(28):9479–9482. doi:10.1021/jacs.7b05003

80. Cécile Mons, Thomas Botzanowski, Anton Nikolaev, Petra Hellwig, Sarah Cianférani, Ewen Lescop, Cécile Bouton and M-PG-C. The H2O2-Resistant Fe–S Redox Switch MitoNEET Acts as a pH Sensor To Repair Stress-Damaged Fe–S Protein. *Biochemistry*. 57(38):5616-5628. doi:10.1021/acs.biochem.8b00777

81. Lipper CH, Stofleth JT, Bai F, et al. Redox-dependent gating of VDAC by mitoNEET. *Proc Natl Acad Sci U S A*. 2019;116(40):19924-19929. doi:10.1073/pnas.1908271116

82. Zhou T, Lin J, Feng Y WJ. Binding of Reduced Nicotinamide Adenine Dinucleotide Phosphate Destabilizes the Iron-Sulfur Clusters of Human MitoNEET. *Biochemistry*. 49(44):9604-9612. doi:10.1021/bi101168c

83. Zuris JA, Ali SS, Yeh H, Nguyen TA, Nechushtai R, Paddock ML JP. NADPH Inhibits [2Fe-2S] Cluster Protein Transfer from Diabetes Drug Target MitoNEET to an Apoacceptor Protein. *J Biol Chem*. 287(15):11649-11655. doi:10.1074/jbc.M111.319731

84. Landry AP, Wang Y, Cheng Z, Crochet RB, Lee YH DH. Flavin nucleotides act as electron shuttles mediating reduction of the [2Fe- 2S] clusters in mitochondrial outer membrane protein mitoNEET. *Free Radic Biol Med*. 102:240-247. doi:10.1016/j.freeradbiomed.2016.12.001

85. Wang Y, Landry AP, Ding H. The mitochondrial outer membrane protein mitoNEET is a redox enzyme catalyzing electron transfer from FMNH2 to oxygen or ubiquinone. *J Biol Chem*. May 2017:jbc.M117.789800. doi:10.1074/jbc.M117.789800

86. Li X, Wang Y, Tan G, Lyu J DH. Electron transfer kinetics of the mitochondrial outer membrane protein mitoNEET. *Free Radic Biol Med*. 121:98-104. doi:10.1016/j.freeradbiomed.2018.04.569

87. Vernay A, Marchetti A, Sabra A, Jauslin TN, Rosselin M, Scherer PE, Demaurex N, Orci L CP. MitoNEET-dependent formation of intermitochondrial junctions. *Proc Natl Acad Sci USA*. 114(31):8277-8282. doi:10.1073/pnas.1706643114

88. Landry AP, Ding H. Redox control of human mitochondrial outer membrane protein MitoNEET [2Fe-2S] clusters by biological thiols and hydrogen peroxide. *J Biol Chem*. 2014;289(7):4307-4315. doi:10.1074/jbc.M113.542050

89. Landry AP, Cheng Z DH. Reduction of mitochondrial protein mitoNEET[2Fe–2S] clusters by human glutathione reductase. *Free Radic Biol Med*. 81:119-127. doi:10.1016/j.freeradbiomed.2015.01.017

90. Ola Karmi , Sarah H. Holt , Luhua Song , Sagi Tamir, Yuting Luo, Fang Bai, Ammar Adenwalla, Merav Darash-Yahana, Yang-Sung Sohn, Patricia A. Jennings, Rajeev K. Azad, Jose' N. Onuchic, Faruck Morcos, Rachel Nechushtai RM. Interactions between mitoNEET and NAF-1 in cells. *PLoS One*. 12(4):e0175796. doi:10.1371/journal.pone.0175796

91. Skylar D. King, Chipo F. Gray, Luhua Song, Rachel Nechushtai, Tina L. Gumienny RM and PAP. The cisd gene family regulates physiological germline apoptosis through ced-13 and the canonical cell death pathway in Caenorhabditis elegans. *Cell Death Differ*. 26(1):162-178. doi:10.1038/s41418-018-0108-5.

92. Sauerbeck A, Gao J, Readnower R, et al. Pioglitazone attenuates mitochondrial dysfunction, cognitive impairment, cortical tissue loss, and inflammation following traumatic brain injury. *Exp Neurol*. 2011;227(1):128-135. doi:10.1016/j.expneurol.2010.10.003

93. Zatta P, Lucchini R, van Rensburg SJ, Taylor A. The role of metals in neurodegenerative processes: aluminum, manganese, and zinc. *Brain Res Bull*. 2003;62(1):15-28. doi:10.1016/S0361-9230(03)00182-5

94. Duce JA, Tsatsanis A, Cater MA, et al. Iron-Export Ferroxidase Activity of β-Amyloid Precursor Protein Is Inhibited by Zinc in Alzheimer's Disease. *Cell*. 2010;142(6):857-867. doi:10.1016/j.cell.2010.08.014

95. Shabanzadeh AP-., Shuaib A, Yang T, Salam A, Wang CX. Effect of zinc in ischemic brain injury in an embolic model of stroke in rats. *Neurosci Lett*. 2004;356(1):69-71. doi:10.1016/J.NEULET.2003.10.073

96. Pagani MA, Casamayor A, Serrano R, Atrian S, Ariño J. Disruption of iron homeostasis in Saccharomyces cerevisiae by high zinc levels: a genome-wide study. *Mol Microbiol*. 2007;65(2):521-537. doi:10.1111/j.1365-2958.2007.05807.x

97. He Q-Q, Xiong L-L, Liu F, et al. MicroRNA-127 targeting of mitoNEET inhibits neurite outgrowth, induces cell apoptosis and contributes to physiological dysfunction after spinal cord transection. *Sci Rep*. 2016;6:35205. doi:10.1038/srep35205

98. Geldenhuys WJ, Benkovic SA, Lin L, et al. MitoNEET (CISD1) Knockout Mice Show Signs of Striatal Mitochondrial Dysfunction and a Parkinson's Disease Phenotype. *ACS Chem Neurosci*. 2017;8(12):2759-2765. doi:10.1021/acschemneuro.7b00287

99. Shi, Guangyao; Cui, Lei; Chen, Rui; Liang, Shaodong; Wang, Chunlei; Wu P. TT01001 attenuates oxidative stress and neuronal apoptosis by preventing mitoNEET-mediated mitochondrial dysfunction after subarachnoid hemorrhage in rats. *Neuroreport*. 2020;31(11):845-850. doi:10.1097/WNR.0000000000001492

100. Stauch KL, Villeneuve LM, Totusek S, Lamberty B, Ciborowski P FH. Quantitative Proteomics of Presynaptic Mitochondria Reveal an Overexpression and Biological Relevance of Neuronal MitoNEET in Postnatal Brain Development. *Dev Neurobiol*. doi:10.1002/dneu.22684

101. Geldenhuys WJ, Funk MO, Barnes KF, Carroll RT. Structure-based design of a thiazolidinedione which targets the mitochondrial protein mitoNEET. *Bioorganic Med Chem Lett*. 2010;20(3):819-823. doi:10.1016/j.bmcl.2009.12.088

102. Logan SJ, Yin L, Geldenhuys WJ, et al. Novel thiazolidinedione mitoNEET ligand-1 acutely improves cardiac stem cell survival under oxidative stress. *Basic Res Cardiol*. 2015;110(2):19. doi:10.1007/s00395-015-0471-z

103. Geldenhuys WJ, Nair RR, Piktel D, Martin KH, Gibson LF, Byrd RC. The mitoNEET ligand NL-1 mediates anti-leukemic activity in drug resistant B-cell acute lymphoblastic leukemia. doi:10.1124/jpet.118.255984

104. Saralkar P, Geldenhuys WJ. Screening for anticancer properties of thiazolidinedione compounds in a galactose media metastatic breast cancer cell model. *Med Chem Res*. 2019;28(12):2165-2170. doi:10.1007/s00044-019-02444-z

105. Pedada KK, Zhou X, Jogiraju H, et al. A quantitative LC?MS/MS method for determination of thiazolidinedione mitoNEET ligand NL-1 in mouse serum suitable for pharmacokinetic studies. *J Chromatogr B*. 2014;945-946:141-146. doi:10.1016/j.jchromb.2013.11.048

106. Geldenhuys WJ, Funk MO, Awale PS, Lin L, Carroll RT. A novel binding assay identifies high affinity ligands to the rosiglitazone binding site of mitoNEET. *Bioorg Med Chem Lett*. 2011;21(18):5498-5501. doi:10.1016/j.bmcl.2011.06.111
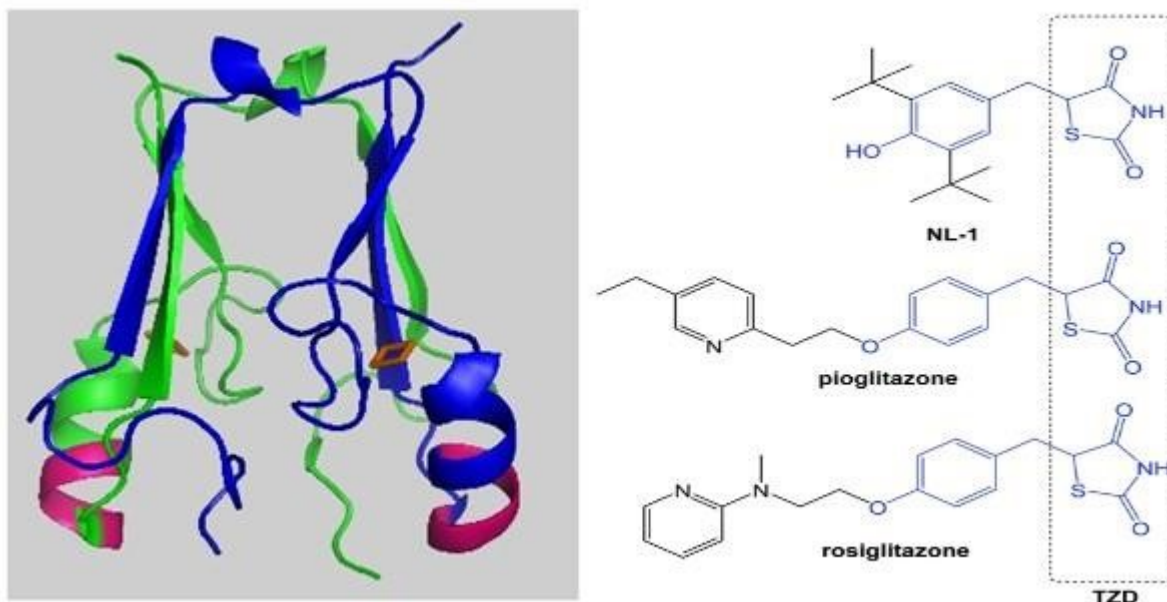
Figure 2.1: Structures of mitoNEET and NL-1: The homodimeric structure of mitoNEET (left) with the two iron-sulfur clusters (orange). Structure of the TZD analogs pioglitazone and NL-1.
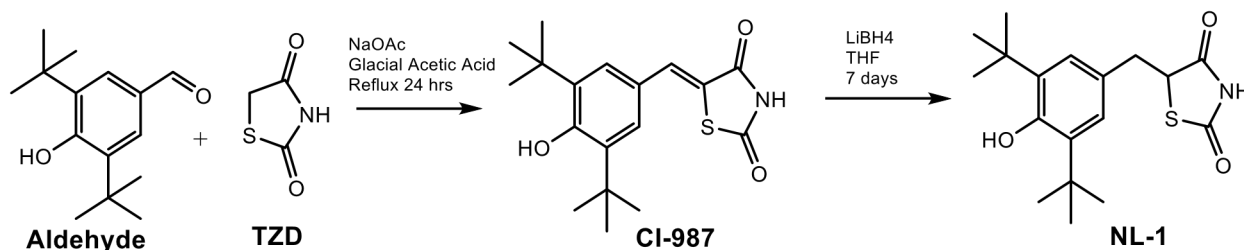
Figure 2.2: Synthesis of NL-1 using Knoevenagel condensation reaction

CHAPTER 3

Evaluation of the mitochondrial mitoNEET ligand NL-1 as a protective agent in ischemia

Chapter included in the following manuscript:

The mitochondrial mitoNEET ligand NL-1 is protective in a murine model of transient cerebral ischemic stroke

Pushkar Saralkar, Alexander Mdzinarishvili, Tasneem Arsiwala, Yoon-Kwang Lee, Patrick G. Sullivan, Mark V. Pinti, John M. Hollander, Eric E. Kelley, Xuefang Ren, Heng Hu, James Simpkins, Candice Brown, Lori E. Hazlehurst, Jason D. Huber and Werner J. Geldenhuys

3.1. Introduction

Ischemic stroke presents significant challenges to human health in United States, and the world. About 800,000 Americans suffer from stroke each year, which results in 150,000 deaths. Stroke is the fifth leading cause of death, and the leading cause of permanent disability in the nation[1]. The consequences of stroke, i.e. lifelong disabilities due to irreversible death of neurons go unmitigated due to a lack of efficient neuroprotective strategies in humans[2,3]. Stroke occurs due to an occlusion in the vasculature supplying oxygen and nutrients to the brain, causing an energy crisis in that region which progresses into tissue death. The part of the brain suffering irreversible damage is called the ischemic core, whereas the area surrounding the core is called the penumbra. The stroke penumbra consists of the tissue in duress that could be salvaged with a time dependent intervention[4]. The current treatment strategy for stroke is aimed at removing the occlusion to blood flow, and restoring the blood supply to the ischemic penumbra in a timely manner. To date, the only therapeutic used to restore blood supply is the thrombolytic agent tissue plasminogen activator (t-PA)[3,5]. However, when the blood supply is restored and the ischemic tissue is reperfused, secondary tissue damage is observed, which is generally referred to as ischemiareperfusion (IR) injury[6]. The t-PA therapy does not address the local and systemic neurodegeneration associated with the IR injury. Neurodegeneration occurs due to a complex interplay between factors such as oxidative stress, apoptosis, inflammatory mediators and excitotoxicity[7]. A prominent reason for the rapid and significant mortality after stroke is the onset of edema in the brain[8,9]. A key player in the IR injury is the mitochondrion, an organelle central to cellular energetics, apoptosis and ROS generation. In the literature there have been over 1000 candidate compounds tested with the hopes of eventual clinical use[10]. However, not a single compound has been successfully translated into a

viable clinically useful drug. Therefore, an urgent need exists to develop compounds which can mitigate the damage from IR injury in brain stroke pathology.

MitoNEET (gene: *CISD1*) is a recently discovered novel mitochondrial protein located on the outer surface of mitochondria. Colca et al. described the identification of mitoNEET as a mitochondrial target for the anti-diabetic drug pioglitazone[11]. By using a photo-affinity probe, they identified this ~17 kDa protein which carries a CDGSH domain. The mitoNEET was found to belong to a group of zinc-finger proteins, although it contains two iron-sulfur clusters [2Fe-2S], instead of zinc[12]. This protein is also present in several other species, including thermophiles[13] as well as in plants[14]. This suggests that mitoNEET belongs to an ancient family of proteins with an as yet unknown function[15]. There are numerous presumed functions for mitoNEET in normal physiology and pathophysiology, particularly in the central nervous system11. For example, it was shown that downregulation of mitoNEET by microRNA-127 leads to inhibition of neurite outgrowth and can induce neuronal cell apoptosis[16]. Recently, also it was shown that mitoNEET ligands such as TT01001 may have neuroprotective activity in stroke[17] which prompted the current study using the mitoNEET ligand NL-1.

Our overarching goal is to develop mitoNEET ligands which can be used as clinical leads[18], and NL-1 represents a promising small molecule mitoNEET ligand which was derived from the parent compound pioglitazone (Figure 1). We have previously shown that the mitoNEET ligand NL-1 is neuroprotective in Parkinson's disease model[19], NL-1 can protect stem cells from reperfusioninjury before being transplanted[20] and mitigates tissue loss post traumatic brain injury (TBI)[21]. These promising reports led us to explore the effect of NL-1 on mitochondrial function in cells of the central nervous system. The work presented in this chapter investigates the role of

NL-1 in mechanisms that improve cell survival and thus lays the foundational premise for its possible use as a stroke therapeutic.

3.2. Materials and Methods

Materials

All reagents were purchased from Sigma-Aldrich (St. Louis, MO) unless otherwise noted. NL-1 was prepared as described previously[22].

Methods

Experimental animals

All mice were housed in the vivarium facilities, and all experiments were done in accordance with the West Virginia University Institutional Animal Care and Use Committees, and according to the Guide for the Care and Use of Laboratory Animals as adopted and promulgated by the U.S. National Institutes of Health. Male C57BL/6J mice (3-4 months) were used for the glucose tolerance testing. Each group of mice were randomly assigned to each treatment group, with number of animals 4-5 in each group.

PPAR-g binding test

PPAR-□ activation was determined using the IndigoBiosciencs PPAR-□ activity kit. The cells containing a PPAR-g luciferase construct were reconstituted in the cell recovery medium and 100 µL of the reconstituted cell suspension was seeded into white 96 well plate. The plated cells were treated with the positive control rosiglitazone (4 □M) and the test compound NL-1 (10 □M). The plate was transferred to an incubator at 37°C for 24 hours. After 24 hours, the cell media was aspirated and 100 µL of luciferase detection reagent was added to each well, allowing the plate to

rest at room temperature for at least five minutes. The luciferase activity was measured by quantifying the luminescence on a plate reader.

Glucose tolerance test

Glucose tolerance test (GTT) was performed in C57BL/6J mice by intraperitoneal injection of glucose (1.5 g/kg of bodyweight) after overnight fasting. The mice were injected with either DMSO as the vehicle control or 10 mg/kg NL-1, IP. Blood was collected from tail vein at the time points of 30, 60, 90 and 120 minutes following glucose injection. The glucose levels were measured using a OneTouch glucometer (LifeScan, Milipitas, CA).

Kinase Panel

NL-1 was screened against a panel of kinases from Reaction Biology at 10 µM (www.reactionbiology.com). The panel included a set of 349 typical kinases, while 20 atypical kinases were tested for inhibition. NL-1 was tested at 10 µM in DMSO, and the concentration of ATP used for the kinase screen was 10 µM ATP. Staurosporine was used as positive control to show expected inhibition of kinase assay.

Cell culture

N2A cells, a mouse neuroblastoma cell line, were obtained from ATCC (Manassas, VA). N2a cells were used to determine the effect of NL-1 on cellular physiology in a neuronal cell line. The cells were cultured in DMEM medium supplemented with 10% fetal bovine serum and 1% penicillin/streptomycin (all from Thermo-Fisher Scientific, Pittsburgh PA), and cultured at 37°C and 5% CO_2. For the oxygen-glucose deprivation study, we followed our previously published methods.

Cell oxidative stress and mitochondrial membrane potential

To evaluate the effect of oxidative stress, N2A cells were treated with NL-1 in a dose-dependent manner spanning a concentration range of 8 log units for 1 hour, followed by addition of Amplex Red (Invitrogen) to all wells of the plate, and fluorescence recorded using a BioTek Cytation 3 (Winooski, VT) plate reader (540/590 Ex/Em) 25 minutes later.

Calcium flux assay

Calcium movement in N2A cells were determined using the Enzo FLUOFORTE calcium assay kit, according to the manufactures instructions. Cells were prepared the day before and plated in black 96-well plates at 10000 cells per well. The following day, the culture medium was removed and the cells were treated with the non-fluorescent FLUOFORTE Dye-loading solution and incubated for 45 min at 37ºC after which the media was changed to HBSS buffer with calcium and no phenol red. The cells were treated with DMSO as a control and NL-1 at 10 ☐M. The effect on calcium movement was expressed as relative fluorescence measured on a BioTek Synergy 4 plate reader with Ex: 485 and Em: 528 at a kinetic setting. As control, calcium influx was stimulated by depolarizing the cells with the addition of 50 mM KCl in HBSS[23].

Electron Transport Chain Complex Activities

Electron transport chain (ETC) complexes I, IV, activities were measured spectrophotometrically as previously described[24]. Briefly, brain was resected from mice. Mitochondria were isolated from organs using BioVision Mammalian Mitochondria Isolation Kit for Tissue & Cultured Cells (Catalog #: K288), resuspended in 1 mL KME buffer each, and stored at -80°C. Complex I (NADH dehydrogenase) activity was determined by measuring NADH oxidation at 340nm. Complex IV

(cytochrome c oxidase) activity was evaluated by measuring the oxidation of cytochrome c at 550 nm. Each treatment group was comprised of 8 replicate wells in a 96-well plate. Bradford assay was used to measure protein concentration in isolated mitochondria from brain and liver that was used when performing calculations to obtain measurements expressed as nanomoles substrate converted/min/mg of protein. The mean measurement of each treatment group was compared with the mean of the control group (DMSO-only) with a One-Way ANOVA using GraphPad Prism 8 software program following the exclusion of outliers as determined by ROUT (Q = 1%) outlier method.

Effect of NL-1 on mitochondrial membrane potential

The effect of NL-1 on mitochondrial membrane potential was assessed using previously published method[25]. Briefly, N2A cells were seeded into black 96 well plates. The next day, this was followed by the addition of ursodeoxycholic acid (500 nM) as a positive control, and NL-1 at 10 μM for 30 minutes, followed by the addition of TMRM (10 nM final concentration) for an additional 10 minutes. Brilliant Black (1 mg/ml stock) was added the plates to quench background fluorescence. The plate was read using a BioTek Cytation 3 plate reader at 540 nm excitation and 590 nm emission wavelengths.

Effect of NL-1 on lipid peroxidation

The effect of NL-1 on lipid peroxidation was determined using the TBARS assay quantifying of thiobarbituric acid derivatives (TBARS). Briefly, N2A cells were seeded in 6 well plates, at 500,000 cells per well, and were treated with NL-1 (10 ☐M) and hydrogen peroxide H_2O_2 (100 ☐M) for 24 hours. Cells were lysed with 200 ☐L RIPA buffer and placed in 1.5 ml centrifuge tubes.

The lysates were then treated with 200 µL of 10% trichloroacetic acid for 15 minutes on ice. After centrifugation at 2000 x g, the supernatant was mixed 1:1 with 0.67% w/v thiobarbituric acid and boiled for 10 min. Absorbance was measured at 532 nm using a BioTek multimodal plate reader.

Effect of NL-1 on cellular respiration

The Seahorse assay using the Seahorse XF96 (Agilent Technologies, Santa Clara, CA) was used to assess the impact of NL-1 treatment on cellular respiration and glycolysis. N2a cells were seeded into collagen-coated Seahorse 96-well XF Cell culture microplate at a density of 20000 cells per well. Cells reached confluence after 24 hours and were then subjected to treatment with vehicle control or 10 µM NL-1 for either 3 or 24 hours. The Seahorse XF96 measured oxygen consumption rate (OCR) under different conditions using sequential addition of oligomycin, carbonyl cyanide p-trifluoromethoxyphenylhydrazone (FCCP), antimycin A and rotenone. The assay provided information about the parameters of mitochondrial respiration such as basal respiration, ATPlinked respiration, proton link, maximal respiratory capacity, spare respiratory capacity and nonmitochondrial respiration. The second measurement performed by Seahorse XF96 was that of the extracellular acidification rate (ECAR), which is a measure of cellular glycolysis. The Seahorse XF96 measured ECAR under different conditions using sequential addition of glucose, oligomycin and 2-deoxyglucose. The assay provided information about the parameters such as glycolysis, glycolytic capacity, glycolytic reserve and non-glycolytic acidification.

Oxygen glucose deprivation and reperfusion (OGDR)

An *in vitro* cerebral ischemia and reperfusion model was employed by exposing the cells to oxygen and glucose deprivation (OGD). Cell culture medium was replaced with the glucose deficient

Hank's Balanced Salt Solution (HBSS), containing 10% FBS and transferred to the BioSpherix X3 Xvivo System hypoxia chamber, with 0.1-0.2% oxygen, 5% carbon dioxide. The temperature of hypoxia chamber was maintained at 37°C. The cells were incubated in hypoxia chamber for 3 hours. After the desired period of hypoxia, the glucose-free medium was replaced with normal cell growth medium and cells were incubated in normal growth environment for 24 hours, mimicking the reperfusion following cerebral ischemia.

Effect of NL-1 on hydrogen peroxide generation following OGDR

The *in vitro* efficacy of NL-1 in reducing generation of ROS was studied using Amplex Red assay (Thermo Scientific). N2a cells were plated in a black 96-well plate at a density of 10,000 cells per well. After 24 hours, cells were subjected to OGD. The cells were treated with NL-1 drug during the period of recovery. After the 24-hour recovery, 50 µL of Amplex Red working reagent was added to each well and allowed to react in dark at room temperature for 30 minutes. The amount of hydrogen peroxide in each well was measured by fluorimetry using the BioTek Synergy H1 plate reader (BioTek Instruments, Winooski, VT), at an excitation and emission wavelength of 530 nm and 590 nm, respectively. The data of each plate were normalized for the control wells of that plate, and then compared with other plate replicates.

Statistical analysis

Data were analyzed using GraphPad Prism 6.0 (GraphPad Software, La Jolla, CA). Differences between two or more groups were assessed using Student's t-test and one-way ANOVA, respectively. Data are expressed as mean ± standard error of the mean (SEM). Values of $P < 0.05$ were considered statistically significant in all experiments.

3.3. Results

PPAR-γ binding analysis of NL-1

Figure 3.1 shows the results of luminescence intensities for vehicle, the positive control rosiglitazone and the test compound NL-1. The luminescence intensity of rosiglitazone was found to be significantly higher than that of the vehicle and NL-1. The luminescence intensity for vehicle and NL-1 were comparable, and no statistically significant difference was seen between the two. These results indicate that NL-1 (10 µM) did not activate PPAR-□ at the dose tested, as compared to the positive control compound rosiglitazone (4 µM), which was able to activate PPAR-□ as expected.

Effect of NL-1 on blood glucose levels

The ability of NL-1 to affect blood glucose levels was tested using an intraperitoneal glucose tolerance test. **Figure 3.2** shows a glucose concentration (mg/dL) versus time plot for vehicle and NL-1 treated mice. The near overlay of the two plots showed that NL-1 did not have a significant effect on altering blood glucose levels when dosed at 10 mg/kg. The AUC values for vehicle and NL-1 treated groups were found to be 43860 ± 2155 mg/dL.min and 44120 ± 2820 mg/dL.min, respectively.

NL-1 effect on kinases

To test the kinase inhibition of NL-1, we used a kinase panel consisting of wild type and atypical kinases. The Reaction Biology panel used a radiometric assay which directly measures kinase catalytic activity toward a specific substrate[26]. NL-1 did not appreciably inhibit kinases out of a panel of 349 typical and 20 atypical kinases. Amongst the typical kinases, the results indicate inhibition of the WNK family of kinases. These include WNK1 (76.44% of control), WNK2

(66.89% of control) and WNK3 (54.75% of control), as shown in **Figure 3.3(A)**. The results for 20 atypical kinases are expressed as the percent inhibition of control in **Figure 3.3(B)**. Among the atypical kinases, inhibition was observed for PDK2/PDHK2 (65.5% of control) and PDK3/PDHK3 (73.8% of control).

Calcium flux assay

The fluorescence intensity was measured as a function of calcium mobilization or flux for untreated cells and cells treated with 10 μM NL-1, using the Enzo FLOUFORTE calcium assay kit. **Figure 3.4(A)** shows that the kinetic measurements performed over a period of 25 minutes indicated no significant difference between the relative fluorescence intensities for control and NL-1 treated cells, indicating that the baseline calcium uptake was unaffected by NL-1 treatment. Similar effect was seen on cells that were stimulated by addition of 50 mM KCL **(Figure 3.4B)**, wherein NL-1 did not show significant effect on calcium flux at the dose tested.

Effect of NL-1 on electron transport chain complexes

We evaluated the effect of NL-1 treatment on mitochondrial function. NL-1 interactions with the components of electron transport chain such as complex I (NADH dehydrogenase) and complex IV (cytochrome c oxidase) were studied my measuring the concentrations of NADH and cytochrome c, which are the substrates of these enzymes. At 10 ☐M, NL-1 was found to significantly increase Complex I **(Figure 3.5A)** function by about 33% of the DMSO control. At the same concentration, NL-1 had no significant effect on the complex IV activity **(Figure 3.5B)**.

Effect of NL-1 on mitochondrial membrane potential

Mitochondrial membrane potential was measured using the TMRM assay. TMRM (tetramethyl rhodamine methyl ester) is a lipophilic cationic dye that is accumulated by the mitochondria in

proportion to the membrane potential. It exhibits a red shift in fluorescence spectra upon accumulation in the mitochondrial membrane due to a quenching in the fluorescence intensity[27]. Ursodeoxycholic acid at 500 nM was used as a positive control. **Figure 3.6** shows that the fluorescence intensities of ursodeoxycholic acid and NL-1 were found to be significantly higher than that of the vehicle treated cells. Thus, NL-1 was found to improve the mitochondrial membrane potential at a concentration of 10 μM.

Effect of NL-1 on lipid peroxidation

The thiobarbituric acid reactive substances (TBARS) assay was used to determine the ability of NL-1 to reduce lipid peroxidation. The lipid peroxidation products react with thiobarbituric acid upon heating to yield a pink colored product that can be quantified using colorimetry[28]. N2A cells were treated with H_2O_2 to induce lipid peroxidation, for a period of 24 hours. **Figure 3.7** describes the absorbance intensities for TBARS generated, which is used as index for lipid peroxidation, for the four groups: control, H_2O_2 alone, H_2O_2 and NL-1, and NL-1 alone. Cells treated with H_2O_2 and NL-1 (10 μM) significantly reduced the presence of the TBARS as compared to H_2O_2 alone.

Effect of NL-1 on mitochondrial respiration

The impact of NL-1 on mitochondrial respiration was studied using the Seahorse XF96 assay. The data were obtained for mitochondrial respiration which is expressed as the OCR plotted as a function of time and sequential addition of drugs that modulate respiration **(Figure 3.8A and 3.8C)**. The OCR for different parameters of mitochondrial respiration obtained was plotted as a comparison between DMSO control and 10 μM NL-1 **(Figure 3.8B and 3.8D)**. For the acute treatment period of 3 hours, NL-1 was found to significantly improve the maximal respiration and spare respiratory capacity of N2a cells **(Figure 3.8B)**. For a prolonged drug exposure of 24 hours,

NL-1 treatment also significantly improved the cellular basal respiration along with the maximal respiration and spare respiratory capacity **(Figure 3.8D)**. Similarly, the ECAR was plotted as a function of time and sequential addition of drugs that modulate glycolysis **(Figure 3.9A and 3.9C)**. The ECAR for glycolytic parameters obtained was plotted as a comparison between DMSO control and 10 μM NL-1 **(Figure 3.9B and 3.9D)**. NL-1 acute treatment (3 hours) had no significant impact on the glycolysis in N2a cells, while prolonged exposure of 24 hours improved the cellular glycolytic capacity.

Effect of NL-1 on hydrogen peroxide generation following OGDR

The efficacy of NL-1 in reducing peroxide generation was studied by subjecting N2a cells to OGD conditions for a period of 3 hours, and a reperfusion period of 24 hours **(Figure 3.10)**. The hydrogen peroxide produced was measured using the Amplex Red assay, and each treatment was compared to control. It was found that NL-1 had a significant effect in reducing the peroxide produced at a dose of 10 and 30 μM, for an OGD period of 3 hours.

3.4. Discussion

The aim of this study was to perform preliminary investigation into the viability of the mitoNEET ligand NL-1 as a possible therapeutic for ischemia and reperfusion injury. The protein mitoNEET is a located on mitochondrial and has been suggested to regulate the bioenergetics of mitochondria[29]. Here we evaluated the pharmacological properties of NL-1, a mitoNEET ligand synthesized by our group[22], on its ability to interact with the cellular mitochondrial system, and we found that NL-1 can be used as a potential neuroprotective agent for mitigating the pathology of cerebral ischemia and reperfusion injury[18,30].

MitoNEET belongs to the iron-sulfur protein family (gene: *cisd*), and contains 2Fe-2S clusters, which have been reported to be redox active[31]. Low pH conditions, may lead to the cluster ejection from the protein contributing to ferroptosis downstream. The natural endogenous ligand of mitoNEET remains to be elucidated, but some studies have indicated that it may play a role in glutathione mediated redox reactions[32–34], as well as interacting with related metabolic systems including adiponectin[35] and GDH[36]. MitoNEET was first identified from the binding of pioglitazone, a type II diabetic glitazone[11]. Certain actions of pioglitazone such as lowering of lipid levels were independent of its known target, the PPARγ receptor. Investigation into its off-target actions led to the discovery of the mitochondrial protein mitoNEET. Since pioglitazone has been evaluated by others in brain related injuries, including reperfusion injury[21], stroke[37,38] and traumatic brain injury (TBI), we were interested in using mitoNEET as a target to rescue cells following ischemia and reperfusion injury by mitigating the effect of mediators of cell death following stroke such as ROS and inflammatory markers. However, using a known glitazone drug such as pioglitazone or rosiglitazone would not have been a rational approach for stroke therapy, as the actions of these drugs on PPARγ receptor would lead to unwanted anti-diabetic effect. With this premise, our group previously developed a mitoNEET ligand, NL-1, with conserved the thiazolidinedione pharmacophore[22]. We aimed to use NL-1 to probe the biochemistry and physiology of mitoNEET. We were interested in evaluating NL-1 for similar class profiling as pioglitazone.

The first important step toward establishing NL-1 as a stroke therapeutic was to show that the molecule was bereft of any PPARγ anti-diabetic effects seen from the glitazone drugs. To this effect, we resorted to both, *in vitro* and *in vivo* testing. The *in vitro* assay was performed using a

PPARγ binding kit which has been widely used to test for PPARγ agonists and antagonists[39–41]. The kit contained proprietary cells transfected with a PPARγ-luciferase construct, which comprises of a luciferase reporter gene functionally linked to a PPARγ responsive promoter. The luminescence intensity of the luciferin substrate is directly proportional to the analyte binding to the PPARγ receptor. The significantly higher luminescence intensity for the positive control rosiglitazone compared to NL-1 and vehicle control helped establish that NL-1 was not a PPARγ ligand. We confirmed that NL-1 did not have an anti-diabetic effect using an *in vivo* glucose tolerance test in mice. Intraperitoneal glucose tolerance test is widely utilized to determine the ability of test compounds to lower blood glucose levels[42,43]. The mice used for this study were fasted overnight, which initiates a catabolic state in mice as they food consumption is primarily nocturnal[44]. The concentration-time curves for both, vehicle and NL-1 treated mice nearly overlapped. The similar AUC values for both groups indicated that NL-1 has no impact on lowering of blood glucose levels. These results for NL-1 are in contrast to the published effects of pioglitazone, a PPAR-□ agonist, which reduced serum glucose levels[45].

Protein kinases are a vital category of enzymes as they play a central role in a host of cell signaling pathways. They array of kinases present can serve as targets for different small molecules, which could elicit unwanted effects. The affinity of NL-1 for kinases has been untested and we intended to check for inhibition of kinases by NL-1. The high throughput kinase panel used included members of all major human protein kinase families[26]. Staurosporine is a general kinase inhibitor that is widely used as the positive control for a kinase panel[46,47]. The only kinase family amongst the typical kinases inhibited by NL-1 was the WNK kinase family, particularly WNK3. WNK kinases or With-No-Lysine kinases play an important role in body fluid and ion homeostasis and regulates blood pressure[48,49]. An inhibitor of WNK kinase family, WNK463, was shown to

lower mean arterial pressure, and increase urinary excretion of sodium and potassium[50]. It has been recently reported that WNK3 is upregulated upon onset of intracerebral hemorrhage which in turn deteriorates brain injury via the WNK3/SPAK/NKCC1 pathway[51]. WNK3 knockout in mouse and rat models exhibit significantly reduced infarct volumes, cerebral edema, axonal demyelination, BBB damage and improved neurocognitive behavior following an ischemic stroke[51–53]. Of note is that fact that NL-1 was used at a single concentration of 10 μM, which is a high concentration for kinase inhibition. A more detailed investigation at lower concentrations of NL-1 is necessary to determine its effective inhibitory actions on WNKs and PDKs. Nonetheless, a possible inhibition of WNK3 by NL-1 could contribute to improved outcomes after stroke, and presents a promising mitoNEET-independent axis that warrants further investigation.

Calcium homeostasis plays an important role in neurodegeneration following ischemia and reperfusion injury. Accumulation of intracellular calcium activates the mediators of apoptosis and necrosis. In mitochondria, excess calcium leads to swelling and a loss of membrane potential which increases the permeability of mitochondrial membranes, promoting cytochrome c release[54,55]. It could also lead to loosening of BBB tight junctions, leading to increased permeability[56]. Considering the importance of intracellular calcium in regulation of cell survival after stroke, we performed the calcium flux assay to determine if NL-1 itself affected the calcium levels in the cells. The FLUOFORTE assay kit by Enzo Life Sciences has been used to quantify the intracellular calcium mobilization[57]. The assay utilizes a cell permeable fluorogenic calcium binding dye, which upon hydrolyzed by intracellular esterases, gets converted to a cell impermeable negatively charged form. The dye has a calcium-binding moiety which self-quenches the fluorescence of the dye in absence of calcium. This quenching is relieved by binding of calcium, and thus, the fluorescence signal is directly proportional to the amount of intracellular

calcium. KCl was used to increase the extracellular potassium ion concentrations, which in turn increases the influx of calcium ions through the voltage gated calcium channels[23,58]. This study shows that NL-1 neither alters the intracellular calcium concentrations, nor does it prevent the influx of calcium ions when the cells are depolarized with KCl. Thus, NL-1 does not affect the calcium homeostasis *in vitro*.

Next, we decided to focus on the effect of NL-1 on mitochondrial bioenergetics, since the drug target mitoNEET is a mitochondrial enzyme. We examined the electron transport chain complex I and IV activities to see how NL-1 affected cellular respiration. Complex 1 or NADH dehydrogenase activity was measured by spectrophotometry, which involves catalytic oxidation of NADH to NAD+ with subsequent reduction of cytochrome c. Complex I activity has been shown to be decreased following ischemia and is not restored upon reperfusion[59,60]. Improvement in complex I activity contributed to a cerebral-protective effect in a mouse stroke model[60–62], while an impairment in complex I activity exacerbates stroke[63]. Thus, improvement in complex I activity with NL-1 treatment bodes well for cell survival after ischemia. While ischemia is the primary cause of hampered complex I activity, complex IV activity is mainly inhibited by a period of prolonged reperfusion[64]. NL-1 caused no significant change in the complex IV activity. The results possibly suggest that the protective actions of NL-1 on the respiratory could be predominantly seen during the ischemic phase.

The mitochondrial membrane potential is the electrochemical gradient across the mitochondrial inner membrane that is the driving force for the ATP generation process. In ischemia and reperfusion injury, oxidative stress and calcium ion build-up can lead to a loss of membrane potential which accelerates cellular apoptosis. We tried to determine if NL-1 had an effect in altering the mitochondrial membrane potential using TMRM, a commonly used fluorimetric

assay[65–67]. TMRM can be used to measure mitochondrial potential in both, live cells as well as isolated mitochondria. Its advantages include that it readily equilibrates in the mitochondria, shows little membrane potential independent binding, does not inhibit the electron transport chain and has low toxicity to the cells[65,67]. Ursodeoxycholic acid has been reported to improve mitochondrial membrane potential, and hence was used as a positive control. The improvement in mitochondrial membrane potential by NL-1 was comparable to ursodeoxycholic acid. Thus NL-1 could have a positive impact on the membrane potential and could provide an impetus to ATP production[68].

The mitoNEET has several lysine residues in its structure, and these lysine residues seem to be susceptible to modification by the oxidative stress by-product of lipid peroxidation, 4hydoxynonenoal (4-HNE). Proteomics studies indicated that LYS55 is modified by 4-HNE, via an aldehyde covalent bond[69]. Since we show that NL-1 reduces lipid peroxidation, we theorize that NL-1 might be augmenting in part, the modification of this LYS55. Lipid peroxidation is a consequence of oxidative stress and elevated levels of TBARS due to lipid peroxidation have been reported in rats models as well as patients with ischemic stroke[70,71]. In a clinical trial for acute ischemic stroke, glycine has been found to lower the levels of TBARS in CSF; one of the reasons for its neuroprotective actions[72]. Although the effect observed was modest, the potential lowering of TBARS by NL-1 could benefit in the mitigation of stroke pathology.

The Seahorse XF96 instrument effectively measures the two important components of ATP production, glycolysis and mitochondrial respiration, within a 200 μm area in the vicinity of the cells. The sensor sleeves that cover each well of a 96-well plate consists of two fluorophores, one quenched by oxygen measuring the mitochondrial respiration and the second one that senses protons and measures glycolysis[73,74]. The instrument has means to sequentially add compounds

that modulate respiration and glycolysis. The instrument first measures the baseline respiration in cells pre-treated with NL-1. Following the establishment of a baseline, complex V inhibitor oligomycin is injected with blocks any ATP-linked respiration. ATP-linked respiration is obtained by subtracting OCR pre and post oligomycin addition. The proton gradient can be calculated by subtracting non-mitochondrial respiration from oligomycin OCR. Next, FCCP is added which removes the inner mitochondrial membrane gradient such that the maximal respiratory capacity is reached. Maximal respiratory capacity is calculated by subtracting non-mitochondrial respiration from FCCP OCR. Mitochondrial reserve capacity can be calculated by subtracting basal respiration from maximal respiration. The last addition consists of antimycin A (complex III inhibitor) and rotenone (complex I inhibitor), which essentially stops the ETC functioning and shows the non-mitochondrial respiration. In a similar manner, glycolytic parameters can be determined by sequential addition of compounds and measuring the ECAR. Upon the

establishment of the baseline ECAR, glucose is added, and the cells undertake glycolysis which is denoted as the basal glycolysis. The next injection is of oligomycin which inhibits ATP synthase (complex V) and shifts the energy production to glycolysis, to reveal the maximum glycolytic capacity. Finally, 2-deoxyglucose which competes with glucose to bind glucose hexokinase is added, thus inhibiting glycolysis and revealing the non-glycolytic acidification. The reserve glycolytic capacity can be calculated by subtracting basal glycolysis rate from the maximal glycolytic capacity. Our experiments reveal that NL-1 primarily helps to improve the mitochondrial respiration, compared to glycolysis. These actions of NL-1 at the mitochondria seem logical as the NL-1 target mitoNEET is a mitochondrial membrane protein. Further, it is possible that the improvement in respiration brought about by NL-1 is a time dependent phenomenon, since a prolonged 24-hour exposure was found to improve the basal respiration, which was not seen in

cells treated for 3 hours. Overall, this experiment reveals a potential for NL-1 to improve mitochondrial respiration and ATP production in cells that might suffer from a massive ATP deficit following ischemia.

Finally, in order to establish NL-1 as a potential stroke therapeutic, we needed to investigate the effect of NL-1 in mitigating at least one of the multiple axes that cause cell death in ischemia and reperfusion injury. For this purpose, we developed an *in vitro* ischemia and reperfusion model using mouse neuroblastoma (N2a) cells. HBSS supplemented with 10% FBS was used as the glucose-free medium for cell incubation in the hypoxia chamber[75,76]. We studied the effect of NL-1 on the levels of hydrogen peroxide, which is an important constituent of the ROS milieu. Hydrogen peroxide is formed as a dismutation product of superoxide radical by mitochondrial manganese superoxide dismutase enzyme[77]. It diffuses across the outer mitochondrial membrane into the extra mitochondrial space, wherein it can be quantified[78]. We determined the effect of NL-1 nanoparticles on peroxide generation using the sensitive fluorimetric Amplex Red assay[79]. Amplex Red is a colorless substance that reacts with hydrogen peroxide in presence of horseradish peroxidase in a 1:1 stoichiometry to yield a stable fluorescent compound called resorufin[80,81]. The primary challenge with this assay involves prevention of light exposure of Amplex red reagent for longer periods, and artificial generation of hydrogen peroxide by light exposure of resorufin[82,83]. Our results showed that NL-1 had the ability to reduce peroxide generation for a 3 hour ischemia period at a dose of 10 μM. Thus, NL-1 was found to have a potential to address the elevated levels of ROS following stroke, which could aid in neuroprotection.

In summary, this chapter describes the preliminary studies performed to investigate the viability of using NL-1 as a stroke therapeutic. Our data indicate that the thiazolidinedione analog

NL-1 is devoid of redundant anti-diabetic effects. Importantly, NL-1 acts on the mitochondrial system to improve respiration, cell survival and lower ROS mediated adverse effects following ischemia. This *in vitro* work lays the foundation for pursuing NL-1 as a potential stroke therapeutic.

3.5. References:

1.   Mozaffarian D, Benjamin EJ, Go AS, et al. Executive summary: Heart disease and stroke statistics-2016 update: A Report from the American Heart Association. *Circulation*. 2016;133(4):447-454. doi:10.1161/CIR.0000000000000366

2.   Price-Haywood EG, Harden-Barrios J, Carr C, Reddy L, Bazzano LA, van Driel ML. Patient-reported outcomes in stroke clinical trials 2002–2016: a systematic review. *Qual Life Res*. 2019;28(5):1119-1128. doi:10.1007/s11136-018-2053-7

3.   Kim JS. tPA helpers in the treatment of acute ischemic stroke: Are they ready for clinical use? *J Stroke*. 2019;21(2):160-174. doi:10.5853/jos.2019.00584

4.   Shi H, Liu KJ. Cerebral tissue oxygenation and oxidative brain injury during ischemia and reperfusion. *Front Biosci*. 2007;12(4):1318-1328. doi:10.2741/2150

5.   Gravanis I, Tsirka SE. Tissue-type plasminogen activator as a therapeutic target in stroke. *Expert Opin Ther Targets*. 2008;12(2):159-170. doi:10.1517/14728222.12.2.159

6.   Choi JH, Pile-Spellman J. Reperfusion Changes After Stroke and Practical Approaches for Neuroprotection. *Neuroimaging Clin N Am*. 2018;28(4):663-682. doi:10.1016/j.nic.2018.06.008

7.   Meng-Yu Wu, Giou-Teng Yiang, Wan-Ting Liao, Andy Po-Yi Tsai, Yeung-Leung Cheng, Pei-Wen Cheng, Chia-Ying Li C-JL. Current Mechanistic Concepts in Ischemia and Reperfusion Injury. *Cell Physiol Biochem*. 2018;46(4):1650-1667. doi:10.1159/000489241

8.   Raslan A, Bhardwaj A. Medical management of cerebral edema. *Neurosurg Focus*. 2007;22(5):1-12. doi:10.3171/foc.2007.22.5.13

9.   Jha SK. Cerebral edema and its management. *Med J Armed Forces India*. 2003;59(4):326-331. doi:10.1016/S0377-1237(03)80147-8

10.   Green AR. Pharmacological approaches to acute ischaemic stroke: Reperfusion certainly, neuroprotection possibly. In: *British Journal of Pharmacology*. Vol 153. Wiley-Blackwell; 2008:S325. doi:10.1038/sj.bjp.0707594

11.   Colca JR, McDonald WG, Waldon DJ, et al. Identification of a novel mitochondrial protein ("mitoNEET") cross-linked specifically by a thiazolidinedione photoprobe. *Am J Physiol - Endocrinol Metab*. 2003;286(2). http://ajpendo.physiology.org/content/286/2/E252.long. Accessed June 10, 2017.

12.   Paddock ML, Wiley SE, Axelrod HL, Cohen AE, Roy M, Abresch EC, Capraro D, Murphy AN, Nechushtai R, Dixon JE JP. MitoNEET is a uniquely folded 2Fe–2S outer mitochondrial membrane protein stabilized by pioglitazone. *Proc Natl Acad Sci U S A*. 104(36):14342-14347. doi:10.1073/pnas.0707189104

13.   Asako Kounosu T, Iwasaki, Seiki Baba Y, Hayashi-Iwasaki, Tairo Oshima T, Kumasaka. Crystallization and preliminary X-ray diffraction studies of the prototypal homologue of mitoNEET (Tth-NEET0026) from the extreme thermophile Thermus thermophilus HB8.

Struct Biol Cryst Commun. 2008;64(12):1146–1148. doi:10.1107/S1744309108035975

14. Nechushtai R, Conlan AR, Harir Y, et al. Characterization of Arabidopsis NEET reveals an ancient role for NEET proteins in iron metabolism. *Plant Cell*. 2012;24(5):2139-2154. doi:10.1105/tpc.112.097634

15. Inupakutika MA, Sengupta S, Nechushtai R, et al. Phylogenetic analysis of eukaryotic NEET proteins uncovers a link between a key gene duplication event and the evolution of vertebrates. *Sci Rep*. 2017;7. doi:10.1038/srep42571

16. He Q-Q, Xiong L-L, Liu F, et al. MicroRNA-127 targeting of mitoNEET inhibits neurite outgrowth, induces cell apoptosis and contributes to physiological dysfunction after spinal cord transection. *Sci Rep*. 2016;6:35205. doi:10.1038/srep35205

17. Takehiro Takahashi, Masashi Yamamoto, Kazutoshi Amikura, Kozue Kato TS, Kanako Serizawa, Daisuke Akazawa, Takumi Aoki, Koji Kawai, Emi Ogasawara J-IH, Kazuto Nakada and MK. A Novel MitoNEET Ligand, TT01001, Improves Diabetes and Ameliorates Mitochondrial Function in db/db Mice. *TheJournal Pharmacol Exp Ther*. 352(2):338-345. doi:10.1124/jpet.114.220673

18. Geldenhuys WJ, Yonutas HM, Morris DL, Sullivan PG, Darvesh AS, Leeper TC. *Identification of Small Molecules That Bind to the Mitochondrial Protein MitoNEET*. Vol 26.; 2016. doi:10.1016/j.bmcl.2016.09.009

19. Geldenhuys WJ, Benkovic SA, Lin L, et al. MitoNEET (CISD1) Knockout Mice Show Signs of Striatal Mitochondrial Dysfunction and a Parkinson's Disease Phenotype. *ACS Chem Neurosci*. 2017;8(12):2759-2765. doi:10.1021/acschemneuro.7b00287

20.   Logan SJ, Yin L, Geldenhuys WJ, et al. Novel thiazolidinedione mitoNEET ligand-1 acutely improves cardiac stem cell survival under oxidative stress. *Basic Res Cardiol*. 2015;110(2):19. doi:10.1007/s00395-015-0471-z

21.   Yonutas HM, Hubbard WB, Pandya JD, Vekaria HJ, Geldenhuys WJ, Sullivan PG. Bioenergetic restoration and neuroprotection after therapeutic targeting of mitoNEET: New mechanism of pioglitazone following traumatic brain injury. *Exp Neurol*. 2020;327:113243. doi:10.1016/j.expneurol.2020.113243

22.   Geldenhuys WJ, Funk MO, Barnes KF, Carroll RT. Structure-based design of a thiazolidinedione which targets the mitochondrial protein mitoNEET. *Bioorganic Med Chem Lett*. 2010;20(3):819-823. doi:10.1016/j.bmcl.2009.12.088

23.   Young LM, Geldenhuys WJ, Domingo OC, Malan SF, Van Der Schyf CJ. Synthesis and Biological Evaluation of Pentacycloundecylamines and Triquinylamines as Voltage-Gated Calcium Channel Blockers. *Arch Pharm (Weinheim)*. 2016;349(4):252-267. doi:10.1002/ardp.201500293

24.   Hathaway QA, Nichols CE, Shepherd DL, et al. Maternal-engineered nanomaterial exposure disrupts progeny cardiac function and bioenergetics. *Am J Physiol - Hear Circ Physiol*. 2017;312(3):H446-H458. doi:10.1152/ajpheart.00634.2016

25.   Vongs A, Solly KJ, Kiss L, MacNeil DJ, Rosenblum CI. A miniaturized homogenous assay of mitochondrial membrane potential. *Assay Drug Dev Technol*. 2011;9(4):373-381. doi:10.1089/adt.2010.0301

26.   Anastassiadis T, Deacon SW, Devarajan K, Ma H, Peterson JR. Comprehensive assay of kinase catalytic activity reveals features of kinase inhibitor selectivity. *Nat Biotechnol*.

2011;29(11):1039-1045. doi:10.1038/nbt.2017

27. Scaduto RC, Grotyohann LW. Measurement of mitochondrial membrane potential using fluorescent rhodamine derivatives. *Biophys J.* 1999;76(1 I):469-477. doi:10.1016/S00063495(99)77214-0

28. Ghani MA, Barril C, Bedgood DR, Prenzler PD. Measurement of antioxidant activity with the thiobarbituric acid reactive substances assay. *Food Chem.* 2017;230:195-207. doi:10.1016/j.foodchem.2017.02.127

29. Wiley SE, Murphy AN, Ross SA, van der Geer P, Dixon JE. MitoNEET is an ironcontaining outer mitochondrial membrane protein that regulates oxidative capacity. *Proc Natl Acad Sci U S A*. 2007;104(13):5318-5323. doi:10.1073/pnas.0701078104

30. Geldenhuys WJ, Leeper TC, Carroll RT. mitoNEET as a novel drug target for mitochondrial dysfunction. *Drug Discov Today*. 2014;19(10):1601-1606. doi:10.1016/j.drudis.2014.05.001

31. Lipper CH, Stofleth JT, Bai F, et al. Redox-dependent gating of VDAC by mitoNEET. *Proc Natl Acad Sci U S A*. 2019;116(40):19924-19929. doi:10.1073/pnas.1908271116

32. Landry AP, Ding H. Redox control of human mitochondrial outer membrane protein MitoNEET [2Fe-2S] clusters by biological thiols and hydrogen peroxide. *J Biol Chem*. 2014;289(7):4307-4315. doi:10.1074/jbc.M113.542050

33. Landry AP, Cheng Z DH. Reduction of mitochondrial protein mitoNEET[2Fe–2S] clusters by human glutathione reductase. *Free Radic Biol Med*. 81:119-127. doi:10.1016/j.freeradbiomed.2015.01.017

34.   Habener A, Chowdhury A, Echtermeyer F, et al. MitoNEET Protects HL-1 Cardiomyocytes

from Oxidative Stress Mediated Apoptosis in an *In vitro* Model of

Hypoxia and Reoxygenation. Vanella L, ed. *PLoS One*. 2016;11(5):e0156054.
doi:10.1371/journal.pone.0156054

35.   Christine M Kusminski, William L Holland, Kai Sun, Jiyoung Park, Stephen B Spurgin YL,

G Roger Askew, Judith A Simcox, Don A McClain CL& PES. MitoNEET-driven

alterations in adipocyte mitochondrial activity reveal a crucial adaptive process that

preserves insulin sensitivity in obesity. *Nat Med*. 18 (10):1539-1549. doi:10.1038/nm.2899

36.   Roberts ME, Crail JP, Laffoon MM, Fernandez WG, Menze MA KM. Identification of

disulfide bond formation between MitoNEET and glutamate dehydrogenase 1.

Biochemistry. 52 (50),:8969–8971. doi:10.1021/bi401038w

37.   Culman J, Nguyen-Ngoc M, Glatz T, Gohlke P, Herdegen T, Zhao Y. Treatment of rats with

pioglitazone in the reperfusion phase of focal cerebral ischemia: A preclinical stroke trial.

Exp Neurol. 2012;238(2):243-253. doi:10.1016/j.expneurol.2012.09.003

38.   Blankenship D, Niemi J, Hilow E, Karl M, Sundararajan S. Oral pioglitazone reduces

infarction volume and improves neurologic function following MCAO in rats. In:

Advances in Experimental Medicine and Biology. Vol 701. Springer New York LLC;

2011:157-162. doi:10.1007/978-1-4419-7756-4_22

39.   Bisgaier CL, Oniciu DC, Srivastava RAK. Comparative evaluation of gemcabene and

peroxisome proliferator-activated receptor ligands in transcriptional assays of peroxisome

proliferator-activated receptors: Implication for the treatment of hyperlipidemia and

cardiovascular disease. *J Cardiovasc Pharmacol*. 2018;72(1):3-10. doi:10.1097/FJC.0000000000000580

40. Gugnani KS, Vu N, Rondón-Ortiz AN, Böhlke M, Maher TJ, Pino-Figueroa AJ. Neuroprotective activity of macamides on manganese-induced mitochondrial disruption in U-87 MG glioblastoma cells. *Toxicol Appl Pharmacol*. 2018;340:67-76. doi:10.1016/j.taap.2017.12.014

41. Jang JY, Koh M, Bae H, et al. Structural basis for differential activities of enantiomeric PPARγ agonists: Binding of S35 to the alternate site. *Biochim Biophys Acta - Proteins Proteomics*. 2017;1865(6):674-681. doi:10.1016/j.bbapap.2017.03.008

42. Andrikopoulos S, Blair AR, Deluca N, Fam BC, Proietto J. Evaluating the glucose tolerance test in mice. *Am J Physiol - Endocrinol Metab*. 2008;295(6):1323-1332. doi:10.1152/ajpendo.90617.2008

43. Arora T, Wegmann U, Bobhate A, et al. Microbially produced glucagon-like peptide 1 improves glucose tolerance in mice. *Mol Metab*. 2016;5(8):725-730. doi:10.1016/j.molmet.2016.06.006

44. Ayala JE, Samuel VT, Morton GJ, et al. Standard operating procedures for describing and performing metabolic tests of glucose homeostasis in mice. *DMM Dis Model Mech*. 2010;3(9-10):525-534. doi:10.1242/dmm.006239

45. Kubota N, Terauchi Y, Kubota T, et al. Pioglitazone ameliorates insulin resistance and diabetes by both adiponectin-dependent and -independent pathways. *J Biol Chem*. 2006;281(13):8748-8755. doi:10.1074/jbc.M505649200

46. Elkamhawy A, Park JE, Cho NC, Sim T, Pae AN, Roh EJ. Discovery of a broad spectrum antiproliferative agent with selectivity for DDR1 kinase: Cell line-based assay, kinase panel, molecular docking, and toxicity studies. *J Enzyme Inhib Med Chem*. 2016;31(1):158-166. doi:10.3109/14756366.2015.1004057

47. El-Deeb IM, Park BS, Jung SJ, et al. Design, synthesis, screening, and molecular modeling study of a new series of ROS1 receptor tyrosine kinase inhibitors. *Bioorganic Med Chem Lett*. 2009;19(19):5622-5626. doi:10.1016/j.bmcl.2009.08.029

48. Shekarabi M, Zhang J, Khanna AR, Ellison DH, Delpire E, Kahle KT. WNK Kinase Signaling in Ion Homeostasis and Human Disease. *Cell Metab*. 2017;25(2):285-299. doi:10.1016/j.cmet.2017.01.007

49. Veríssimo F, Jordan P. WNK kinases, a novel protein kinase subfamily in multi-cellular organisms. *Oncogene*. 2001;20(39):5562-5569. doi:10.1038/sj.onc.1204726

50. Yamada K, Park HM, Rigel DF, et al. Small-molecule WNK inhibition regulates cardiovascular and renal function. *Nat Chem Biol*. 2016;12(11):896-898. doi:10.1038/nchembio.2168

51. Wu D, Lai N, Deng R, et al. Activated WNK3 induced by intracerebral hemorrhage deteriorates brain injury maybe via WNK3/SPAK/NKCC1 pathway. *Exp Neurol*. 2020;332:113386. doi:10.1016/j.expneurol.2020.113386

52. Begum G, Yuan H, Kahle KT, et al. Inhibition of WNK3 Kinase Signaling Reduces Brain Damage and Accelerates Neurological Recovery after Stroke. *Stroke*. 2015;46(7):1956-1965. doi:10.1161/STROKEAHA.115.008939

53. Zhao H, Nepomuceno R, Gao X, et al. Deletion of the WNK3-SPAK kinase complex in mice improves radiographic and clinical outcomes in malignant cerebral edema after ischemic stroke. *J Cereb Blood Flow Metab*. 2017;37(2):550-563. doi:10.1177/0271678X16631561

54. Nagy Z, Nardai S. Cerebral ischemia/repefusion injury: From bench space to bedside. *Brain Res Bull*. 2017;134:30-37. doi:10.1016/j.brainresbull.2017.06.011

55. Tohru Kobayashi, Satoshi Kuroda, Mitsuhiro Tada, Kiyohiro Houkin, Yoshinobu Iwasaki HA. Calcium-induced mitochondrial swelling and cytochrome c release in the brain: its biochemical characteristics and implication in ischemic neuronal injury. *Brain Res*. 2003;960(1-2):62-70. doi:10.1016/s0006-8993(02)03767-8

56. Nagy Z, Goehlert UG, Wolfe LS, Hüttner I. Ca2+ depletion-induced disconnection of tight junctions in isolated rat brain microvessels. *Acta Neuropathol*. 1985;68(1):48-52. doi:10.1007/BF00688955

57. Singh SK, Mishra MK, Eltoum IEA, Bae S, Lillard JW, Singh R. CCR5/CCL5 axis interaction promotes migratory and invasiveness of pancreatic cancer cells. *Sci Rep*. 2018;8(1):1-12. doi:10.1038/s41598-018-19643-0

58. Geldenhuys WJ, Bezuidenhout LM, Dluzen DE. Effects of a novel dopamine uptake inhibitor upon extracellular dopamine from superfused murine striatal tissue. *Eur J Pharmacol*. 2009;619(1-3):38-43. doi:10.1016/j.ejphar.2009.08.012

59. Allen KL, Almeida A, Bates TE, Clark JB. Changes of Respiratory Chain Activity in Mitochondrial and Synaptosomal Fractions Isolated from the Gerbil Brain After Graded Ischaemia. *J Neurochem*. 2002;64(5):2222-2229. doi:10.1046/j.1471-

4159.1995.64052222.x

60.   Gaur V, Aggarwal A, Kumar A. Protective effect of naringin against ischemic reperfusion cerebral injury: Possible neurobehavioral, biochemical and cellular alterations in rat brain. *Eur J Pharmacol*. 2009;616(1-3):147-154. doi:10.1016/j.ejphar.2009.06.056

61.   Miao Y, Zhao S, Gao Y, et al. Curcumin pretreatment attenuates inflammation and mitochondrial dysfunction in experimental stroke: The possible role of Sirt1 signaling. *Brain Res Bull*. 2016;121:9-15. doi:10.1016/j.brainresbull.2015.11.019

62.   Yang Y, Jiang S, Dong Y, et al. Melatonin prevents cell death and mitochondrial dysfunction via a SIRT1-dependent mechanism during ischemic-stroke in mice. *J Pineal Res*. 2015;58(1):61-70. doi:10.1111/jpi.12193

63.   Wolff V, Schlagowski A-I, Rouyer O, et al. Tetrahydrocannabinol Induces Brain Mitochondrial Respiratory Chain Dysfunction and Increases Oxidative Stress: A Potential Mechanism Involved in Cannabis-Related Stroke. 2015. doi:10.1155/2015/323706

64.   Almeida A, Allen KL, Bates TE, Clark JB. Effect of reperfusion following cerebral ischaemia on the activity of the mitochondrial respiratory chain in the gerbil brain. *J Neurochem*. 1995;65(4):1698-1703. doi:10.1046/j.1471-4159.1995.65041698.x

65.   Huang S-G. Development of a High Throughput Screening Assay for Mitochondrial Membrane Potential in Living Cells. *J Biomol Screen*. 2002;7(4):383-389. doi:10.1177/108705710200700411

66.   Chowdhury SR, Djordjevic J, Albensi BC, Fernyhough P. Simultaneous evaluation of substrate-dependent oxygen consumption rates and mitochondrial membrane potential by TMRM and safranin in cortical mitochondria. *Biosci Rep*. 2016;36(1):286.

doi:10.1042/BSR20150244

67.   Creed S, McKenzie M. Measurement of mitochondrial membrane potential with the fluorescent dye tetramethylrhodamine methyl ester (TMRM). In: *Methods in Molecular Biology*. Vol 1928. Humana Press Inc.; 2019:69-76. doi:10.1007/978-1-4939-9027-6_5

68.   Mortiboys H, Aasly J, Bandmann O. Ursocholanic acid rescues mitochondrial function in common forms of familial Parkinson's disease. *Brain*. 2013;136(10):3038-3050. doi:10.1093/brain/awt224

69.   Arnett D, Quillin A, Geldenhuys WJ, Menze MA, Konkle M. 4-Hydroxynonenal and 4-Oxononenal Differentially Bind to the Redox Sensor MitoNEET. *Chem Res Toxicol*. 2019;32(6):977-981. doi:10.1021/acs.chemrestox.9b00166

70.   Şeneş M, Kazan N, Coşkun Ö, Zengi O, Inan L, Yücel D. Oxidative and nitrosative stress in acute ischaemic stroke. *Ann Clin Biochem*. 2007;44(1):43-47. doi:10.1258/000456307779596057

71.   Akhtar M, Maikiyo AM, Najmi AK, Khanam R, Mujeeb M, Aqil M. Neuroprotective effects of chloroform and petroleum ether extracts of Nigella sativa seeds in stroke model of rat. *J Pharm Bioallied Sci*. 2013;5(2):119-125. doi:10.4103/0975-7406.111825

72.   Gusev EI, Skvortsova VI, Dambinova SA, et al. Neuroprotective effects of glycine for therapy of acute ischaemic stroke. *Cerebrovasc Dis*. 2000;10(1):49-60. doi:10.1159/000016025

73.   Rose S, Frye RE, Slattery J, et al. Oxidative stress induces mitochondrial dysfunction in a subset of autism lymphoblastoid cell lines in a well-matched case control cohort. *PLoS*

One. 2014;9(1). doi:10.1371/journal.pone.0085436

74.   Guide□ U. *Agilent Technologies Agilent Seahorse XF Glycolysis Stress Test Kit*.

75.   Farajdokht F, Mohaddes G, Karimi-Sales E, et al. Inhibition of PTEN protects PC12 cells against oxygen-glucose deprivation induced cell death through mitoprotection. *Brain Res*. 2018;1692:100-109. doi:10.1016/J.BRAINRES.2018.05.026

76.   Minaei Beyrami S, Khadem Ansari MH, Rasemi Y, Shakib N, Karimi P. Complete inhibition of phosphatase and tensin homolog promotes the normal and oxygen-glucose deprivation/reperfusion-injured PC12 cells to cell death. *J Cardiovasc Thorac Res*. 2018;10(2):83-89. doi:10.15171/jcvtr.2018.13

77.   Chan SHH, Tai M-H, Li C-Y, Chan JYH. Reduction in molecular synthesis or enzyme activity of superoxide dismutases and catalase contributes to oxidative stress and neurogenic hypertension in spontaneously hypertensive rats. *Free Radic Biol Med*. 2006;40(11):2028-2039. doi:10.1016/J.FREERADBIOMED.2006.01.032

78.   Staniek K, Nohl H. Are mitochondria a permanent source of reactive oxygen species? *Biochim Biophys Acta - Bioenerg*. 2000;1460(2-3):268-275. doi:10.1016/S0005-2728(00)00152-3

79.   Zhou M, Diwu Z, Panchuk-Voloshina N, Haugland RP. A Stable Nonfluorescent Derivative of Resorufin for the Fluorometric Determination of Trace Hydrogen Peroxide: Applications in Detecting the Activity of Phagocyte NADPH Oxidase and Other Oxidases. *Anal Biochem*. 1997;253(2):162-168. doi:10.1006/ABIO.1997.2391

80.   Liu Y, Ai K, Ji X, et al. Comprehensive Insights into the Multi-Antioxidative Mechanisms of Melanin Nanoparticles and Their Application To Protect Brain from Injury in Ischemic Stroke. *J Am Chem Soc*. 2017;139(2):856-862. doi:10.1021/jacs.6b11013

81.   Rodrigues J V., Gomes CM. Enhanced superoxide and hydrogen peroxide detection in biological assays. *Free Radic Biol Med*. 2010;49(1):61-66. doi:10.1016/J.FREERADBIOMED.2010.03.014

82.   Kalyanaraman B, Darley-Usmar V, Davies KJA, et al. Measuring reactive oxygen and nitrogen species with fluorescent probes: challenges and limitations. *Free Radic Biol Med*. 2012;52(1):1-6. doi:10.1016/J.FREERADBIOMED.2011.09.030

83.   Zhao B, Summers FA, Mason RP. Photooxidation of Amplex red to resorufin: Implications of exposing the Amplex red assay to light. *Free Radic Biol Med*. 2012;53(5):1080-1087. doi:10.1016/J.FREERADBIOMED.2012.06.034
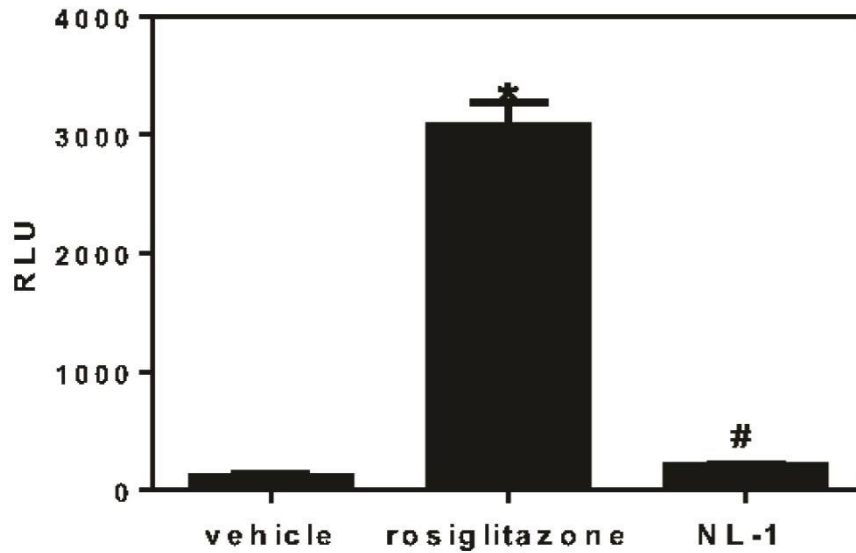
Figure 3.1: The mitoNEET ligand NL-1 (10 µM) does not activate PPAR-gamma using a reporter assay system. As a positive control rosiglitazone was used to activate PPAR-gamma (4 µM) with increased luciferase activity. NL-1 showed a statistically significant (P<0.05) difference compared to vehicle control* and #compared to rosiglitazone. N = 4.
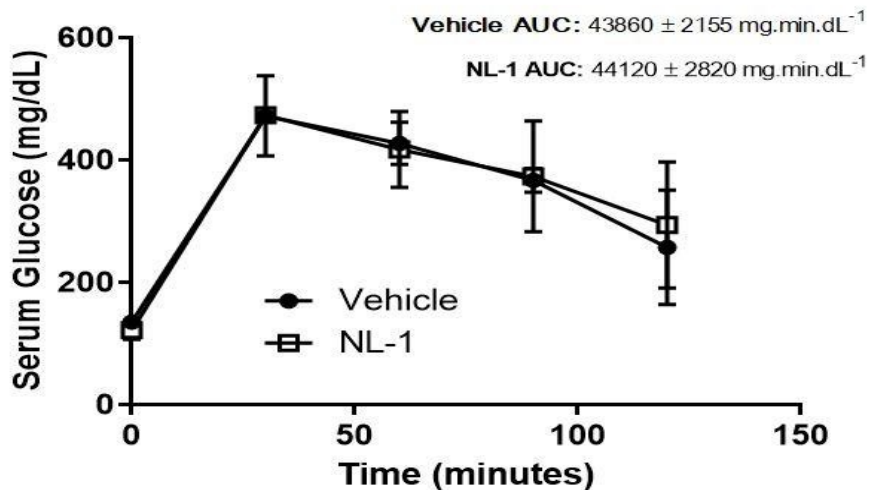
Figure 3.2: Effect of an acute treatment of NL-1 on glucose levels in mice. NL-1 at 10 mg/kg did not lower blood glucose after glucose tolerance test. Each data point represents mean $\pm$ S.D. where N = 4.
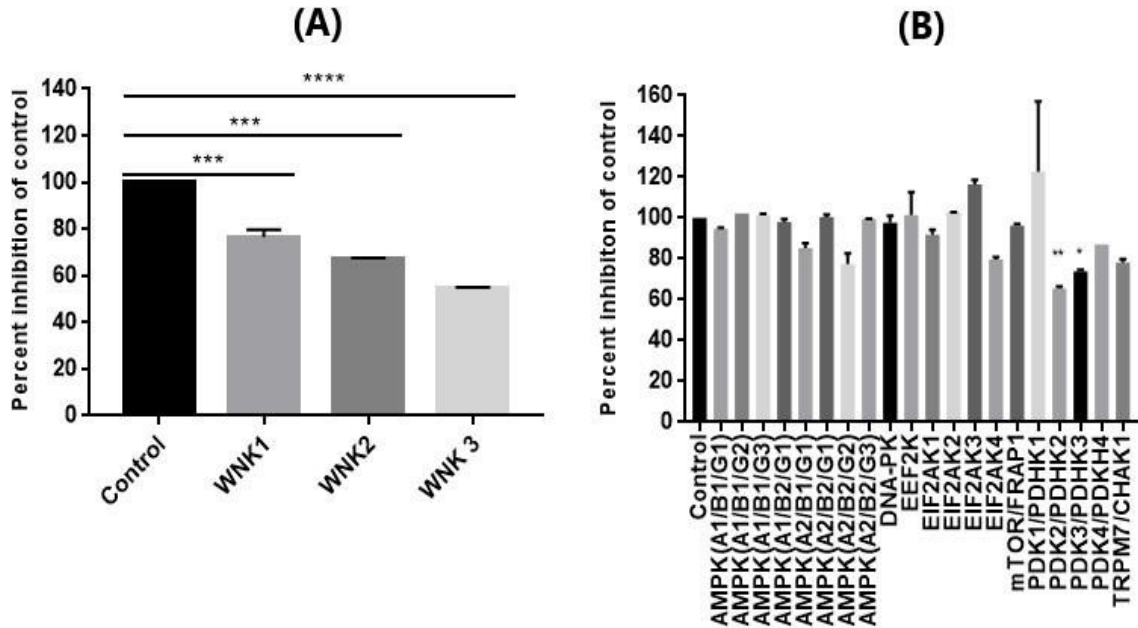
Figure 3.3: Testing for inhibitory effects of NL-1 using a kinase panel. (A) Typical kinase panel shows that the only notable inhibition for the WNK kinase family, out of 349 kinases, and (B) Atypical kinase panel showing significant inhibition of PDK2 and PDK3. Results are expressed as the percent inhibition of control (*p<0.05, **p<0.01, ***p<0.001, ****p<0.0001).
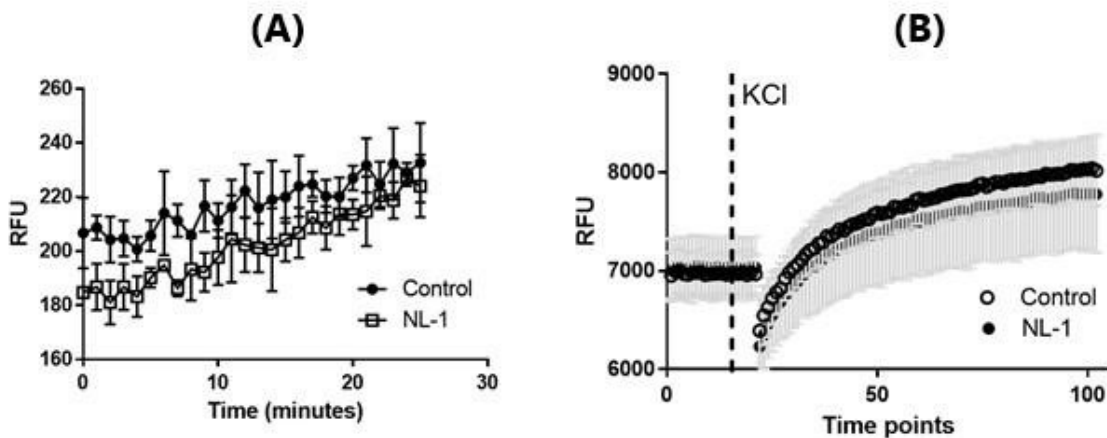
Figure 3.4: NL-1 (10 ☐M) effect on endogenous calcium and calcium influx in N2A cells. Cells were treated with NL-1 for 15 minutes and the calcium flux measure with the Fluoforte calcium kit. Control cells received DMSO only, with a final concentration of DSMO 1%. (A)

Effect of NL-1 on baseline calcium uptake. (B) Effect of NL-1 on cells which have been stimulated by KCl (50 mM) to stimulate voltage gated ion channels. The cells treated with NL-1 did not show significant effects on calcium flux at the dose tested. Each data point represented by average +/- S.D. were N = 3 -5 for each group. Abbreviation: relative fluorescent units (RFU).

(A) Complex I   **(B) Complex IV**
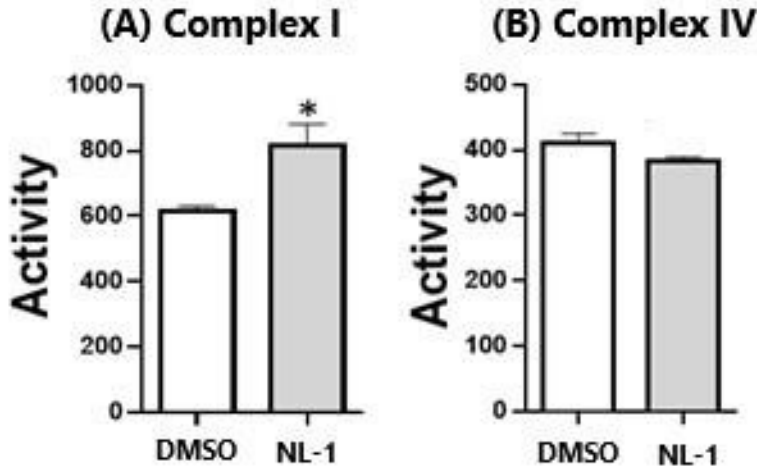
Figure 3.5: Effect of NL-1 on mitochondrial complexes of the electron transport chain. A) NL-1 (10 ☐M) stimulates complex I activity in isolated mitochondria; B) NL-1 does not affect complex IV in isolated mitochondria. Each bar represents average +/- S.D, where N = 3 (*p<0.05).

Membrane potential
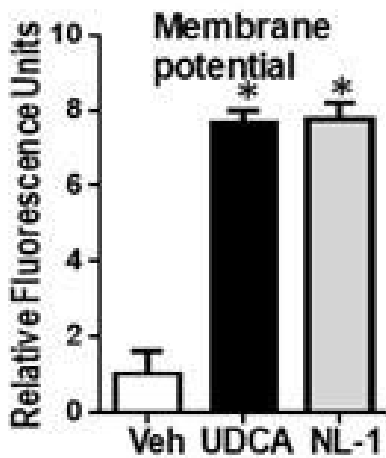
Figure 3.6: NL-1 (10 □M) stimulates mitochondrial membrane potential in N2A cells, with ursodeoxycholic acid used as control (500 nM). Each bar represents average +/- S.D, where N = 3 (*p<0.05).
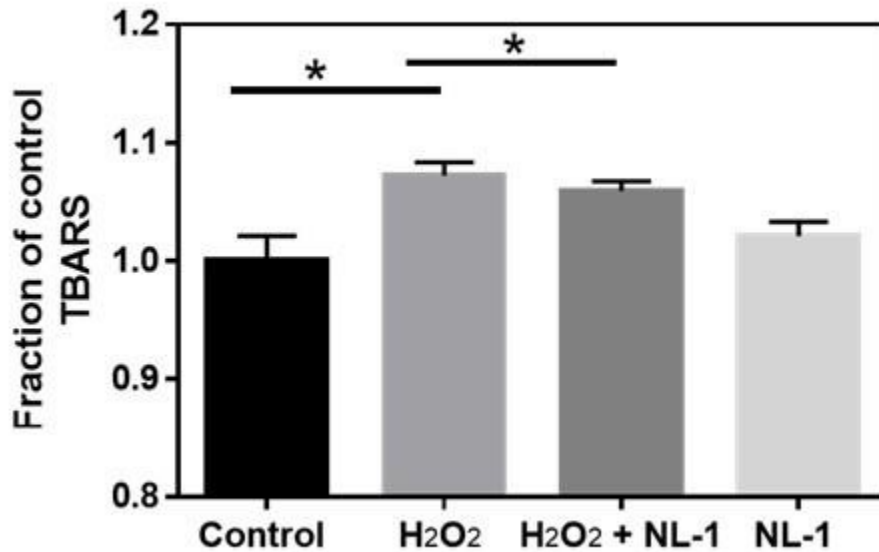
Figure 3.7: Lipid peroxidation assay (TBARS) show attenuation in N2A cells treated with NL-1 (10 □M). Cells were treated with hydrogen peroxide (100 □M) for 24 hours. TBARS levels were found to be significantly reduced for cells treated with NL-1 and hydrogen peroxide as compared to hydrogen peroxide alone. Each bar represents average +/- SD were N = 3 (*p<0.05).
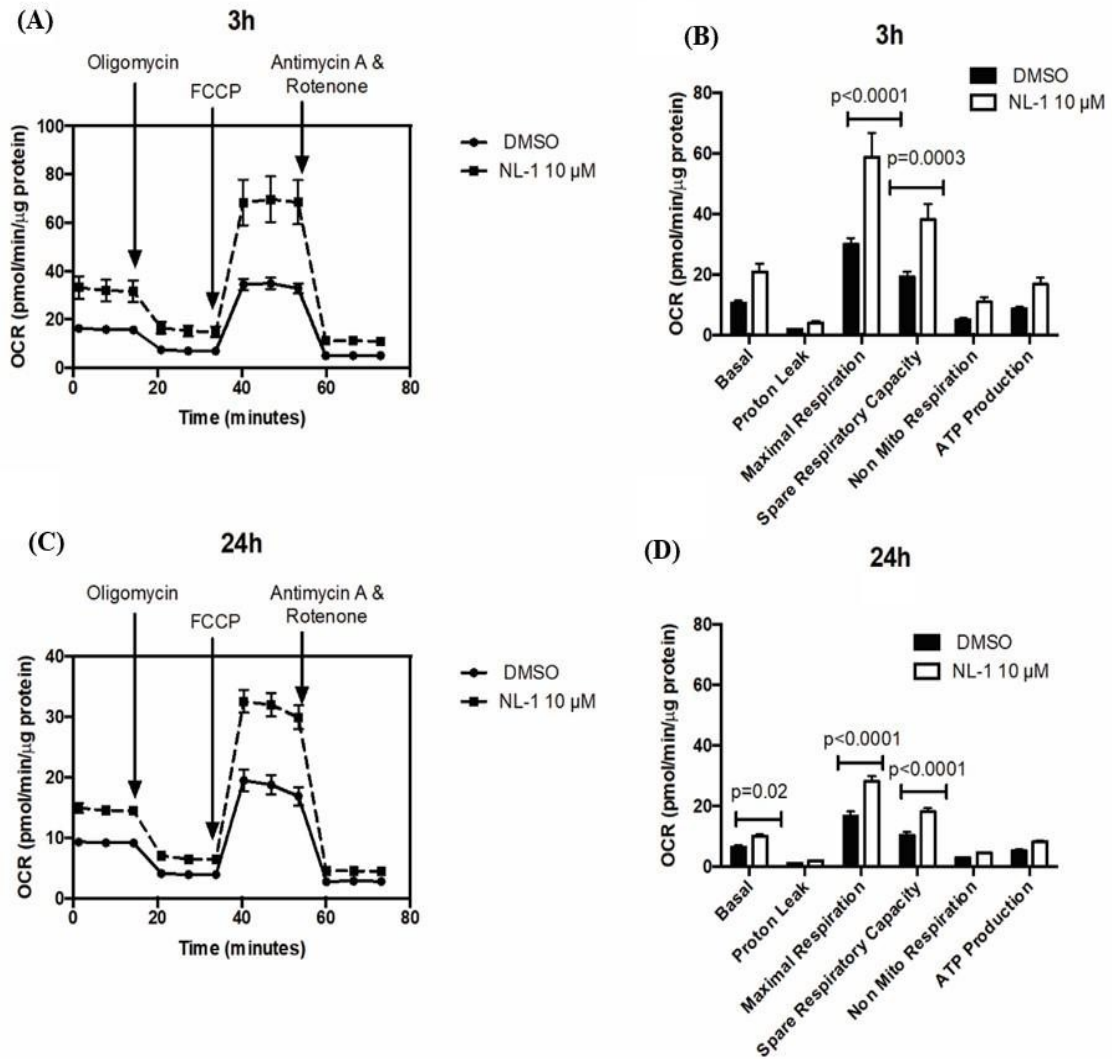
Figure 3.8: Measurement of oxygen consumption rate (OCR) of N2a cells as a function of mitochondrial respiration. The OCR is plotted over time with sequential addition of modulators of respiration for (A) 3 hour and (C) 24 hour treatment. The OCR for parameters of mitochondrial respiration are compared for control and 10 μM NL-1 for (B) 3 hour and (D) 24 hour treatment.
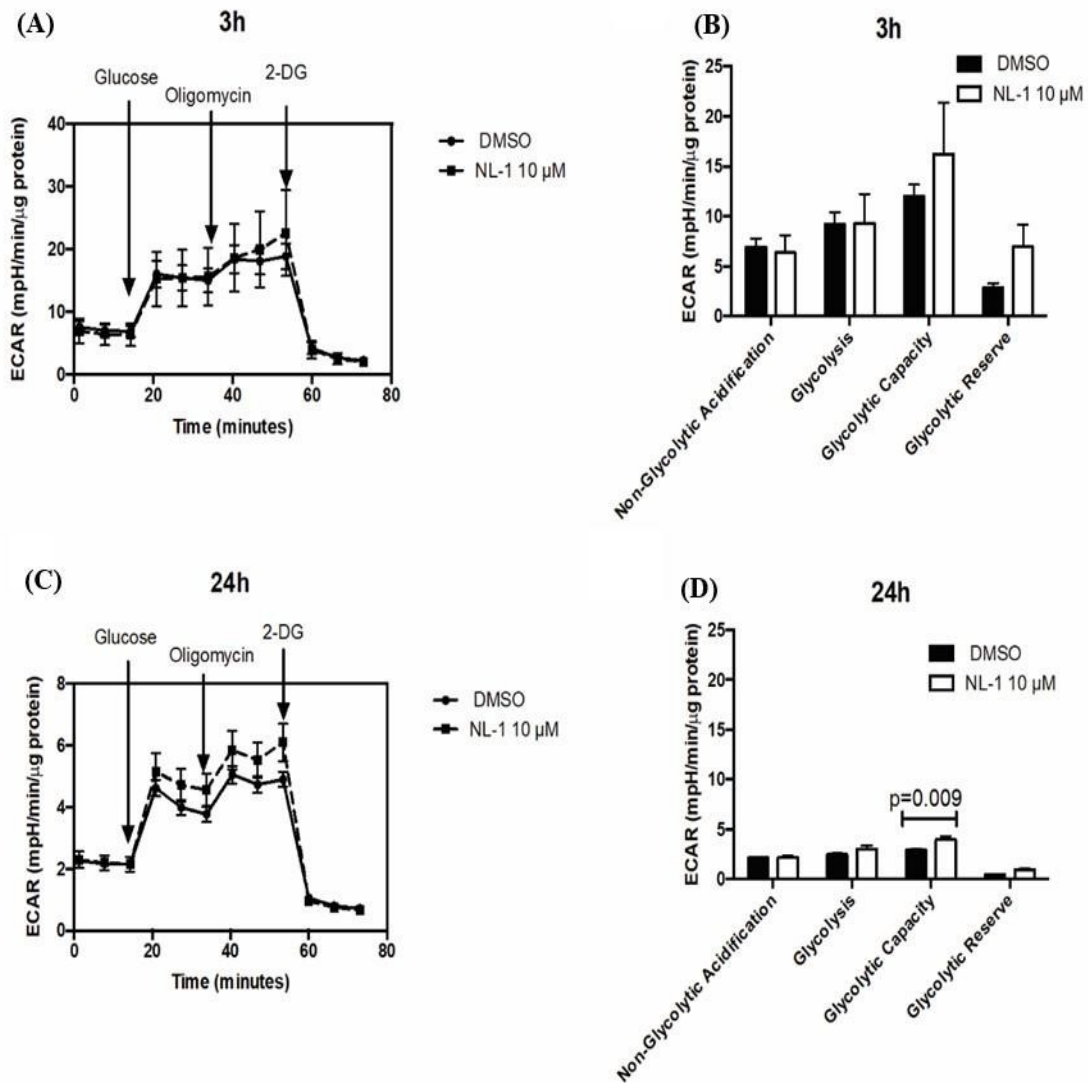
Figure 3.9: Measurement of extracellular acidification rate (ECAR) of N2a cells as a function of glycolysis. The ECAR is plotted over time with sequential addition of modulators of glycolysis for (A) 3 hour and (C) 24 hour treatment. The ECAR for parameters of glycolysis are compared for control and 10 μM NL-1 for (B) 3 hour and (D) 24 hour treatment.
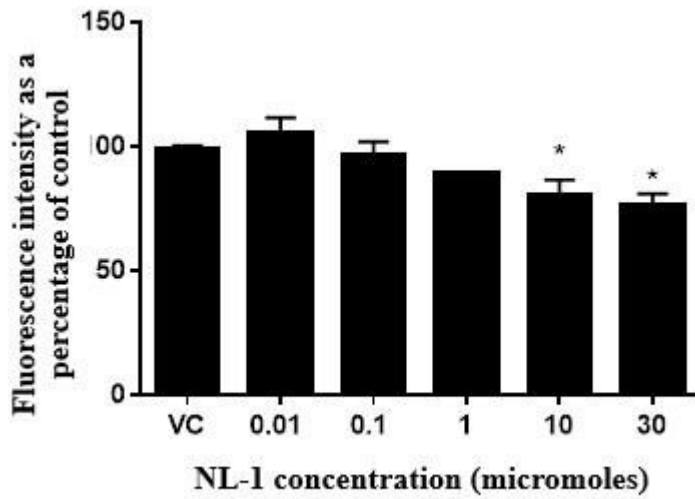
Figure 3.10: NL-1 protects neuronal cells against oxygen glucose deprivation and reperfusion (OGDR). N2a cells were exposed to OGD conditions for 3 hours and reperfused for 24 hours. The fluorescence intensity from Amplex Red assay is plotted as a percentage on control cells for a series of NL-1 concentrations (*p<0.05).

CHAPTER 4

Formulation, characterization and *in vitro* evaluation of NL-1 polymeric nanoparticle system

Chapter published:

Nanoparticle formulation and in vitro efficacy testing of the mitoNEET ligand NL-1 for drug delivery in a brain endothelial model of ischemic reperfusioninjury

Pushkar Saralkar, Tasneem Arsiwala and Werner J. Geldenhuys

4.1. Introduction

Stroke is a leading cause of mortality and morbidity worldwide, with no proven therapies to slow down the neuronal cell death after a stroke.[1] About 80% of stroke cases consist of ischemic stroke, wherein the blood supply to a brain region is impeded. As a result, the brain tissue is deprived of vital nutrients such as oxygen and glucose. Unless the occlusion is removed and blood supply is restored, prolonged deprivation of nutrients leads to formation of an infarct in the brain tissue which is a result of cell damage to neurons, microglia, astrocytes and endothelial cells. Multiple mechanisms of cell damage are activated following cerebral ischemia and reperfusion which can be a function of location in the brain as well as the time elapsed since the onset of ischemia. Although it might seem counterintuitive, restoration of blood supply, known as reperfusion, can cause further damage. Effects of reperfusion, also known as reperfusion injury, are the causative factors for cerebral edema and blood brain barrier (BBB) disruption[2].

Energy failure is the immediate consequence of this ischemic event, as the brain cells are unable to generate ATP molecules due to lack of glucose and oxygen. A decline in ATP generation results in many downstream events such as the dysfunction of ATP pumps, loss of membrane potential, prevention of neurotransmitter reuptake leading to excitotoxicity of neurotransmitters such as glutamate. A direct effect of lack of impeded glucose and oxygen delivery is the alternation of mitochondrial function. The mitochondria are involved in two important physiological functions that include the generation of ATP and regulation of cellular apoptotic pathways. Oxidative stress is a principle mechanism of cell damage following cerebral ischemia and reperfusion, mediated by reactive oxygen species (ROS) such as superoxide radical, hydrogen peroxide, and the product of nitric oxide and superoxide interaction: peroxynitrite. Ischemic events are known to activate enzymes that produce ROS, which also see a surge in generation following reperfusion. These

ROS can interact with matrix metalloproteases leading to BBB disruption, and also recruit neutrophils and other leukocytes, adding an inflammatory dimension to the cellular damage[3]. Mitochondria are the upstream regulators of the intrinsic pathway of neuronal cellular apoptosis, with changes in the mitochondrial membrane integrity following ischemia and reperfusion injury lead to the initiation of cellular apoptosis, resulting in eventual cell death.

MitoNEET is a protein present in the outer mitochondrial membrane, which was discovered as an off-target binding site for the thiazolidinedione category of anti-diabetic drug pioglitazone[4,5]. It is a 14 kD protein that exists as a homodimer. MitoNEET contains two ironsulfur clusters (2Fe-2S) that are responsible for its physiological actions[6,7]. The iron-sulfur cluster is labile, and its stability within the protein is dependent on its oxidation state[8]. It participates in redox processes thereby regulating the bioenergetics of the cell, and can act as a sensor for ROS[9]. MitoNEET interacts with endogenous molecules that are involved in cellular respiration[10,11]. MitoNEET has been discovered to play a role in metabolic conditions, cancer as well as in neurodegenerative diseases[12,13]. Loss of MitoNEET has been implicated to cause

neurodegeneration in Parkinson's Disease and in spinal cord injury[14,15]. Pioglitazone, a mitoNEET ligand has shown to have neuroprotective effects after spinal cord injury[16]. However, keeping in mind about the anti-diabetic actions of pioglitazone, a mitoNEET specific ligand, NL-1, has been previously developed in our lab[17]. NL-1 has been shown to reduce rotenone induced cell death, and caused uncoupling of mitochondrial respiration. When tested with cardiac stem cells, it has been found to improve their survival under an environment of oxidative stress[18]. With the current background about mitoNEET and its ligand NL-1, we investigated the potential of NL-1 in treatment of cerebral ischemia reperfusion injury, by targeting the mitochondrial pathways of cell damage such as oxidative stress and apoptosis. The work presented involves development and

characterization of polymeric nanoparticles for NL-1 delivery, and the *in vitro* efficacy testing. Although this study focuses only on the *in vitro* efficacy of NL-1 nanoparticles, the long term aim of this project is delivery of NL-1 to the brain for treatment of cerebral ischemia. This is the first report of the formulation of NL-1, a first in class mitoNEET ligand into a nanoparticle drug delivery system.

4.2. Materials and Methods

Materials

Acid end-capped PLGA Resomer RG 530H (50:50), amiloride hydrochloride hydrate, chlorpromazine hydrochloride, genistein, and thiazolyl blue tetrazolium bromide (MTT) were purchased from Sigma-Aldrich (St. Louis, MO). Polyvinyl alcohol was obtained from MP Biochemicals (Solon, OH). Kolliphor P188 was a generous gift from BASF Chemicals Company (Ludwigshafen, Germany). Rhodamine B was purchased from Fisher Chemicals (Fair Lawn, NJ). Solvents such as dichloromethane, ethyl acetate, methanol and LC-MS grade acetonitrile were also obtained from Fisher Chemicals. Triton-X 100 detergent was purchased from Acros Organics. Btubulin primary antibody for immunostaining was purchased from Abcam (ab15568). AlexaFluor
488-conjugated Affinipure donkey anti-rabbit secondary antibody was purchased from Jackson Immunoresearch Laboratories (West Grove, PA). Amplex Red Hydrogen Peroxide Kit was purchased from Invitrogen (A22188) (Carlsbad, CA). FITC Annexin V Apoptosis Detection Kit was obtained from BD Biosciences (catalog number: 556547) (Franklin Lane, NJ). The bEnd.3 cells and Dulbecco's Modified Eagle's Medium (DMEM) (catalog number 30-2002) were purchased from American Type Cell Culture (ATCC, Manasas, VA). TrypLE Express and Fetal

Bovine Serum (FBS) were purchased from Gibco.
Methods

Preparation of nanoparticles

PLGA nanoparticles loaded with NL-1 were prepared using emulsification and solvent evaporation technique. Acid-end capped PLGA was dissolved (2% w/v) in organic phase consisting of dichloromethane and ethyl acetate in a 1:1 ratio. This was emulsified with the aqueous phase consisting of 1% w/v PVA and 0.5% w/v Kolliphor P188 as emulsifying agents. The primary emulsion was achieved using ultrasonication process (Heat Systems Ultrasonics Inc., Model W225). The nanoparticles were obtained after evaporation of the solvent by overnight stirring. The nanoparticles were separated from the unentrapped drug using a 10 cm Sephadex G-50 column. Finally, for long term storage, the nanoparticles were freeze dried using 5% mannitol as a cryoprotectant. The blank nanoparticles were prepared using the same procedure without adding NL-1 to the organic phase.

Characterization of PLGA nanoparticles

Both blank and NL-1 loaded nanoparticles were characterized for their particle size. The particle size and polydispersity index analyses were carried out using the Malvern Zetasizer. The nanoparticle samples were diluted 1:100, and each formulation was measured in triplicate. The zeta potential of the nanoparticles was also measured using the Malvern Zetasizer. The particle size of freeze-dried nanoparticles was measured by resuspending the nanoparticle powder in pure water at a concentration of 1 mg/mL. The stability of resuspended nanoparticles was determined by measuring the particle size of the suspension every week, for 60 days. Upon optimization of the formulations, Scanning Electron Microscopy (SEM) was used to determine the particle morphology as well as the size. The nanoparticle suspension was coated on a silica wafer and

allowed to air dry. The dry film of nanoparticles was sputter coated with gold-palladium thin film using Denton Desk V sputter coater (Denton Vacuun, Moorestown, NJ). Subsequently, the particles were visualized using the Hitachi S4700 scanning electron microscope, at an operating voltage of 5 KV.

The physical state of nanoparticles was assessed using X-ray diffraction (XRD) technique. Four separate samples were analyzed that included the NL-1 drug in its pure form, blank PLGA nanoparticles, NL-1 loaded PLGA nanoparticles and a physical mixture of NL-1 drug and NL-1 loaded PLGA nanoparticles. Powder X-ray diffraction measurement was performed at room temperature using a PANalytical X'Pert Pro XRD equipped with Copper k-alpha 8047.2 eV X-ray source.

A modified LC-MS/MS method for NL-1 quantification was developed based on a previously described method[19]. The system comprised of ExionLC (SCIEX, Farmingham, MA) and an ABSciEx QTrap 5500 mass spectrometer. A Phenomenex Luna Omega UPLC column (100 x 2.1 mm, 1.6 μM) was used to elute NL-1 with an isocratic flow of acetonitrile and water (85:15) at 0.3 mL/minute. NL-1 fragment at 263.1 Daltons was used for quantification.

The entrapment efficiency of NL-1 loaded PLGA nanoparticles was calculated by extracting the drug from about 10 mg lyophilized nanoparticles. One milliliter acetonitrile was added to the nanoparticles and subjected to ultrasonication for two minutes. The solution was then centrifuged at 12,000 rpm for ten minutes and the supernatant was used to quantify NL-1 content. The percent entrapment efficiency of NL-1 was calculated using the following formula:

$Percent\ entrapment\ efficiency\ of\ NL-1$

$$= \frac{Amount\ of\ NL-1\ measured\ upon\ extraction}{\rule{6cm}{0.4pt}}\ x\ 100$$

$$Amount\ of\ NL-1\ used\ in\ formulation$$

In vitro release of NL-1

The *in vitro* release of NL-1 from the lyophilized nanoparticles was studied using Slide-A-Lyzer MINI Dialysis Units (Thermo Scientific, Waltham, MA), with a molecular weight cut-off of 3,500 Daltons. The release medium consisted of 20% v/v methanol in 0.1 M ammonium acetate buffer pH 7.4. About 10 mg nanoparticles were weighed and dispersed in 600 µL of release medium. Five hundred microliters of this suspension was packed in the dialysis units (donor compartment), and the units were set afloat in 10 mL of release medium in a 50 mL tube (recipient compartment). The tubes were incubated at 37 °C. For pure NL-1, an equivalent amount of NL-1 was prepared as a dilution in the release medium, using a methanol stock solution (5 mg/mL) of the drug. Five hundred microliters of the NL-1 dilution were added to the dialysis units, using the same set-up used for NL-1 nanoparticles. At fixed time points, 500 µL of liquid was sampled from the recipient compartments of both, pure NL-1 and NL-1 nanoparticles. An equivalent volume of release medium was replaced to keep the volume constant. Sink conditions were maintained throughout the release study. The sampled release medium was analyzed for NL-1 content using the LCMS/MS method. The amount of NL-1 was plotted as percent cumulative released from the nanoparticles versus time.

Nanoparticle uptake studies

The nanoparticle uptake study was performed in mouse endothelial bEnd.3 cells (ATCC, Manassas, VA). Rhodamine labelled fluorescent nanoparticles were prepared using the aforementioned procedure, with the addition of rhodamine B to aqueous phase prior to ultrasonication. The nanoparticles were gel filtered to remove excess rhodamine, and were further cleaned by centrifugation. The pellet obtained after second wash was used for uptake studies on

the cells. This optimization to reduce background fluorescence was performed using Nanosight NS300 (Malvern Panalytical) with a 532 nm laser, and 565 nm filter. For the uptake study, cells were plated in 6-well plates at a seeding density of 150,000 cells per plate. Cells were incubated with rhodamine nanoparticles dispersed in cell culture medium, for different time periods of 1, 3, 6, and 24 hours. Once the incubation time was complete, the cells were washed thrice with PBS, trypsinized and collected in flow cytometry tubes. The cells were further washed and pelleted thrice with PBS within the tubes, and fixed with 0.4% paraformaldehyde. The samples were analyzed for rhodamine fluorescence by flow cytometry using the BD LSRFortessa 4 laser analyzer (Becton, Dickinson and Company, Franklin Lanes, NJ). The data were analyzed using the BD FACS Diva 8.0 software. To determine the effect of energy dependence of nanoparticle uptake, one plate of cells was pre-incubated at 4°C for 1 hour, after which the cells were treated with rhodamine nanoparticles at 4°C for a single time point of 6 hours. The rhodamine nanoparticle uptake was analyzed using flow cytometry, following the same procedure. The mechanism of nanoparticle uptake was studied using specific uptake mechanism inhibitors. These included amiloride hydrochloride hydrate (100 µM) for phagocytosis, chlorpromazine hydrochloride (3 µM) for clathrin mediated endocytosis, and genistein (400 µM) for lipid raft/ caveolar mediated endocytosis. The cells were pre-treated with the inhibitors separately for 1 hour, after which they were treated with rhodamine nanoparticles for a single time period of 6 hours, and analyzed for cellular uptake using flow cytometry.

Nanoparticle localization studies

Rhodamine nanoparticle localization was studied qualitatively by with immunohistochemistry. bEnd.3 cells were plated on coverslips and incubated with rhodamine labelled nanoparticles for a period of six hours. Upon completion of the incubation period, the cells were washed three times

with PBS, fixed with 4% paraformaldehyde for 15 minutes, and permeabilized with 0.1% TritonX100 for 10 minutes. Upon permeabilization, the cells were blocked with 10% v/v goat serum in 5% w/v bovine serum albumin (BSA). Subsequently, the cells were incubated in β-tubulin primary antibody (Abcam ab15568) overnight at 4°C. Alexa Fluor 488-conjugated AffiniPure donkey antirabbit IgG (Jackson Immuno Research Laboratories, West Grove, PA) was used as the secondary antibody in 5% BSA for two hours at room temperature. Finally, the cell nuclei were stained with DAPI (Thermo Scientific) for ten minutes, prior to mounting the coverslips on to slides. Cells were washed thrice with PBS between each step. The cells were imaged using Nikon A1R/SIM confocal and super resolution imaging microscope (Nikon, Tokyo, Japan).

In vitro ischemia model

The efficacy of NL-1 loaded nanoparticles to achieve neuroprotection following stroke was determined as a function of their ability to reduce generation of hydrogen peroxide and occurrence of apoptosis. An *in vitro* cerebral ischemia and reperfusion model was employed by exposing the cells to Oxygen and Glucose Deprivation (OGD). The process involved removal of regular cell culture medium and replacing the medium with the glucose deficient Hank's Balanced Salt Solution (HBSS), containing 10% FBS. The cell plates were then transferred to the BioSpherix X3 Xvivo System hypoxia chamber, with 0.1-0.2% oxygen, 5% carbon dioxide with nitrogen making up the rest of gaseous flow. The temperature of hypoxia chamber was maintained at 37°C. The cells were incubated in hypoxia chamber for a specific time period of either 3 or 6 hours. After the desired period of hypoxia, the glucose-free medium was replaced with normal cell growth medium and cells were incubated in normal growth environment for 24 hours, mimicking the reperfusion following cerebral ischemia.

Effect of NL-1 nanoparticles on hydrogen peroxide generation following OGD

The *in vitro* efficacy of NL-1 nanoparticles in reducing generation of ROS was studied using Amplex Red assay (Thermo Scientific). bEnd.3 cells were plated in a black 96-well plate at a density of 10,000 cells per well. After 24 hours, cells were subjected to OGD. The cells were treated with NL-1 drug and an equivalent dose of NL-1 nanoparticles during the period of recovery. After the 24-hour recovery, 50 µL of Amplex Red working reagent was added to each well and allowed to react in dark at room temperature for 30 minutes. The amount of hydrogen peroxide in each well was measured by fluorimetry using the BioTek Synergy H1 plate reader (BioTek Instruments, Winooski, VT), at an excitation and emission wavelength of 530 nm and 590 nm, respectively. The data of each plate was normalized for the control wells of that plate, and then compared with other plate replicates.

Effect of NL-1 nanoparticles on cellular apoptosis following OGD

The ability of NL-1 nanoparticles to reduce apoptosis and enhance cell survival was determined in bEnd.3 cells using the Annexin V assay. Cells were plated in 6-well plates at a seeding density of 150,000 cells per well. After approximately 24 hours, cells were subjected to OGD, and allowed to recover with concurrent drug and nanoparticle treatments. 1 µM and 10 µM were the two concentrations of NL-1 and an equivalent dose of nanoparticles tested. After about 24 hours, cells were stained with Annexin V-FITC and propidium iodide, following which, they were sorted into live, early apoptotic, late apoptotic and necrotic populations using BD LSRFortessa analyzer, and analyzed using the BD FACS Diva 8.0 software. The cytoprotective ability of NL-1 nanoparticles was determined as a function of percentage of live cells present.

Toxicity studies on PLGA nanoparticles

The cytotoxicity of blank and NL-1 loaded PLGA nanoparticles was tested on hepatic HepG2 cells, using the MTT assay. Cells were plated in clear 96-well plates at a seeding density of 10,000 cells per well. The cells were treated with blank nanoparticle suspensions over a range of concentrations. A highest concentration of 10 mg/mL freeze dried nanoparticles was used for treatment. The cells were allowed to grow for 72 hours after treatments. Upon completion of the treatment incubation period, 50 µL of 1 mg/mL MTT solution was added to each well and the plates were incubated for two hours. After two hours, the MTT and media mix was aspirated, and the formazan crystals were dissolved in DMSO at 37°C, for one hour on a shaker at 150 rpm (Benchmark Incu-shaker mini). The analysis was carried out by measuring the absorbance at 570 nm using the BioTek Synergy H1 plate reader (BioTek Instruments, Winooski, VT). All treatments were performed in triplicates.

Hemolysis studies on PLGA nanoparticles were performed based on a previously used method[20], using mouse blood. The blood was centrifuged to remove plasma and serum. The blood was subsequently washed thrice with 0.9% normal saline, and the volume was made up to original volume after the third wash. The blood solution was further diluted 1:10 in normal saline for the assay. An approximate dose of 5 mg/kg for a mouse was calculated, and the required amount of freeze dried nanoparticles were weighed and resuspended in 0.9% normal saline. Following treatments were used: blank nanoparticles, NL-1 loaded nanoparticles, 10 µM NL-1 drug, negative control (0.9% normal saline), and positive control (1% Triton X-100). One hundred microliters of the treatment solutions were diluted with 700 µL 0.9% normal saline, to which 200 µL of blood cells were added. The tubes were incubated at 37°C for 1 hour. After incubation, the tubes were centrifuged, and the supernatant was used for analysis. The sample absorbance was measured at 405 nm and the percent hemolysis was calculated using the following formula:

$$\frac{Sample\ absorbance - absorbance\ of\ negative\ control}{Absorbance\ of\ positive\ control - absorbance\ of\ negative\ control} \, x \, 100$$

Statistical analysis:

Statistical analysis of data obtained was carried out by GraphPad Prism 7.04 (GraphPad Software, CA) using one-way ANOVA followed by Dunnett's post hoc test for comparison of multiple groups. The graphs were prepared using GraphPad Prism 7.04. Data are presented as mean with standard deviations. A statistically significant difference between groups was considered if the p value was <0.05.

4.3. Results

Preparation and characterization of NL-1 loaded PLGA nanoparticles

The nanosuspension and the freeze-dried nanoparticles were characterized for their particle size and zeta potential. The particle size of blank and NL-1 loaded nanoparticles was found to be 121.9 $\pm$ 20.6 nm (n=5) and 123.9 $\pm$ 17.1 nm (n=12), respectively. The polydispersity index (PDI) of blank nanoparticles was found to be 0.17 $\pm$ 0.09, whereas the NL-1 loaded nanoparticles have a greater PDI of 0.27 $\pm$ 0.08. The particle size of freeze-dried nanoparticles upon resuspension was found to have increased to 175.6 $\pm$ 6.8 nm (n=12), while the PDI was found to be 0.10 $\pm$ 0.02. The zeta potential of blank and NL-1 loaded nanoparticles was found to be -16.8 $\pm$ 5.8 m V (n=3) and -26.2 $\pm$ 1.3 mV (n=3), respectively. The results for particle size and zeta potential results are summarized in **Table 4.1**. The freeze-dried nanoparticles in suspension were found to maintain their particle size in the range of 168-180 nm over a period of 60 days (data not shown). SEM imaging showed a spherical morphology for blank and NL-1 loaded nanoparticles. **Figure 4.1** shows the SEM

images for blank and NL-1 loaded nanoparticles. Scanning electron microscopy confirmed the particle sizing results, as the nanoparticles were found to be in the general size range of 100 nm.

The LC-MS/MS method for analysis of NL-1 was successfully modified and used for studying the entrapment efficiency of NL-1 and the *in vitro* release. The entrapment efficiency of NL-1 in the current PLGA formulation was found to be 59.7 ± 10.1 %. To determine the physical state of NL1 in the nanoparticles, X-ray diffraction was performed on NL-1 drug, blank nanoparticles, NL-1 loaded nanoparticles, and a physical mixture of NL-1 drug and blank nanoparticles, as shown in **Figure 4.2**. NL-1 drug was found to show a very specific X-ray diffraction pattern, with multiple sharp peaks. The patterns of blank and NL-1 loaded nanoparticles were found to almost coincide, showing that these have similar physical character. The pattern obtained for physical mixture of NL-1 drug and blank nanoparticles showed an intermediate pattern. The NL-1 peaks were clearly seen, along with the peaks seen with the nanoparticle only samples, albeit of lesser intensity.

In vitro release of NL-1 from nanoparticles

The *in vitro* release of NL-1 and NL-1 from the PLGA nanoparticles was plotted as cumulative percent release as a function of time, shown in **Figure 4.3**. It was seen that NL-1 drug and NL-1 nanoparticles had a $78.7 \pm 21.6\%$ and $79.1 \pm 7.2\%$ drug release after a time period of 24 hours, respectively. NL-1 drug was found to have a faster diffusion as compared to the release of NL-1 from formulation up to a 12-hour period. NL-1 and NL-1 nanoparticles have a 50% release at about 4 and 14 hours, respectively. The *in vitro* release studies demonstrate that the PLGA nanoparticles have a slower release of NL-1 as compared to the pure NL-1 drug. The release is slower during the phase between 6-20 hours. The nanoparticles do not sustain the release of NL-1, as the eventual plateau phase of release is reached almost concurrently for both, the pure drug and the nanoparticles, at 48 hours.

Cellular uptake of nanoparticles

The time-dependent uptake of rhodamine nanoparticles in bEnd.3 cells was analyzed using flow cytometry analysis. **Figure 4.4** shows an overlay for the representative flow cytometry histograms for each time point, along with the uptake quantification. Two negative controls, untreated cells and cells treated with blank nanoparticles showed low fluorescence intensities as seen in the histograms. The positive control of rhodamine nanoparticles had high fluorescence intensity, indicated with a right shift in the histogram (data not shown). The rhodamine nanoparticle treated cells showed a marginal shift beyond the threshold value. Upon quantification, it was found that 1-hour incubation showed a significantly higher rhodamine fluorescence as compared to the negative controls. The uptake was found to be significantly higher at 3 hours as compared to 1 hour. However, after 3 hours the uptake showed a plateauing as there was no statistically significant difference in fluorescence intensities at 3, 6 and 24 hours. We tested the energy dependence of rhodamine nanoparticle uptake by comparing uptake at 37°C to that of 4°C **(Figure 4.5)**. Compared to the nanoparticle uptake at 37°C, the uptake was significantly lowered during treatment at 4°C, as seen from the left shift in the fluorescence histogram. The fluorescence intensity at 4°C was similar to the negative control with no significant difference between the two. We further tried to delineate the mechanism of nanoparticle uptake by treating cells with specific uptake inhibitors, such as amiloride hydrochloride hydrate for phagocytosis, chlorpromazine hydrochloride for receptor mediated endocytosis, and genistein for caveolar mediated endocytosis. The uptake was quantified by measuring the rhodamine fluorescence by flow cytometry **(Figure 4.6)**. The caveolar endocytosis inhibitor genistein was found to significantly reduce the uptake of rhodamine nanoparticles into bEnd.3 cells to 61.8% as compared to the uptake into untreated cells.

Amiloride HCl and Chlorpromazine HCl which inhibit phagocytosis and clathrin mediated endocytosis, respectively, were found to have no significant effect on rhodamine nanoparticle uptake.

Cellular localization of nanoparticles

The cellular localization studies were performed using fluorescent rhodamine nanoparticles as seen in F**igure 4.7**. Confocal microscopy was used to image the nanoparticles in bEnd.3 cells that were immune stained for β-tubulin (green) and nucleus was stained with DAPI (blue). The images are shown as individual channels of DAPI for nucleus, FITC for β-tubulin and red for rhodamine. The merged image shows localization of nanoparticles in the cytoplasmic region of the cells, within the tubulin cytoskeleton. The second panel **(Figure 4.7, E-H)** shows the z-stack images of cells, which confirm the presence of rhodamine nanoparticles in the cytoplasm of the cells. **Figure 4.7I** shows a super resolution image, with nanoparticle localization in the cytoplasm.

NL-1 nanoparticles reduce hydrogen peroxide generation

The efficacy of NL-1 nanoparticles in reducing ROS generation was studied by subjecting bEnd.3 cells to OGD conditions for a period of 3 or 6 hours, and a reperfusion period of 24 hours **(Figure 4.8)**. The hydrogen peroxide produced was measured using the Amplex Red assay, and each treatment was compared to control. It was found that the NL-1 nanoparticles had a significant effect in reducing the peroxide produced at a NL-1 dose of 2.5 μM, for a stroke period of 3 hours. However, the efficacy of NL-1 nanoparticles was seen to decrease for a stroke period of 6 hours, as significant reduction in peroxide levels was only seen at 10 μM and 20 μM NL-1 dose. **Figures 4.8C and 4.8D** compare the effect of nanoparticles against that of pure NL-1 drug. For 3 hour

OGDR, NL-1 loaded nanoparticles were found to be more efficacious as compared to NL-1 drug, while such an effect was not seen at 6-hour ischemia period.

NL-1 nanoparticles improve cell survival and reduce apoptosis

The cells were exposed to either 3 or 6 hours of ischemia, with subsequent treatment with 1 μM and 10 μM of NL-1 and equivalent dose of NL-1 nanoparticles. The cells were differentiated into four categories based on their staining. The live cells are unstained, the cells in early apoptosis pick up a stronger signal of Annexin V-FITC, while the cells in late apoptosis and necrotic phase have a strong PI signal. The results are expressed as percent survival of cells and percent of cells in late apoptotic phase. **Figure 4.9 A-D** are representative images showing flow cytometry data, and quantified in **Figure 4.9 E-H**. The cells undergoing apoptosis were predominantly found to be in the late apoptotic stage. The cell survival for control for 3-hour ischemia was found to be 44.4 ± 2.8%. NL-1 drug improved cells survival to 58.3 ± 2.3% at a concentration of 10 μM, however no significant improvement in cell survival was seen at 1 μM concentration. In contrast, the equivalent dose of nanoparticles significantly improved cell survival at both 1 μM (57.5 ± 3.0%) and 10 μM dose (65.7 ± 0.2 %). Correspondingly, there was a decrease in the percent of cells in late apoptosis for 10 μM NL-1, 1 μM NL-1 nanoparticles and 10 μM NL-1 nanoparticles. The NL-1 nanoparticles showed a significantly higher efficacy as compared to the corresponding concentration of NL-1 drug. For an ischemic period of 6 hours, the control showed a survival of 40.4 ± 1.1%. NL-1 drug showed improved cell survival at both 1 μM (56.2 ± 1.4%) and 10 μM (71.0 ± 1.4%). Enhanced cell survival was also seen for NL-1 nanoparticles at 1 μM (57.3 ± 2.3%) and 10 μM (69.8 ± 4.3%) concentrations. A corresponding significant decrease was seen in the percentage of cells in late apoptosis for all treatments. However, there was no significant difference in the efficacy of NL-1 nanoparticles and the NL-1 drug for the 6-hour ischemic period.

NL-1 nanoparticle formulation was non-toxic

The inherent toxicity of blank and NL-1 loaded PLGA nanoparticles was studied using MTT cytotoxicity assay on hepatic HepG2 cells **(Figure 4.10A)**. A wide concentration range of blank nanoparticles was used for the assay, with the highest concentration of 10 mg/mL. HepG2 cell survival was found to be about $95.9 \pm 5.6\%$ at a nanoparticle concentration of 1 mg/mL and was found to reduce to $68.2 \pm 2.5\%$ at the highest treatment concentration of 10 mg/mL, in blank PLGA nanoparticles. For NL-1 loaded nanoparticles, the cell survival was found to be $80.4 \pm 11.4\%$, and $58.1 \pm 7.8\%$ at 1 mg/mL and 10 mg/mL, respectively. The second toxicity parameter that was investigated was the potential of PLGA nanoparticles to cause hemolysis of erythrocytes, since the nanoparticles are intended for intravenous administration **(Figure 4.10B)**. The positive control of 1% v/v Triton X-100 NL-1 showed 100% hemolysis. The NL-1 drug was found to have a slightly higher hemolysis as compared to blank and NL-1 loaded nanoparticles, which showed an almost zero percent hemolysis. The results obtained show that neither the blank nor the NL-1 loaded nanoparticles showed any hemolytic activity.

4.4. Discussion

The goal of the current study was to formulate the mitoNEET ligand, NL-1, into a nanoparticle dosage form, for use in ischemia reperfusion injury. Targeting mitochondrial dysfunction post-stroke is an attractive drug target, as both neuronal cells and blood—brain barrier endothelium cells are affected with ischemia reperfusion injury. Here we were able to develop formulation strategy for NL-1, with an optimized activity profile in contrast to the drug alone.

The blank and NL-1 loaded PLGA nanoparticles were prepared successfully using emulsification and solvent evaporation technique. The formulation employed acid end capped

PLGA, a biodegradable polymer, which hydrolyzes into the inert lactic acid and glycolic acid residues[21]. Emulsification and solvent evaporation is a commonly used technique for the preparation of PLGA nanoparticles. The polymer is dissolved in organic solvent that is present as globules in the continuous aqueous phase, stabilized on the interface by the surfactants (PVA and Kolliphor P188). During solvent evaporation, the solvent diffuses into the continuous external phase, causing the formation of nanoparticles upon aggregation and desolvation of the globules[22]. Formulation parameters such as solvent, surfactants and their concentrations, polymer concentrations were studied to arrive at the final formulation. The choice of solvent used to dissolve polymer can be critical, as the nanoparticle size is a function of solvent diffusion out of the droplets during evaporation[23]. Dichloromethane, ethyl acetate and acetone were tried as solvents alone and in combination. Surfactants align at the organic-aqueous interface and stabilize the system by reducing the interfacial tension[24]. Thus, the use of an ideal surfactant would dictate the stability of the formulation. Non-ionic surfactants such as PVA, Kolliphor P188, and Kolliphor P407 were tried at concentrations of 0.5% w/v and 1% w/v, as well as in combinations. The surfactant combination yielding the most stable formulation, without affecting the particle size range was found to be 1% w/v PVA and 0.5% w/v Kolliphor P188. Finally, the concentration of PLGA to be used (2% w/v) was decided based upon the gradual increase in particle size observed with increasing PLGA concentration. Higher aggregation observed at PLGA concentrations above 3% w/v made it imperative to limit the PLGA concentrations at 2%. Size exclusion chromatography is a frequently used technique for the separation of the unentrapped drug from the obtained nanoparticles[25–27]. The free NL-1 was separated from the PLGA nanoparticles using the Sephadex G-50 column for size exclusion. PLGA nanoparticles in aqueous solution could be vulnerable to hydrolytic cleavage, resulting in instability of the nanoparticles. Hence, the formulation was freeze dried for long-term storage. The use of a cryoprotectant such as mannitol

during freeze drying was warranted in order to prevent physical damage to the nanoparticles due to mechanical stress of freezing and dehydration[28,29]. The use of cryoprotectant also allows for rapid redispersion of the nanoparticles back into an aqueous solution[28]. The NL-1 nanoparticles are intended for delivery to treat ischemic stroke in the long term, which would require them to traverse the blood brain barrier (BBB). A nanoparticle size of under 200 nm has been found to be desirable for effective treatment of diseases of the CNS[30–32]. The particle size of NL-1 loaded PLGA nanoparticles in suspension as well as upon redispersion was found to be under 200 nm. The zeta potential of the nanoparticles was found to be in the moderately negative range (anionic). This was expected due to the use of acid-end capped PLGA during nanoparticle synthesis. For the purposes of formulation stability, a zeta potential further away from the neutral range is preferred, as repulsion between similarly charged particles is likely to prevent their aggregation. Nanoparticle surface charge has been found to have an impact on the BBB and their brain uptake as well. A low concentration anionic nanoparticles were found to be non-toxic to the BBB, and also showed a higher brain uptake[33]. This formulation thus has a potential for efficient delivery of NL-1 to the ischemic region in the brain, and at the same time not have a global BBB disruptive effect.

These results indicate that NL-1 is present in a different physical state in the nanoparticles, in contrast to its native crystalline form, and there is a definite reduction in crystallinity of the drug. The physical state of drug can impact the release of the drug from the nanoparticles, with crystalline form offering impedance[34]. The presence of NL-1 in a non-crystalline form (amorphous or dissolved) could lead to an efficient drug release. The nanoparticles do not sustain the release of NL-1, as the eventual plateau phase of release is reached almost concurrently for both, the pure drug and the nanoparticles, at 48 hours. The non-sustained release of NL-1 could be required, since neurodegeneration following stroke is a time dependent phenomenon. A successful rescue of

greater percentage of cells would require a quicker drug treatment. The release models that showed the best fit include Korsmeyer-Peppas (R^2: 0.9933), and first order release model (R^2: 0.9812).

The R^2 values obtained for the other models are summarized in **table 4.2**. The exponent for Korsmeyer-Peppas fit was found to be 0.768. The Korsmeyer-Peppas model of drug release is used for the first 60% of the release data, and can be helpful in determining the mechanism of drug release[35,36]. The exponent of 0.768 in the Korsmeyer-Peppas fit of the release kinetics points toward non-Fickian or anomalous release being the primary release mechanism of NL-1. The release of NL-1 from PLGA nanoparticles is a possible combination of NL-1 diffusion and PLGA erosion. A drawback of Korsmeyer-Peppas release model is that fact that it is used only for first 60% of the drug released. When the entire release data was fit to a model, it was found to be close to first-order model. First order kinetics imply that the release of drug from the nanoparticles is dependent on the concentration of the drug present in the system.

The first step toward effective treatment of cells by nanoparticles would require uptake of the nanoparticles by the cells. Rhodamine nanoparticles were prepared and characterized for particle size under a fluorescent filter on the Nanosight (data not shown). This was useful in optimizing the wash-outs needed for the nanoparticles to eliminate background fluorescence, and to confirm the presence of fluorescent nanoparticles. The studies were performed in bEnd.3 endothelial cells, a commonly used model for *in vitro* stroke studies[37–39]. The time-dependent uptake of rhodamine nanoparticles in bEnd.3 cells was analyzed using flow cytometry analysis. The significantly higher uptake after 1 hour could possibly be beneficial for cell rescue, which can be a time sensitive phenomenon. The significantly lowered nanoparticle uptake at 4°C could suggest that the functioning of proteins and enzymes involved in endocytosis is inhibited at lower temperatures and is an energy-dependent active process. We further tried to delineate the

mechanism of nanoparticle uptake by treating cells with specific uptake inhibitors, such as amiloride hydrochloride hydrate for phagocytosis, chlorpromazine hydrochloride for receptor mediated endocytosis, and genistein for caveolar mediated endocytosis. The uptake was quantified by measuring the rhodamine fluorescence by flow cytometry **(Figure 4.6)**. The most prominent mechanisms of nanoparticle uptake into cells include phagocytosis, clathrin mediated endocytosis, and caveolar/lipid raft endocytosis. Phagocytosis is an actin-dependent uptake mechanism, which is generally mediated by specialized cells such as macrophages, suitable to particles around 500 nm in size[40]. Clathrin mediated endocytosis involves binding of cargo (nanoparticles) to specific receptors on the cell surface, leading to downstream recruitment of proteins that help internalize the nanoparticles into a 'coated pits'[41]. Caveolar endocytosis is mediated by components of lipid rafts and occurs in cholesterol rich regions of the plasma membrane. These are vesicles formed by cell membrane invaginations[42]. Each of the above mechanism was individually inhibited by using specific inhibitors. A single concentration of inhibitors was used for each mechanism, based on literature[41–43]. Lipid raft or caveolar mediated endocytosis was thus found to be the prominent mode of nanoparticle uptake. Genistein is an inhibitor of receptor associated tyrosine kinases, involved in the caveolar uptake mechanism[44]. The caveolar invaginations can be in the size range of 50-200 nm, which would explain the endocytosis of these nanoparticles through this mechanism. Moreover, nanoparticles with an anionic surface charge are known to interact with the cationic lipid components of the lipid rafts in the cell membrane which further explains the mechanism used by the nanoparticles for their uptake[45]. Upon their uptake, it is important that the nanoparticles localize around the site of action of the drug they intend to deliver. The advantage of using confocal microscopy was the ability to image z-stacks, which provides a better understanding of the position of the nanoparticles within the cell, as compared to a twodimensional image. Cytoplasmic

localization of nanoparticles is necessary for the activity of NL1 as a mitoNEET ligand. MitoNEET is present in the outer mitochondrial membrane, and is oriented toward the cytoplasm[46].

The efficacy studies for NL-1 loaded PLGA nanoparticles were performed using the *in vitro* OGD model to mimic stroke. The studies were performed in bEnd.3 endothelial cells, a commonly used model for *in vitro* stroke studies[37–39]. HBSS supplemented with 10% FBS was used as the glucose-free medium for cell incubation in the hypoxia chamber[47,48]. Cellular toxicity following ischemic stroke is multimodal, mediated via multiple mechanisms. Cell damage due to generation of ROS and induction of apoptosis cascade are two of the primary causes of cytotoxicity. Both of these mechanisms are mitochondrial in origin and relevant sites of intervention for NL-1, since it binds the mitochondrial protein mitoNEET. We investigated the effect of NL-1 nanoparticle treatment on both of these physiologic events.

An important ROS mediator generated in mitochondria is the superoxide radical. However, measurement of superoxide produced in the mitochondria can be challenging due to the inability of probes to permeate the outer mitochondrial membrane. Hydrogen peroxide is formed as a dismutation product of superoxide radical by mitochondrial manganese superoxide dismutase enzyme[49]. It diffuses across the outer mitochondrial membrane into the extra mitochondrial space, wherein it can be quantified[50]. We determined the effect of NL-1 nanoparticles on peroxide generation using the sensitive fluorimetric Amplex Red assay[51]. Amplex Red is a colorless substance that reacts with hydrogen peroxide in presence of horseradish peroxidase in a 1:1 stoichiometry to yield a stable fluorescent compound called resorufin[52,53]. The primary challenge with this assay involves prevention of light exposure of Amplex red reagent for longer periods, and artificial generation of hydrogen peroxide by light exposure of resorufin[54,55]. The results indicate that NL-1 nanoparticles are more effective at the shorter ischemic period of 3 hours as

seen from the dose response of NL-1 nanoparticles in reducing the peroxide generation. A possible explanation for this could be that other mechanisms of cell damage might predominate for a longer duration of ischemia. ROS generation could likely be the predominant mode of cell toxicity at the shorter ischemic period. Cell damage due to ROS has been implicated in the earlier time period of ischemia[56]. We also compared the NL-1 nanoparticles to pure NL-1 drug in their ability to reduce the peroxide generation. NL-1 nanoparticles had a greater efficacy as compared to NL-1 drug during the shorter ischemia period. However, this effect was not seen for 6-hour ischemia period.

The second mechanism of cell death that has a mitochondrial dimension is apoptosis. The ability of NL-1 nanoparticles in checking apoptosis and in turn improving the cell survival was determined with the Annexin V apoptosis assay, which is commonly employed to detect apoptotic and necrotic cell populations[57,58]. We found higher protective activity of the NL-1 nanoparticles as compared to NL-1 drug-alone at the 3-hour ischemia period, however these results are not seen at the longer ischemia duration of 6 hours. Although the NL-1 nanoparticles showed a greater cell survival at both concentrations, the drug by itself was not effective at 1 µM for 3 hour ischemia period. Apoptosis in cerebral ischemia has previously been described to be a biphasic event, in which the apoptosis mediated by mitochondria occurs at a later stage[59]. It can be speculated that improved activity of NL-1 for longer ischemia period is a possible result of increased mitochondrial involvement in the apoptotic mechanisms. Further studies are needed to confirm this hypothesis. Overall, the system helped reduce apoptotic populations of bEnd.3 cells.

The inherent toxicity of blank and NL-1 loaded PLGA nanoparticles was studied using MTT cytotoxicity assay on hepatic HepG2 cells. Since liver is a primary metabolic organ, we chose to perform this test on liver cells. The survival curve shows that even the highest concentration of both, blank and NL-1-loaded PLGA nanoparticles did not induce a 50% cell death, and an IC_{50}

value could not be established. The concentration of 10 mg/mL was at least five times higher than the highest concentration of nanoparticles used for efficacy studies. This is indicative that the results obtained were not affected by any inherent nanoparticle toxicity. The second toxicity parameter that was investigated was the potential of PLGA nanoparticles to cause hemolysis of erythrocytes, since the nanoparticles are intended for intravenous administration. This assay is indicative of effect of the nanoparticles on cell membrane integrity[60]. The blood cells were incubated with NL-1 drug, blank nanoparticles and NL-1 loaded nanoparticles, and the absorbance was measured as a function of hemolysis. PLGA nanoparticles have been found to have non-existent hemolysis[60], which was confirmed with the current assay. Thus, the formulation was deemed safe for intravenous administration.

In summary, we report a successful formulation of the hydrophobic drug NL-1 into a PLGA polymeric nanoparticle system, with a reasonable entrapment efficiency. Our data indicate that the NL-1 loaded nanoparticles are effective in reducing oxidative stress arising from peroxide, and improving the cell survival, in an *in vitro* stroke model.

4.5. References:

1.   Stroke Facts | cdc.gov. https://www.cdc.gov/stroke/facts.htm. Accessed September 6, 2019.

2.   Jung JE, Kim GS, Chen H, et al. Reperfusion and Neurovascular Dysfunction in Stroke: from Basic Mechanisms to Potential Strategies for Neuroprotection. *Mol Neurobiol*. 2010;41(2-3):172-179. doi:10.1007/s12035-010-8102-z

3.   Doyle KP, Simon RP, Stenzel-Poore MP. Mechanisms of ischemic brain damage. *Neuropharmacology*. 2008;55(3):310-318. doi:10.1016/J.NEUROPHARM.2008.01.005

4. Colca JR, McDonald WG, Waldon DJ, et al. Identification of a novel mitochondrial protein ("mitoNEET") cross-linked specifically by a thiazolidinedione photoprobe. *Am J Physiol - Endocrinol Metab*. 2003;286(2). http://ajpendo.physiology.org/content/286/2/E252.long. Accessed June 10, 2017.

5. Lin J, Zhou T, Ye K, Wang J. Crystal structure of human mitoNEET reveals distinct groups of iron-sulfur proteins. *Proc Natl Acad Sci U S A*. 2007;104(37):14640-14645. doi:10.1073/pnas.0702426104

6. Sandra E. Wiley, Mark L. Paddock ECA, Larry Gross, Peter van der Geer RN, Anne N. Murphy, Patricia A. Jennings and JED. The Outer Mitochondrial Membrane Protein mitoNEET Contains a Novel Redox-active 2Fe-2S Cluster. *J Biol Chem*. 282(33):23745-23749. doi:10.1074/jbc.C700107200

7. Tamir S, Paddock ML, Darash-Yahana-Baram M, et al. Structure-function analysis of NEET proteins uncovers their role as key regulators of iron and ROS homeostasis in health and disease. *Biochim Biophys Acta - Mol Cell Res*. 2015;1853(6):1294-1315. doi:10.1016/j.bbamcr.2014.10.014

8. Golinelli-Cohen MP, Lescop E, Mons C, et al. Redox control of the human iron-sulfur repair protein MitoNEET activity via its iron-sulfur cluster. *J Biol Chem*. 2016;291(14):7583-7593. doi:10.1074/jbc.M115.711218

9. Landry AP, Ding H. Redox control of human mitochondrial outer membrane protein MitoNEET [2Fe-2S] clusters by biological thiols and hydrogen peroxide. *J Biol Chem*. 2014;289(7):4307-4315. doi:10.1074/jbc.M113.542050

10. Zhou T, Lin J, Feng Y WJ. Binding of Reduced Nicotinamide Adenine Dinucleotide Phosphate Destabilizes the Iron-Sulfur Clusters of Human MitoNEET. *Biochemistry*. 49(44):9604-9612. doi:10.1021/bi101168c

11. Landry AP, Wang Y, Cheng Z, Crochet RB, Lee YH DH. Flavin nucleotides act as electron shuttles mediating reduction of the [2Fe- 2S] clusters in mitochondrial outer membrane protein mitoNEET. *Free Radic Biol Med*. 102:240-247. doi:10.1016/j.freeradbiomed.2016.12.001

12. Mittler R, Darash-Yahana M, Sohn YS, et al. NEET Proteins: A new link between iron metabolism, reactive oxygen species, and cancer. *Antioxidants Redox Signal*. 2019;30(8):1083-1095. doi:10.1089/ars.2018.7502

13. Lipper CH, Paddock ML, Onuchic JN, Mittler R, Nechushtai R, Jennings PA. CancerRelated NEET Proteins Transfer 2Fe-2S Clusters to Anamorsin, a Protein Required for
Cytosolic Iron-Sulfur Cluster Biogenesis. Levy YK, ed. *PLoS One*. 2015;10(10):e0139699. doi:10.1371/journal.pone.0139699

14. He Q-Q, Xiong L-L, Liu F, et al. MicroRNA-127 targeting of mitoNEET inhibits neurite outgrowth, induces cell apoptosis and contributes to physiological dysfunction after spinal cord transection. *Sci Rep*. 2016;6:35205. doi:10.1038/srep35205

15. Geldenhuys WJ, Benkovic SA, Lin L, et al. MitoNEET (CISD1) Knockout Mice Show Signs of Striatal Mitochondrial Dysfunction and a Parkinson's Disease Phenotype. *ACS Chem Neurosci*. 2017;8(12):2759-2765. doi:10.1021/acschemneuro.7b00287

16. Patel SP, Cox DH, Gollihue JL, et al. Pioglitazone treatment following spinal cord injury maintains acute mitochondrial integrity and increases chronic tissue sparing and functional recovery. *Exp Neurol*. 2017;293:74-82. doi:10.1016/j.expneurol.2017.03.021

17. Geldenhuys WJ, Funk MO, Barnes KF, Carroll RT. Structure-based design of a thiazolidinedione which targets the mitochondrial protein mitoNEET. *Bioorganic Med Chem Lett*. 2010;20(3):819-823. doi:10.1016/j.bmcl.2009.12.088

18. Logan SJ, Yin L, Geldenhuys WJ, et al. Novel thiazolidinedione mitoNEET ligand-1 acutely improves cardiac stem cell survival under oxidative stress. *Basic Res Cardiol*. 2015;110(2):19. doi:10.1007/s00395-015-0471-z

19. Pedada KK, Zhou X, Jogiraju H, et al. A quantitative LC?MS/MS method for determination of thiazolidinedione mitoNEET ligand NL-1 in mouse serum suitable for pharmacokinetic studies. *J Chromatogr B*. 2014;945-946:141-146. doi:10.1016/j.jchromb.2013.11.048

20. Saralkar P, Dash AK. Alginate Nanoparticles Containing Curcumin and Resveratrol: Preparation, Characterization, and *In vitro* Evaluation Against DU145 Prostate Cancer Cell Line. *AAPS PharmSciTech*. 2017;18(7). doi:10.1208/s12249-017-0772-7

21. Lemoine D, Francois C, Kedzierewicz F, Preat V, Hoffman M, Maincent P. Stability study of nanoparticles of poly(ε-caprolactone), poly(D,L-lactide) and poly(D,L-lactide-coglycolide). *Biomaterials*. 1996;17(22):2191-2197. doi:10.1016/0142-9612(96)00049-X

22. Kwon H-Y, Lee J-Y, Choi S-W, Jang Y, Kim J-H. Preparation of PLGA nanoparticles containing estrogen by emulsification–diffusion method. *Colloids Surfaces A Physicochem Eng Asp*. 2001;182(1-3):123-130. doi:10.1016/S0927-7757(00)00825-6

23. Cooper DL, Harirforoosh S. Design and Optimization of PLGA-Based Diclofenac Loaded Nanoparticles. Sem DS, ed. *PLoS One*. 2014;9(1):e87326. doi:10.1371/journal.pone.0087326

24. Sharma N, Madan P, Lin S. Effect of process and formulation variables on the preparation of parenteral paclitaxel-loaded biodegradable polymeric nanoparticles: A co-surfactant study. *Asian J Pharm Sci*. 2016;11(3):404-416. doi:10.1016/J.AJPS.2015.09.004

25. Dangi RS, Shakya S. Preparation, optimization and characterization of PLGA nanoparticle. *Int J Pharm Life Sci*. 2013;4(7):2810-2818.

26. Guo J, Gao X, Su L, et al. Aptamer-functionalized PEG–PLGA nanoparticles for enhanced anti-glioma drug delivery. *Biomaterials*. 2011;32(31):8010-8020. doi:10.1016/J.BIOMATERIALS.2011.07.004

27. Wen Z, Yan Z, Hu K, et al. Odorranalectin-conjugated nanoparticles: Preparation, brain delivery and pharmacodynamic study on Parkinson's disease following intranasal administration. *J Control Release*. 2011;151(2):131-138. doi:10.1016/J.JCONREL.2011.02.022

28. Fonte P, Soares S, Costa A, et al. Effect of cryoprotectants on the porosity and stability of insulin-loaded PLGA nanoparticles after freeze-drying. *Biomatter*. 2012;2(4):329-339. doi:10.4161/biom.23246

29. Abdelwahed W, Degobert G, Stainmesse S, Fessi H. Freeze-drying of nanoparticles: Formulation, process and storage considerations. *Adv Drug Deliv Rev*. 2006;58(15):1688-1713. doi:10.1016/J.ADDR.2006.09.017

30. Cruz LJ, Stammes MA, Que I, et al. Effect of PLGA NP size on efficiency to target traumatic brain injury. *J Control Release*. 2016;223:31-41. doi:10.1016/J.JCONREL.2015.12.029

31. Hu K, Shi Y, Jiang W, Han J, Huang S, Jiang X. Lactoferrin conjugated PEG-PLGA nanoparticles for brain delivery: Preparation, characterization and efficacy in Parkinson's disease. *Int J Pharm*. 2011;415(1-2):273-283. doi:10.1016/J.IJPHARM.2011.05.062

32. Saraiva C, Praça C, Ferreira R, Santos T, Ferreira L, Bernardino L. Nanoparticle-mediated brain drug delivery: Overcoming blood–brain barrier to treat neurodegenerative diseases. *J Control Release*. 2016;235:34-47. doi:10.1016/J.JCONREL.2016.05.044

33. Lockman PR, Koziara JM, Mumper RJ, Allen DD. Nanoparticle Surface Charges Alter Blood–Brain Barrier Integrity and Permeability. *J Drug Target*. 2004;12(9-10):635-641. doi:10.1080/10611860400015936

34. Mohanty C, Sahoo SK. The *in vitro* stability and *in vivo* pharmacokinetics of curcumin prepared as an aqueous nanoparticulate formulation. *Biomaterials*. 2010;31(25):6597-6611. doi:10.1016/j.biomaterials.2010.04.062

35. Gautam Singhvi MS. In-vitro drug release characterization models. *Int J Pharm Stud Res*. 2011;2(1):77-84.

36. Jose S, Fangueiro JF, Smitha J, et al. Predictive modeling of insulin release profile from cross-linked chitosan microspheres. *Eur J Med Chem*. 2013;60:249-253. doi:10.1016/J.EJMECH.2012.12.011

37. Comajoan P, Gubern C, Huguet G, Serena J, Kádár E, Castellanos M. Evaluation of common housekeeping proteins under ischemic conditions and/or rt-PA treatment in bEnd.3 cells. *J Proteomics*. 2018;184:10-15. doi:10.1016/J.JPROT.2018.06.011

38. Wang L, Niu Y, He G, Wang J. Down-regulation of lncRNA GAS5 attenuates neuronal cell injury through regulating miR-9/FOXO3 axis in cerebral ischemic stroke. *RSC Adv*. 2019;9(28):16158-16166. doi:10.1039/C9RA01544B

39. Zhao M, Wang J, Xi X, Tan N, Zhang L. SNHG12 Promotes Angiogenesis Following Ischemic Stroke via Regulating miR-150/VEGF Pathway. *Neuroscience*. 2018;390:231-240. doi:10.1016/J.NEUROSCIENCE.2018.08.029

40. Oh N, Park J-H. Endocytosis and exocytosis of nanoparticles in mammalian cells. *Int J Nanomedicine*. 2014;9 Suppl 1:51-63. doi:10.2147/IJN.S26592

41. dos Santos T, Varela J, Lynch I, Salvati A, Dawson KA. Effects of Transport Inhibitors on the Cellular Uptake of Carboxylated Polystyrene Nanoparticles in Different Cell Lines. Schnur JM, ed. *PLoS One*. 2011;6(9):e24438. doi:10.1371/journal.pone.0024438

42. Ha S-W, Weitzmann MN, Beck GR. Bioactive Silica Nanoparticles Promote Osteoblast Differentiation through Stimulation of Autophagy and Direct Association with LC3 and p62. *ACS Nano*. 2014;8(6):5898-5910. doi:10.1021/nn5009879

43. Díaz-Moscoso A, Vercauteren D, Rejman J, et al. Insights in cellular uptake mechanisms of pDNA–polycationic amphiphilic cyclodextrin nanoparticles (CDplexes). *J Control Release*. 2010;143(3):318-325. doi:10.1016/J.JCONREL.2010.01.016

44. Parton RG, Richards AA. Lipid Rafts and Caveolae as Portals for Endocytosis: New Insights and Common Mechanisms. *Traffic*. 2003;4(11):724-738. doi:10.1034/j.1600-

0854.2003.00128.x

45. Adjei IM, Sharma B, Labhasetwar V. Nanoparticles: Cellular Uptake and Cytotoxicity. In: Springer, Dordrecht; 2014:73-91. doi:10.1007/978-94-017-8739-0_5

46. Conlan AR, Paddock ML, Axelrod HL, et al. The novel 2Fe-2S outer mitochondrial protein mitoNEET displays conformational flexibility in its N-terminal cytoplasmic tethering domain. *Acta Crystallogr Sect F Struct Biol Cryst Commun*. 2009;65(7):554-559. doi:10.1107/S1744309109019605

47. Farajdokht F, Mohaddes G, Karimi-Sales E, et al. Inhibition of PTEN protects PC12 cells against oxygen-glucose deprivation induced cell death through mitoprotection. *Brain Res*. 2018;1692:100-109. doi:10.1016/J.BRAINRES.2018.05.026

48. Minaei Beyrami S, Khadem Ansari MH, Rasemi Y, Shakib N, Karimi P. Complete inhibition of phosphatase and tensin homolog promotes the normal and oxygen-glucose deprivation/reperfusion-injured PC12 cells to cell death. *J Cardiovasc Thorac Res*. 2018;10(2):83-89. doi:10.15171/jcvtr.2018.13

49. Chan SHH, Tai M-H, Li C-Y, Chan JYH. Reduction in molecular synthesis or enzyme activity of superoxide dismutases and catalase contributes to oxidative stress and neurogenic hypertension in spontaneously hypertensive rats. *Free Radic Biol Med*. 2006;40(11):2028-2039. doi:10.1016/J.FREERADBIOMED.2006.01.032

50. Staniek K, Nohl H. Are mitochondria a permanent source of reactive oxygen species? *Biochim Biophys Acta - Bioenerg*. 2000;1460(2-3):268-275. doi:10.1016/S0005-2728(00)00152-3

51. Zhou M, Diwu Z, Panchuk-Voloshina N, Haugland RP. A Stable Nonfluorescent

Derivative of Resorufin for the Fluorometric Determination of Trace Hydrogen Peroxide: Applications in Detecting the Activity of Phagocyte NADPH Oxidase and Other Oxidases. *Anal Biochem*. 1997;253(2):162-168. doi:10.1006/ABIO.1997.2391

52. Liu Y, Ai K, Ji X, et al. Comprehensive Insights into the Multi-Antioxidative Mechanisms of Melanin Nanoparticles and Their Application To Protect Brain from Injury in Ischemic Stroke. *J Am Chem Soc*. 2017;139(2):856-862. doi:10.1021/jacs.6b11013

53. Rodrigues J V., Gomes CM. Enhanced superoxide and hydrogen peroxide detection in biological assays. *Free Radic Biol Med*. 2010;49(1):61-66. doi:10.1016/J.FREERADBIOMED.2010.03.014

54. Kalyanaraman B, Darley-Usmar V, Davies KJA, et al. Measuring reactive oxygen and nitrogen species with fluorescent probes: challenges and limitations. *Free Radic Biol Med*. 2012;52(1):1-6. doi:10.1016/J.FREERADBIOMED.2011.09.030

55. Zhao B, Summers FA, Mason RP. Photooxidation of Amplex red to resorufin: Implications of exposing the Amplex red assay to light. *Free Radic Biol Med*. 2012;53(5):1080-1087. doi:10.1016/J.FREERADBIOMED.2012.06.034

56. Dirnagl U, Simon RP, Hallenbeck JM. Ischemic tolerance and endogenous neuroprotection. *Trends Neurosci*. 2003;26(5):248-254. doi:10.1016/S0166-2236(03)00071-7

57. Ma Q, Zhao H, Tao Z, et al. MicroRNA-181c Exacerbates Brain Injury in Acute Ischemic Stroke. *Aging Dis*. 2016;7(6):705-714. doi:10.14336/AD.2016.0320

58.   Niu F, Zhang X, Hu X, et al. Targeted mutation of Fas ligand gene attenuates brain inflammation in experimental stroke. *Brain Behav Immun*. 2012;26(1):61-71. doi:10.1016/J.BBI.2011.07.235

59.   Benchoua A, Guégan C, Couriaud C, et al. Specific caspase pathways are activated in the two stages of cerebral infarction. *J Neurosci*. 2001;21(18):7127-7134. doi:10.1523/JNEUROSCI.21-18-07127.2001

60.   Fornaguera C, Calderó G, Mitjans M, Vinardell MP, Solans C, Vauthier C. Interactions of PLGA nanoparticles with blood components: protein adsorption, coagulation, activation of the complement system and hemolysis studies. *Nanoscale*. 2015;7(14):6045-6058. doi:10.1039/c5nr00733j
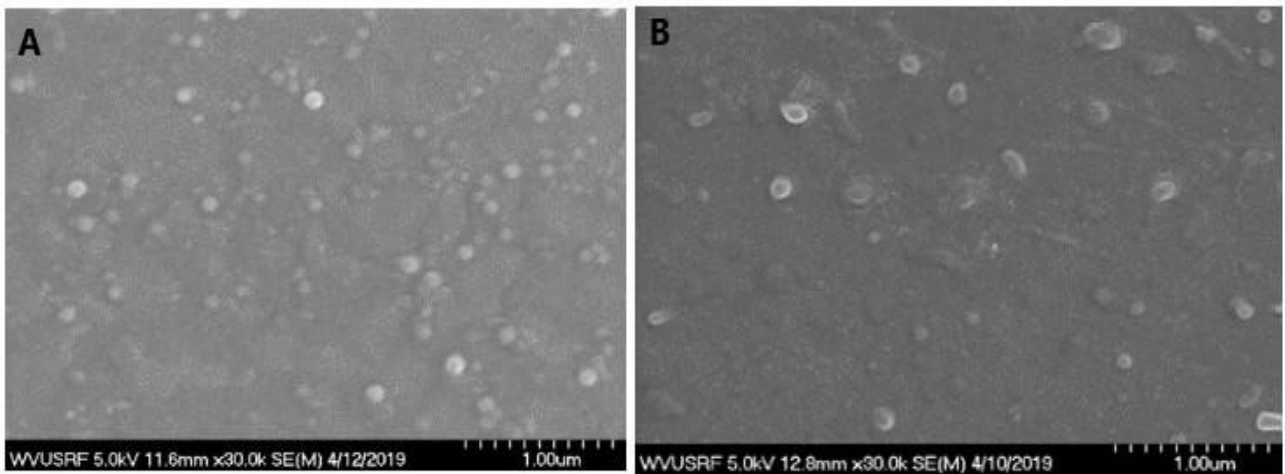
Figure 4.1: SEM images of blank PLGA nanoparticles (A) and NL-1 loaded PLGA nanoparticles (B). Each unit on the scale represents 100 nm.
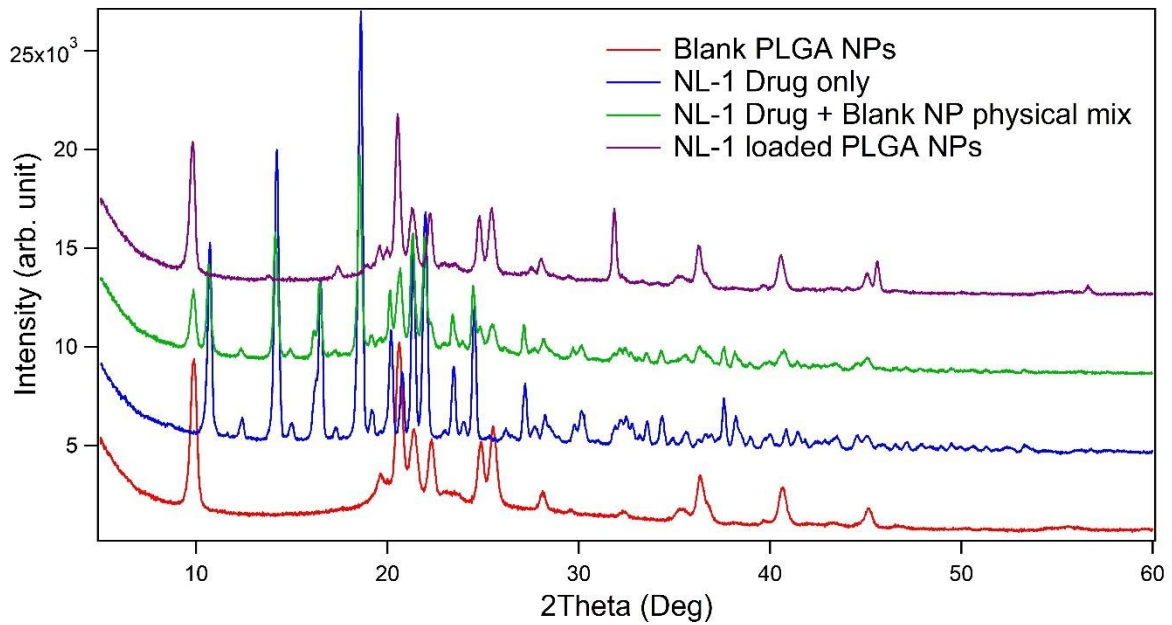
Figure 4.2: Powder X-ray diffraction pattern for NL-1 drug, NL-1 drug and blank nanoparticles physical mixture, blank PLGA nanoparticles, and NL-1 loaded PLGA nanoparticles.
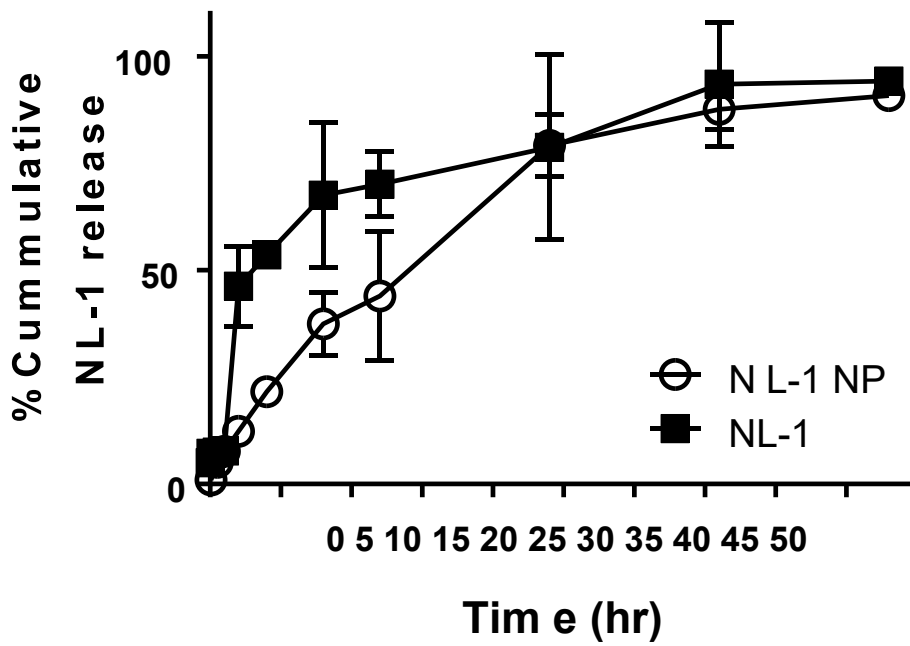

Figure 4.3: *In vitro* drug release profile for NL-1 drug and NL-1 from PLGA nanoparticles. Data are plotted as total percent cumulative NL-1 released versus time.
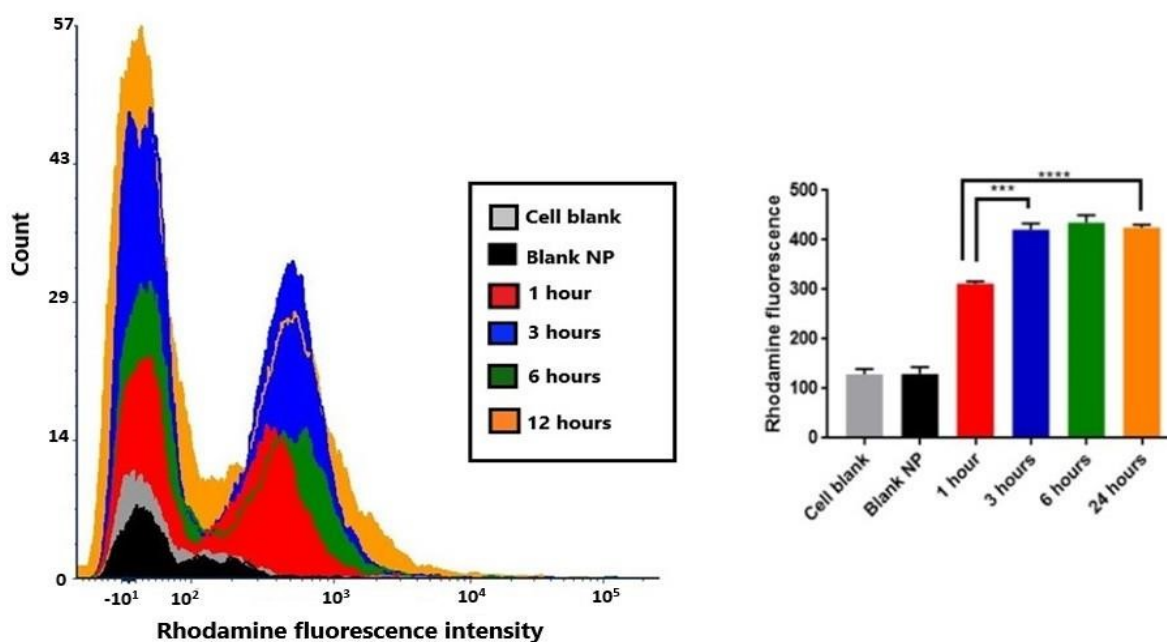
Figure 4.4: Cellular uptake of rhodamine nanoparticles in bEnd.3 cells. The flow cytometry histograms (left) are representatives for cell control, blank nanoparticles, and each time point for rhodamine nanoparticles. The graph (right) shows the quantification of rhodamine nanoparticle uptake ([***]p<0.001, [****]p<0.0001).
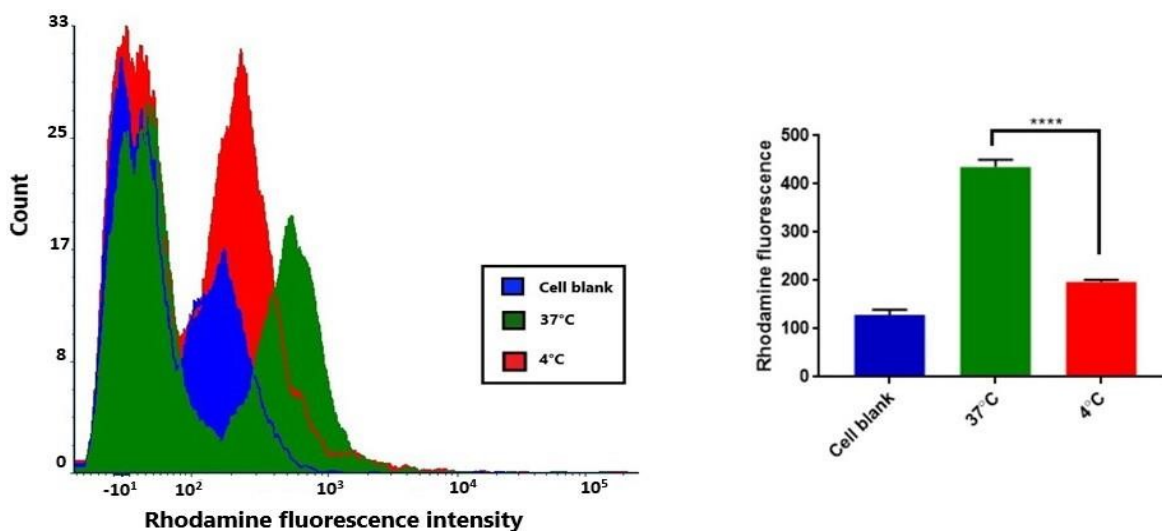

Figure 4.5: Energy dependence of nanoparticle uptake in bEnd.3 cells. Comparative flow cytometry histograms (left) for cell control, and rhodamine nanoparticle uptake at 37°C and at 4°C.

Graphical representation (right) of fluorescence intensities shows a significantly decreased uptake at 4°C (****$p<0.0001$).

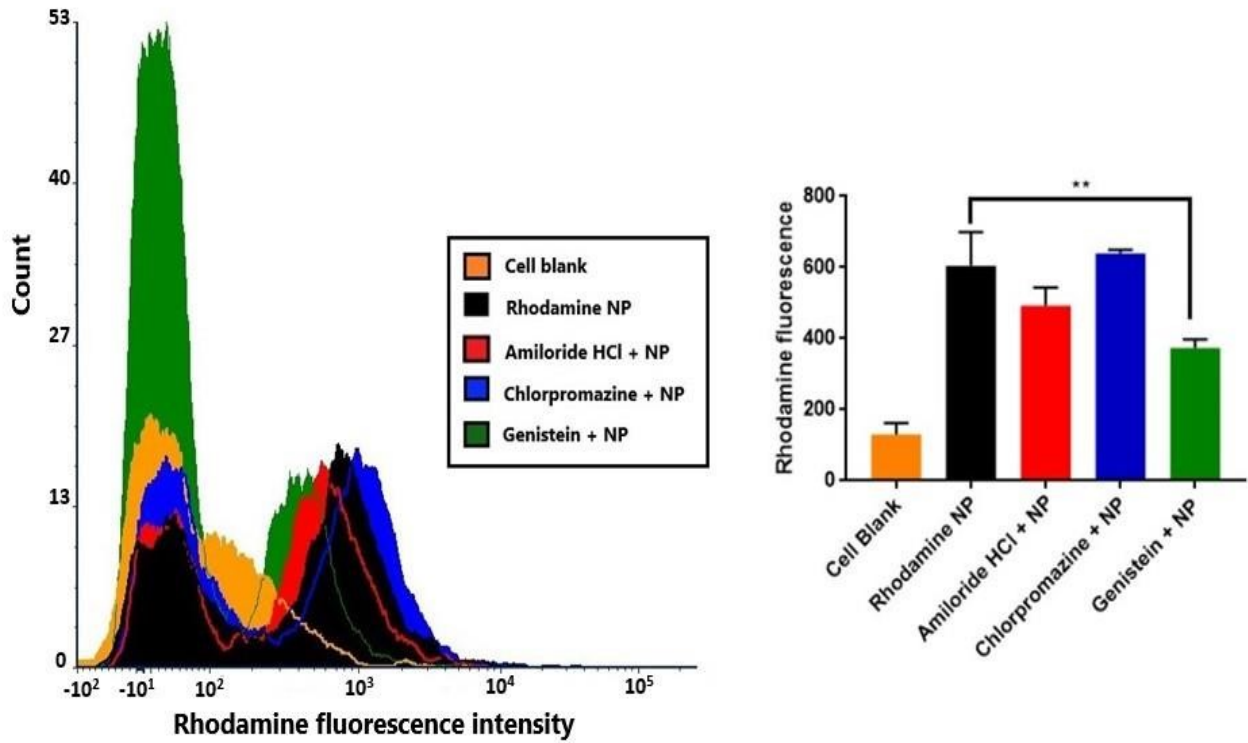**Figure 4.6:** Mechanism of rhodamine nanoparticle uptake in bEnd.3 cells. Flow cytometry histograms (left) are representatives of cell blank, rhodamine nanoparticles alone and with uptake inhibitor treatments. The plot (right) indicates the quantification of fluorescence intensity with respective uptake inhibitors, with genistein treatment showing significant reduction in uptake (**$p<0.01$).
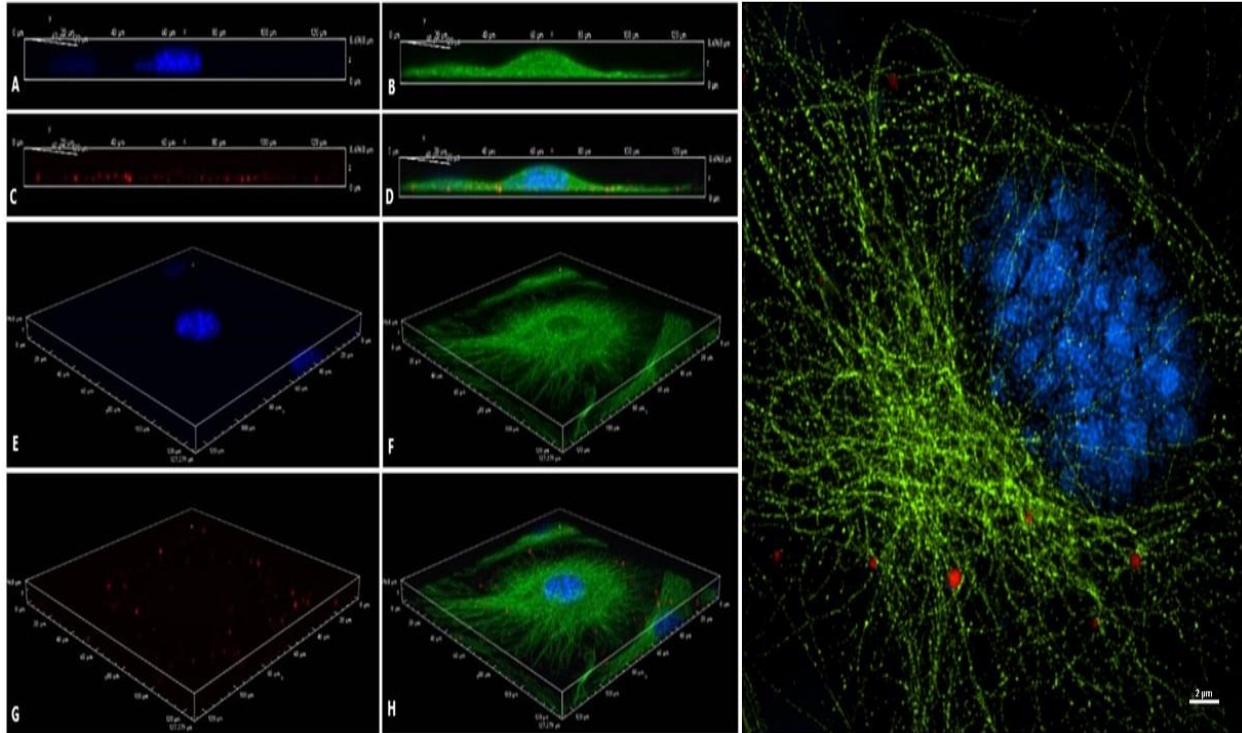
Figure 4.7: Confocal microscopy z-stack images for cellular localization of rhodamine nanoparticles in bEnd.3 cells showing nanoparticle localization in the cytoplasm. Cell nuclei stained blue with DAPI (A and E), tubulin stained green (B and F), red rhodamine nanoparticles (C and G). Images D and H show a merge of individual channels. Image I shows a super resolution image of rhodamine nanoparticles being localized in the cytoplasmic tubulin cytoskeleton.
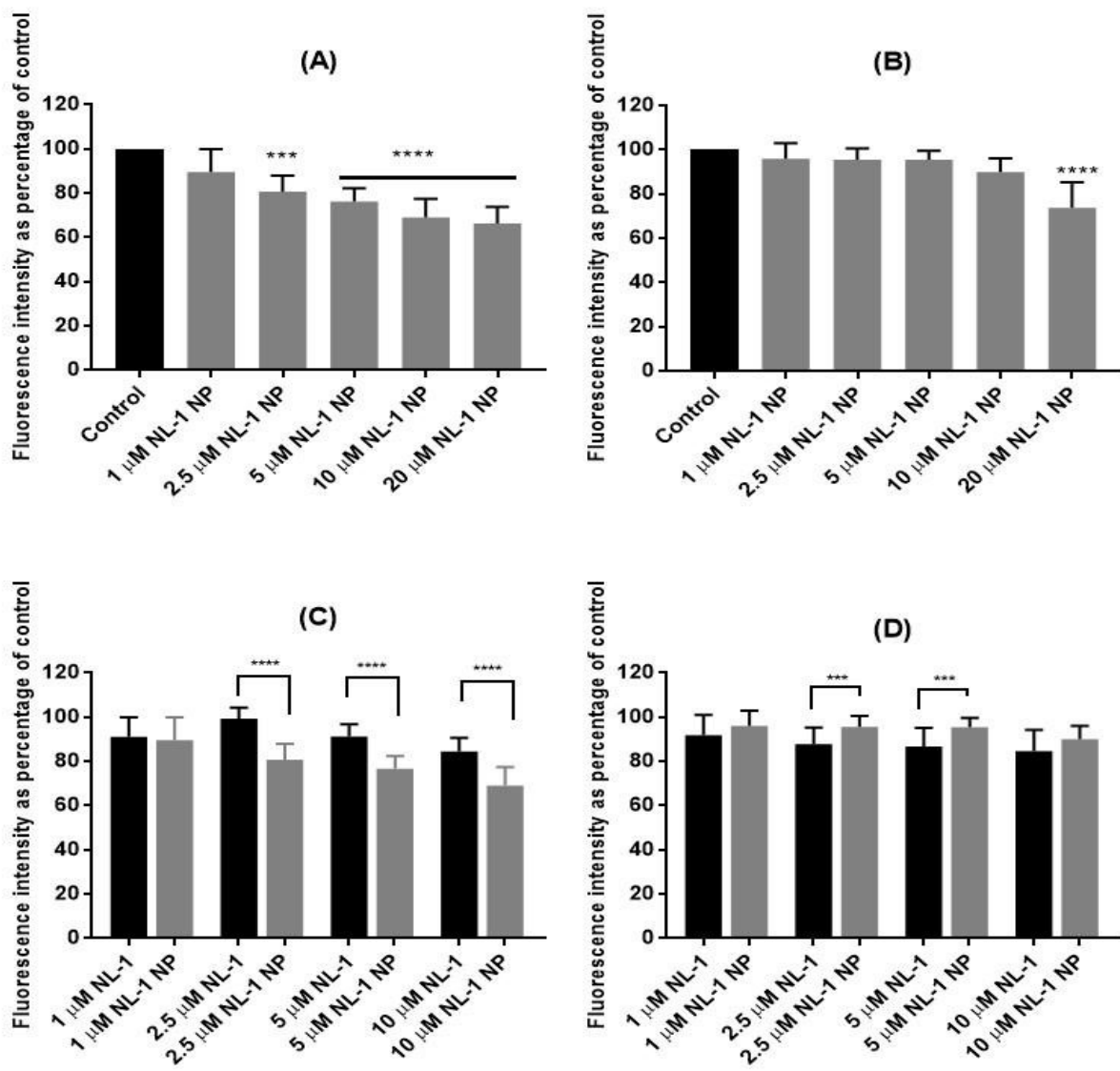
Figure 4.8: Effect of NL-1 nanoparticle treatment on generation of hydrogen peroxide in bEnd.3 cells after 3 hours (A) and 6 hours (B) of OGD. The control was considered as 100% in order to normalize values for multiple plates. The bottom panel shows a comparison in activity of NL-1 drug and NL-1 nanoparticles after 3 hours (C) and 6 hours (D) of OGD (***p<0.001, ****p<0.0001).
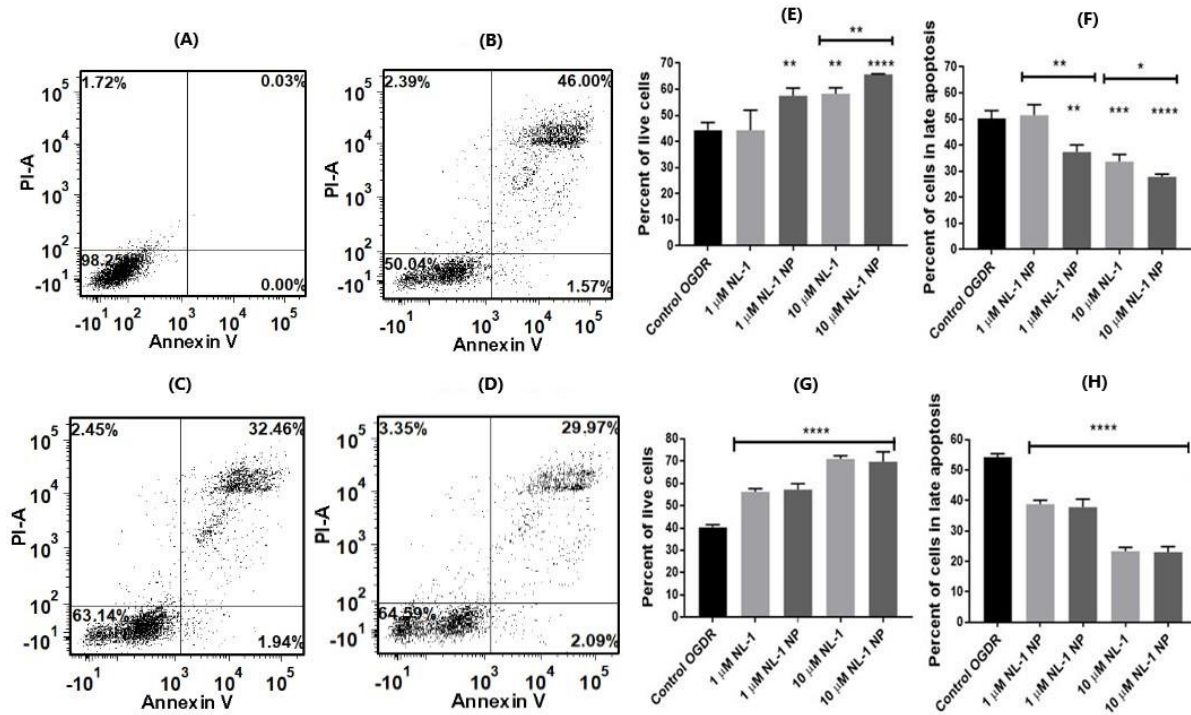
Figure 4.9: Effect of NL-1 and NL-1 nanoparticles on apoptosis in bEnd.3 cells following ischemia and reperfusion. Figures A-D are representative flow cytometry data for cell blank (A), 3 hour OGD (B), and 3 hour OGD with NL-1 (C) and 3 hour OGD with NL-1 nanoparticles (D). Each figure shows four quadrants: live (bottom left), early apoptotic phase (bottom right), late apoptotic phase (top right), and necrotic (top left) cell populations. Results are indicated in terms of improvement in cell survival at 3 hours (E) and 6 hours (F) ischemic period, as well as the reduction in late stage apoptosis after 3 hours (G) and 6 hours (H) of ischemia ($^*p<0.05$, $^{**}p<0.01$, $^{***}p<0.001$, $^{****}p<0.0001$).
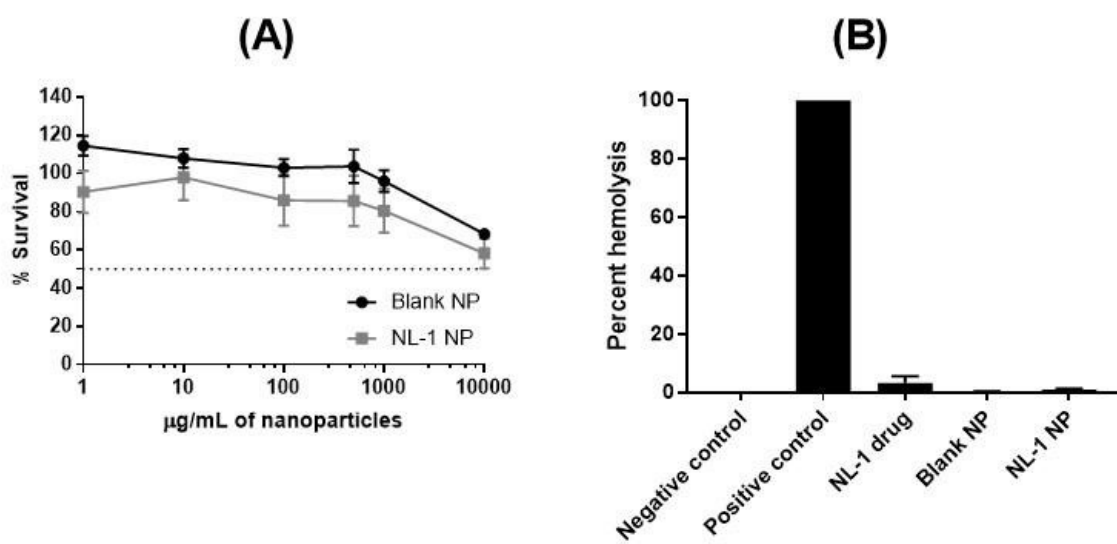
Figure 4.10: Toxicity profile of PLGA nanoparticles. MTT cytotoxicity assay results indicate a relatively safe profile for blank and NL-1 loaded PLGA nanoparticles at the highest concentration of 10 mg/mL (A). NL-1, blank and NL-1 loaded nanoparticles showed a negligible hemolytic activity (B).

Table 4.1: Particle size, polydispersity index and zeta potential of blank, NL-1 loaded and freeze dried nanoparticles

	Particle Size (nm)	Polydispersity Index	Zeta Potential (mV)
Blank PLGA NP	121.9 ± 20.6 (n=5)	0.17 ± 0.09	-16.8 ± 5.8
NL-1 loaded PLGA NP	123.9 ± 17.1 (n=12)	0.27 ± 0.08	-26.2 ± 1.3
Freeze dried nanoparticles upon re-dispersion	175.6 ± 6.8 (n=12)	0.10 ± 0.02	-26.2 ± 1.3

Table 4.2: Summary of plots used for release modelling and the correlation coefficients obtained for the corresponding plots

Model name	Graph plotted	R^2 value
Zero order	% cumulative released vs time	0.9049
First order	Log(cumulative % drug remaining) vs time	0.9812
Hixson-Crowell cube root model	Cube root of % drug remaining vs time	0.9674
Higuchi model	% cumulative released vs square root of time	0.9798
Korsmeyer-Peppas model (first 60%)	Log(% cumulative released) vs log(time)	0.9933

CHAPTER 5

Evaluation of the efficacy of NL-1 nanoparticles in an *in vivo* model of cerebral ischemia and reperfusion injury

5.1. Introduction

Cerebral ischemia and reperfusion injury or stroke is a prime example of a condition with a multimodal pathophysiology, making it the leading cause of permanent disability in the United States[1]. The onset of a stroke occurs with an occlusion in blood supply to the cerebral regions of the brain, which activates pathways for neuronal damage like a domino effect. The lack of oxygen and glucose to the cells of the CNS leads to an energy crisis, causing neurodegeneration via oxidative stress, apoptosis and neuroinflammation. Despite presenting multiple axes as therapeutic targets, stroke therapy in the clinic has remained confined to the use of tissue plasminogen activator (t-PA) to remove the occlusion. However, a greater impact could be from the complications that arise from reperfusion of the ischemic tissue, during which the aforementioned complex interplay between oxidative stress and inflammation predominates. Even with a timely treatment, stroke can lead to a multitude of cognitive, sensory and motor sequelae[2,3]. This makes the assessment of neurological functions an essential in the evaluation of any proposed stroke therapeutic[4].

The hallmark feature of stroke is the advent of cerebral edema, which contributes to the mortality associated with stroke[5]. Edema in stroke occurs in multiple phases and depends on the stage of ischemia or reperfusion. Cytotoxic edema predominates in the ischemic phase, and primarily causes cell swelling and damage. A direct consequence of cytotoxic edema is the vasogenic edema that occurs mainly during the reperfusion phase, aided by the dysfunctional BBB[6,7]. Vasogenic edema causes overall brain swelling with fatal consequences. Thus, there is an immense need to address the issue of cerebral edema from a therapeutic standpoint, as reduction in edema could be potentially life-saving. The major facilitator of vasogenic edema is the dysfunctional BBB. Indeed, a host of factors such as MMPs, infiltrating leukocytes, cytokines and

chemokines contribute to the loosening of BBB tight junctions[8–10]. This allows for extravasation of plasma proteins, which are a component of the edema fluid, and can be used as markers for the histological examination for BBB integrity. The BBB damage, while irreversible in the ischemic core, could still be reversed in the penumbra region[11,12]. A therapeutic intervention that salvages the BBB in stroke penumbra could aid in preventing edema in that region.

At the center of these pathways are the mitochondria. The outer mitochondrial protein mitoNEET participates in redox processes and regulates cellular bioenergetics. Previously, we have shown that the mitoNEET ligand, NL-1, has the potential to be a protective agent in ischemic conditions. *In vitro* testing of a PLGA nanoparticle formulation of NL-1 in an ischemia-reperfusion injury model has shown the drug to be effective in lowering oxidative stress and improving cell survival. Formulation of NL-1 into a polymeric nanoparticle system could help improve drug delivery to the target, prolong drug exposure and hence lower the dose required. In this chapter, we aim to translate the *in vitro* results into a pre-clinical model of cerebral ischemia reperfusion injury. We describe the use of a transient middle cerebral artery occlusion rat model to closely mimic the conditions of ischemia and reperfusion. We report our findings for the effect of NL-1 and NL-1 nanoparticle therapy on stroke outcomes.

5.2. Materials and Methods

Materials

TTC and bupivacaine were purchased from Sigma-Aldrich (St. Louis, MO). 4-Hydroxynonenal primary antibody (MAB3249) and HRP-linked anti-rat IgG secondary antibody (HAF005) were purchased from R&D Systems (Minneapolis, MN). Nitrotyrosine primary antibody (NB11096877) was purchased from Novus Biologicals (Littleton, CO). MitoNEET primary antibody

(16006-1-AP) was purchased from ProteinTech Group (Rosemont, IL). Iba-1 primary antibody (019-19741) was purchased from Fujifilm (Tokyo, Japan). Cytochrome c primary antibody (D18C7) was purchased from Cell Signaling Technology (Danvers, MA). Caspase-3 primary antibody (ab-4051) was purchased from Abcam (Cambridge, UK). GFAP primary antibody (130300), anti-rabbit AlexaFluor 488 secondary antibody, anti-mouse AlexaFluor 568 secondary antibody and anti-rat AlexaFluor 690 secondary antibody were purchased from Invitrogen (Carlsbad, CA). The DAB substrate kit (SK-4100) was purchased from Vector Laboratories (Burlington, ON). The Fluoromount-G mounting medium was purchased from Southern Biotech (Birmingham, AL).

Methods

Study approval and drug treatment

Female Sprague-Dawley rats (22-24 months old) were purchased from Hilltop Laboratories (Scottdale, PA) and housed under 12 hour light-dark conditions with food and water available ad libitum. The West Virginia University Animal Care and Use Committee approved all criteria for procedures prior to experimentation.

Study 1 assessed, neurological score, infarct volume, and hemispheric swelling at 24 hours post MCAO. Study 2 evaluated histological changes at 72 hours post MCAO. Animals were randomly assigned to 4 different treatment groups: control (PBS), 10 mg/kg NL-1, NL-1 nanoparticles with a theoretical dose of 250 µg/kg and 250 µg/kg NL-1. The drug formulation was prepared by dissolving a known amount of NL-1 (based on desired concentration) in methanol and evaporating the solvent. The dried drug residue was reconstituted in ethanol (2% v/v final concentration) and formulated with PBS and Tween 80 (2% w/v). All treatment was administered just before

reperfusion via tail vein. To avoid biases, we also ensured that different treatments were performed on the same day.

Surgical Procedure for MCAO

Rats underwent transient middle cerebral artery occlusion (MCAO) by an intraluminal suture method[13]. All the surgical instruments and materials were autoclaved, and the surgical procedure were performed under sterile conditions. In brief, we anesthetized mice with 4% isoflurane and maintained anesthesia such that animals did not respond to toe pinch with 2% isoflurane via face mask in a mixture of 30% oxygen and 70% nitrous oxide. A servo-controlled homeothermic heating blanket, equipped with a rectal thermometer, was used to maintain body temperature at 37 °C. A 4.0 monofilament suture (Doccol, Sharon, MA) was inserted into the right external carotid artery stump and advanced into the middle cerebral artery. We induced focal cerebral ischemia by occlusion of the right middle cerebral artery for 120 min followed by reperfusion for 24 hour (Study 1) or 72 hour (Study 2). Animals were singly housed and administered 0.5ml of saline to help with dehydration after surgery. We also applied a local analgesia (bupivacaine 1 mg kg−1, subcutaneously (s.c.) at the site of incision. The animals experiencing problems during the induction of MCAO, such as excessive bleeding, and prolonged operation time were excluded.

Neurological Functional Assessment

Neurological functional assessments were carried out by an investigator blinded to treatment groups at WVU rodent behavior core. The health screen and modified Neurological Severity Scores (mNSS) were performed before stroke and 24h post MCAO to evaluate impairments in motor, sensory, balance and reflex measures during the acute period. The scoring range was from

0 to 20 point scale for health screen and 0-18 point scale for mNSS, with higher scores indicating severe neurological injury.

Measurement of infarction volume by 2,3,5-triphenyltetrazolium chloride (TTC)

Measurement of the cerebral infarct size and infarct volume were performed by 2,3,5triphenyltetrazolium chloride (TTC; 2%) staining at 24 h following MCAO. The animals were sacrificed, and the brains were isolated. 2 mm coronal brain slices were made using stainless rat brain slicer matrix and stained for 15 min at 37 °C. Hemispheres were scanned on a flatbed scanner and analyzed using Image J software. On each slice, the non-stained area (ischemic brain) was outlined, and the infarct volume was calculated The corrected infarction volume (CIV) was calculated using the formula: CIV= (CH/IH)*IA*d, where CH was the area of the contralateral hemisphere in mm^2, IH was the area of the ipsilateral hemisphere in mm^2, IA was the infarct area in mm^2, and d was slice thickness (2 mm). CIV (%) = CIV/(CH*d). Edema index was calculated as follows: Hemispheric swelling (%)=[1-(area of contralateral hemisphere/area of ipsilateral hemisphere) ×100%].

Endogenous IgG staining

IgG immune staining was performed on rats that were subjected to 72 hour reperfusion. The slides with 20 µm coronal brain sections were allowed to thaw at room temperature for about 15 minutes. The sections were then fixed with addition of methanol for 3 minutes, upon which, the slides washed once with 1X PBS. The blocking of endogenous peroxidases was performed with a mix of 3% v/v hydrogen peroxide and 4% v/v horse serum in PBS for 30 minutes. The slides were then washed thrice with PBS for 5 minutes each. Subsequently, the brain sections were permeabilized

in a solution of 4% v/v horse serum and 1% w/v TritonX-100 in PBS for one hour, followed by washing thrice with PBS. The slides were then stained for IgG using the HRP-lined rat anti-IgG secondary antibody solution made in 4% v/v horse serum in PBS (R&D Systems dilution: 1:500). The secondary antibody incubation was carried out for 2 hours at room temperature, following which, the slides were washed thrice with PBS. The DAB staining was performed using the DAB staining kit. The staining solution was prepared by adding one drop of the DAB reagent to 1 mL of the dilution buffer. The slides were incubated in this solution for 10 minutes, following which, they were washed thrice with PBS. After the final wash, the slides were cover-slipped using the Flouromount-G (Southern Biotech) mounting medium, and allowed to dry prior to imaging. The slides were imaged by bright field microscopy using the Olympus MVX10 microscope at WVU Imaging Core Facilities.

Immunofluorescence staining

Immunofluorescence staining was performed on rats that were subjected to 72 hour reperfusion. The slides with 20 μm coronal brain sections were allowed to thaw at room temperature for about 15 minutes. The sections were then fixed with addition of methanol for 3 minutes, upon which, the slides washed once with 1X PBS. The tissue permeabilization was carried out in a solution of 4% v/v horse serum and 1% w/v TritonX-100 in PBS for one hour, followed by washing thrice with PBS. The slides were then stained for the various markers using suitable primary antibody cocktails, ensuring to not mix two primary antibodies from the same species. The following primary antibodies were used: mitoNEET (Proteintech, rabbit, 1:200 dilution), cytochrome c (Cell Signaling, rabbit, 1:200 dilution), caspase-3 (Abcam, mouse, 1:200 dilution), 4-hydroxynonenal

(R&D Systems, mouse, 1 µg/mL), nitrotyrosine (Novus biologicals, mouse, 1:200 dilution), Iba-1 (Fujifilm, rabbit, 1:200 dilution) and GFAP (Invitrogen, rat, 1:500 dilution). The primary antibody incubation was carried out in the dark at 4°C, overnight. The following day, the primary antibody was removed and the slides were washed thrice with PBS, prior to secondary antibody incubation. The following fluorescent secondary antibodies were used based on the primary antibody used the previous day: anti-rabbit AlexaFluor 488 (Invitrogen, 1:1000 dilution), anti-mouse AlexaFluor 568 (Invitrogen, 1:1000 dilution) and anti-rat AlexaFluor 680 (Invitrogen, 1:1000 dilution). The secondary antibody incubation was carried out for 2 hours in the dark at room temperature, following which, the slides were washed thrice with PBS. After the final wash, the slides were cover-slipped using the Flouromount-G (Southern Biotech) mounting medium, and allowed to dry prior to imaging. The slides were imaged by fluorescence microscopy using the Olympus Slide Scanner microscope at WVU Imaging Core Facilities.

Statistical analysis:

Statistical analysis of data obtained was carried out by GraphPad Prism 7.04 (GraphPad Software, CA) using one-way ANOVA followed by Dunnett's post hoc test for comparison of multiple groups. The graphs were prepared using GraphPad Prism 7.04. Data are presented as mean with standard deviations. A statistically significant difference between groups was considered if the p value was <0.05.

5.3. Results

Neurological functional assessment

The effectiveness of MCAO procedure in inducing a stroke and the efficacy of drug treatments to improve stroke outcomes was determined using the neurological functional assessment tests, 24hours following tMCAO. This consisted of two tests: the general health screen (0-20 point score) and the mNSS (0-18 point score), with a lower score indicating a better outcome. **Figure 5.1(A)** shows the results for health screen wherein the scores are plotted for each group. All animals showed a very low score between 0-1 pre-tMCAO (0.2 ± 0.6). The highest mean score of 12 ± 2.6 (n=8) was seen for the control group. NL-1 at 10 mg/kg showed a statistically significant improvement in the health score of 9.2 ± 2.8 (n=9), compared to control. The higher dose NL-1 group at 10 mg/kg showed a lower mean health score compared to the low dose group at 250 µg/kg (10.3 ± 2.9, n=6), though the differences were not statistically significant. NL-1 nanoparticles significantly improved the health scores to 8.2 ± 2.6 (n=8), compared to control. The mean health score for NL-1 nanoparticles was found to be lower than NL-1 drug by itself at the same equivalent amount of NL-1, though no statistical significance was seen. For mNSS, a similar trend was observed, shown in **Figure 5.1(B)**. All animals showed a low pre-tMCAO score between 0-2 (0.7 ± 1.1, n=23). The mean score was lowest for NL-1 nanoparticles among all groups (8.1 ± 1.6, n=6). The mean mNSS score for NL-1 at equivalent dose of 250 µg/kg (11 ± 2.9, n=5) was found to be comparable to the control group (11.2 ± 3.3, n=5). The mean score for high dose NL-1 at 10 mg/kg was found to be 10.2 ± 1.7 (n=5) However, no statistical significance was seen for improvement in mNSS scores for any treatment group compared to the control group.

Effect of NL-1 treatment on brain infarcts

The 2 mm coronal sections obtained from the stroke animals were stained with TTC to reveal infarcts in the brain. The infarct volume and hemispheric swelling were calculated for each of the section for all the brains. Both, NL-1 at 10 mg/kg and NL-1 nanoparticles at a dose of 250 μg/kg were able to significantly reduce the infarct volume, as shown in Figure 5.2(A). NL-1 at 10 mg/kg reduced the infarct volume to 69.5% of control, while NL-1 nanoparticles reduced the infarct volume to 49% of control. Similarly, both treatment groups significantly reduced the hemispheric swelling in the brain compared to control treated rats, as shown in **Figure 5.2(B)**. The hemispheric swelling was reduced to 60.6% and 36.5% of control by 10 mg/kg and NL-1 nanoparticles, respectively. The NL-1 nanoparticles significantly lowered the hemispheric swelling compared to NL-1 at a 40-fold higher dose.

Immunohistochemistry

The possible extravasation of endogenous IgG from the brain vasculature was visualized by immune staining brain sections of rats subjected to tMCAO and 72 hour reperfusion. **Figure 5.3** shows the representative IgG stained brain sections for all treatment groups. A qualitative analysis of IgG staining reveals a widespread staining on the ipsilateral side where the infarcts are present. The stained area for NL-1 nanoparticle treated brain sections appears lower than that of the control and 10 mg/mL NL-1 treatment groups. The IgG staining for NL-1 nanoparticle treated brain appears to be confined to the central core of the stroke, with little spillover into the cortical region. The greatest staining in the cortical regions was seen for the control group followed by 10 mg/kg NL-1 treated group.

Immunofluorescence staining was performed for qualitative analysis of the markers of oxidative stress, inflammation and apoptosis after stroke. The images of brain section for all the markers are compiled in a similar panel and include the treatments of **(A)** control, **(B)** 10 mg/kg NL-1 **(C)** NL1 nanoparticles at a theoretical NL-1 dose of 250 µg/kg and **(D)** 250 µg/kg NL-1. The brain sections were stained for the proteins shown in the following figures: mitoNEET **(Figure 5.4)**, nitrotyrosine **(Figure 5.5)**, 4-hydroxynonenal **(Figure 5.6)**, cytochrome c **(Figure 5.7)**, caspase-3 **(Figure 5.8)**, GFAP **(Figure 5.9)** and Iba-1 **(Figure 5.10).**

5.4. Discussion

We used an intraluminal suture tMCAO rat model for testing the *in vivo* efficacy of NL-1 loaded PLGA nanoparticles. Transient MCAO is a widely used model to mimic cerebral ischemia and reperfusion injury[14]. About 70% of human ischemic stroke occur through occlusions in the middle cerebral artery or its branches[15]. The procedure was carried out by intra-arterial suture occlusion, which is a widely used technique to induce stroke in rodents. In this method, the suture is inserted in the external carotid artery, and subsequently advanced into the internal carotid artery, till the blood supply to the middle cerebral artery is occluded[16]. This approach is deemed better for transient MCAO since it maintains the anatomic integrity required for repefusion[17]. This technique has the advantages that it mimics human stroke with the formation of an ischemic penumbra, produces reproducible infarcts, does not need the skull to be opened[16,18,19]. However, the tMCAO technique does not model for the aspect of thromboembolism[18]. Moreover, the outcomes of the procedure depend on the type and length of suture used. Nonetheless, tMCAO remains a gold standard for generating a pre-clinical stroke model. We performed a 120-minute occlusion based on literature, looking at the optimal occlusion period for fewer animal mortalities[20–22].

Four groups of treatments were used. The animals in control group received PBS. Since we had previously performed a short pilot study with 10 mg/kg dose in mice, a group with this dose was selected. The limitations with the volume of liquid that could be injected iv through the rat tail vein and NL-1 entrapment efficiency in the nanoparticles placed a constraint on the NL-1 nanoparticle dose. The effective dose of NL-1 delivered through PLGA nanoparticles was about 250 µg/kg. Finally, we also included a NL-1 low dose group at 250 µg/kg, similar to the nanoparticles.

The primary consequence of stroke is the immediate effect on the overall health of the animals. We determined the effect of stroke and treatments on the animals using the health and sickness scoring, prior to tMCAO and 24 hours following the surgery[23–25]. The sickness scoring was carried out on a scale of 0-20, and is outlined in **Table 5.1**. The parameters evaluated include the animal appearance, posture, body hydration, respiration and deficits in body weight and temperature. Our results indicate that treatment with NL-1 at 10 mg/kg and NL-1 nanoparticles at a dose of 250 µg/kg significantly improved the sickness score of the animals. NL-1 by itself at the low concentration of 250 µg/kg had no significant improvement in the scores. Thus, nanoparticles were able to induce an improvement in the subject health at a 40-fold lower dose. The possible reason for this could be the efficient uptake of NL-1 loaded nanoparticles within the neuronal cells, combined with the relatively slower release of the drug from the nanoparticles. The latter would allow for the drug to act for a longer duration compared to the sudden exposure of NL-1 drug by itself which could be prone to be metabolized faster[26].

Stroke causes deficits in the sensory and motor functioning of the afflicted individual[27]. The mNSS is one of the reliable and most commonly used composite tests for evaluating the

neurological functioning of animals after stroke[28,29]. It uses a scale of 0-18 for rats. The mNSS is called a composite test because it is an amalgamation of sensory (visual, tactile and proprioceptive), motor (muscular movements), brainstem reflex and balance tests. The overall score is the sum of scores received for individual tests. The specific mNSS tests performed in this study are outlined in **Table 5.2** and the include reflex tests, the walking test, the inverted test, the paw-placement test and the beam balance test[30]. The advantage of using mNSS is that it allows for a quick assessment of multiple aspects of stroke induced injuries[31]. mNSS is an effective test right at 24 hours post-stroke and can also be used for a long term neurological evaluation of 30 or even 60 days[29,32,33]. However, the since the score is composite, it could lead to masking of neurological deficits seen for one specific function or modality[31]. One way around this disadvantage could be separation of the scores for each task. Further, mNSS scoring over a prolonged duration of up to 30 days could also help to provide conclusive mNSS results[34,35].

We used mNSS to assess the behavior the following day of the tMCAO surgery, since mNSS is frequently studied 24 hours post-stroke[34–36]. Our results indicate a general improvement in the mNSS scores with treatment, as compared to control. The NL-1 nanoparticles had the lowest means mNSS score amongst all treatments. NL-1 by itself at the equivalent dose has similar mean score as the control group. Although, we don't report statistically significant results, we think improving on the animal numbers would help us achieve significantly reduced mNSS score for NL-1 nanoparticles as compared to NL-1 by itself in equivalent (250 µg/kg) and possibly in high dose (10mg/kg).

Triphenyltetrazolium chloride or TTC staining is one of the most commonly used techniques to quantify brain infarcts. TTC is reduced by succinate dehydrogenase enzyme in the

viable mitochondria to the red colored formazan, leaving the infarcts unstained[37]. TTC staining is quick and reproducible. Although there have been questions raised about TTC staining possibly overestimating infarct area, a study by Tureyen et al., found no significant difference in infarcts quantified by TTC staining and by cresyl violet staining[38]. Infarct volume and hemispheric swelling are two of the most important endpoints used for assessment of outcomes for a stroke therapeutic[39–41]. Infarcts reveal the area of brain damage, whereas hemispheric swelling is indicative of edema that accompanies the reperfusion injury. Our results show an improved stroke outcome with both NL-1 (10 mg/kg) and NL-1 nanoparticles showing a significantly lowered infarct volume and hemispheric swelling. In case of infarct volume, although no significant difference was observed between NL-1 drug and NL-1 nanoparticles, it should be noted that NL1 nanoparticles were dosed at a 40-fold lower dose. A significant difference was seen between drug and nanoparticles for hemispheric swelling, which shows the efficacy of PLGA nanoparticles in reducing the drug dose.

After studying the effect of NL-1 treatment on the primary stroke outcomes, we moved to looking at the status of different markers of damage following cerebral ischemia and reperfusion injury. One of the hallmark features of stroke related damage is the dysfunctional and leaky BBB. The BBB tight junctions are loosened, leading to extravasation of certain biomolecules such as plasma proteins, that are otherwise impermeable[42]. One such commonly used plasma protein surrogate marker to determine BBB leakiness after stroke is the endogenous IgG[43–46]. Our results indicate an intense staining of brain sections treated with control and 10 mg/kg NL-1 in the ipsilateral part of the brain, which received the stroke, with the drug treatment showing staining to a lesser extent in the cortex, compared to the control. The NL-1 nanoparticle shows an overall reduced staining compared to both the groups. Of note is the poor staining in the cortex of the

nanoparticle treated brain. This could possibly indicate an improvement in the integrity of BBB in the stroke penumbra, which could not be seen in control and NL-1 treated brain sections. Thus, although qualitative, IgG staining of brain sections shows a possible rescue of BBB function by NL-1 nanoparticles.

MitoNEET is the target for the NL-1 drug and it was necessary to look at its expression, especially in the region of brain infarcts. For this purpose, we performed fluorescence immunohistochemistry on the brain slices of animals that underwent 72 hour reperfusion, staining for mitoNEET. A qualitative analysis reveals that mitoNEET not changed in the ischemic areas sections of control as well as drug treated groups.

We also performed immunofluorescence staining for markers of the major pathways of ischemia and reperfusion injury associated brain damage, including ROS-RNS, apoptosis and neuroinflammation. Firstly, we looked at the expression of nitrotyrosine, which is a marker for RNS specie peroxynitrite. Excess nitric oxide tends to react with superoxide radical to form the highly cell permeable peroxynitrite. Peroxynitrite causes the nitration of tyrosine residues to form nitrotyrosine[47]. Nitrotyrosine generation has been reported in ischemia and reperfusion injury[48,49]. A qualitative analysis of NT stained brain sections reveal intense staining in the infarcted region. The staining intensity was lowest for NL-1 nanoparticle treated brain compared to control and NL1 drug groups, indicating a possible lowering of NT generation due to a reduced infarct area. The second marker for oxidative stress that we looked at was 4-hydroxynonenal, which is an aldehydic by-product of lipid peroxidation[50,51]. This molecule has been reported to potentiate oxidative cascades and cause impairment of glutamate transport in synapses[52]. The 4-hydroxynonenal stained brain sections reveal an intense staining in the infarct area on the ipsilateral side for all

groups. The intensities are lower for 10 mg/kg NL-1 and NL-1 nanoparticle treated brains, due to the smaller infarct areas.

The next two sets of immune staining were performed for the two most commonly probed markers of intrinsic apoptosis: cytochrome c and caspase-3[53,54]. Cytochrome c is released into the cytoplasm from the mitochondria due to mitochondrial swelling and damage to the mitochondrial membrane potential, wherein it activates the initiator caspases[55]. Caspase-3 is an important effector caspase which mediates apoptosis. The staining of brain sections could not indicate a trend with cytochrome c expression in any of the groups. On the other hand, a more intense staining was seen for caspase-3 in the infarcts of all the groups on the ipsilateral side.

We then turned to determining the expression of markers of inflammation in the brains sections. Astrocytes are often activated in the inflammatory mechanisms surrounding ischemia and reperfusion injury[56], and activated astrocytes overexpress GFAP, which is commonly used as an inflammatory marker in stroke[57,58]. A qualitative analysis of GFAP stained sections reveals widespread staining on the ipsilateral side of the brain. The GFAP staining was seen to be confined to the core infarct regions for 10 mg/kg NL-1 and NL-1 nanoparticle treated brain sections. NL-1 nanoparticles had the smallest area of staining, possibly indicating lack of astrocytic activation in the stroke penumbra upon NL-1 treatment. Finally, we looked at the expression of microglial calcium-binding protein Iba-1. Iba-1 has been found to be upregulated in activated microglia in stroke and Iba-1 immunostaining has been a used as a means to identify activated microglia[59,60]. Iba-1 staining images indicate an intense staining in the region of infarcts for all the groups, with lesser intensity seen for NL-1 nanoparticles due to a reduced infarct size.

In summary, this chapter describes the preliminary *in vivo* efficacy studies performed for NL-1 loaded PLGA nanoparticles. We describe a rat tMCAO model for mimicking cerebral ischemia and reperfusion injury. We found that NL-1 nanoparticles have the potential to improve neurological outcome following a stroke. NL-1 nanoparticles were also effective in reducing the infarct sizes and edema formation in the brain, helping to lower the dose needed to be administered to achieve therapeutic effects. We also report our attempts to visualize the integrity of BBB and expression of markers contributing to cell damage in stroke.

5.5. References:

1. Stroke Statistics | Internet Stroke Center. http://www.strokecenter.org/patients/aboutstroke/stroke-statistics/. Accessed June 10, 2017.

2. Elias GJB, Namasivayam AA, Lozano AM. Deep brain stimulation for stroke: Current uses and future directions. *Brain Stimul*. 2018;11(1):3-28. doi:10.1016/j.brs.2017.10.005

3. Nowak DA. The impact of stroke on the performance of grasping: Usefulness of kinetic and kinematic motion analysis. *Neurosci Biobehav Rev*. 2008;32(8):1439-1450. doi:10.1016/j.neubiorev.2008.05.021

4. Baskett JJ, Marshall HJ, Broad JB, Owen PH, Green G. The good side after stroke: Ipsilateral sensory-motor function needs careful assessment. *Age Ageing*. 1996;25(3):239-244. doi:10.1093/ageing/25.3.239

5. Sara M. Nehring, Prasanna Tadi ST. Cerebral Edema. In: *Treasure Island (FL): StatPearls Publishing*. ; 2020.

6.   Rosenberg GA, Yang Y. Vasogenic edema due to tight junction disruption by matrix metalloproteinases in cerebral ischemia. *Neurosurg Focus*. 2007;22(5). doi:10.3171/foc.2007.22.5.5

7.   Kahle KT, Marc Simard J, Staley KJ, Nahed B V., Jones PS, Sun D. Molecular mechanisms of ischemic cerebral edema: Role of electroneutral ion transport. *Physiology*. 2009;24(4):257-265. doi:10.1152/physiol.00015.2009

8.   Jiang X, Andjelkovic A V., Zhu L, et al. Blood-brain barrier dysfunction and recovery after ischemic stroke. *Prog Neurobiol*. 2018;163-164:144-171. doi:10.1016/j.pneurobio.2017.10.001

9.   Sarvari S, Moakedi F, Hone E, Simpkins JW, Ren X. Mechanisms in blood-brain barrier opening and metabolism-challenged cerebrovascular ischemia with emphasis on ischemic stroke. *Metab Brain Dis*. 2020;35(6):851-868. doi:10.1007/s11011-020-00573-8

10.   Abdullahi W, Tripathi D, Ronaldson PT. Blood-brain barrier dysfunction in ischemic stroke: Targeting tight junctions and transporters for vascular protection. *Am J Physiol - Cell Physiol*. 2018;315(3):C343-C356. doi:10.1152/ajpcell.00095.2018

11.   Nagaraja TN, Karki K, Ewing JR, Croxen RL, Knight RA. Identification of variations in blood-brain barrier opening after cerebral ischemia by dual contrast-enhanced magnetic resonance imaging and T1sat measurements. *Stroke*. 2008;39(2):427-432. doi:10.1161/STROKEAHA.107.496059

12.   Simpkins AN, Dias C, Leigh R. Identification of Reversible Disruption of the Human Blood-Brain Barrier Following Acute Ischemia. *Stroke*. 2016;47(9):2405-2408. doi:10.1161/STROKEAHA.116.013805

13. Uluç K, Miranpuri A, Kujoth GC, Aktüre E, Başkaya MK. Focal cerebral ischemia model by endovascular suture occlusion of the middle cerebral artery in the rat. *J Vis Exp*. 2010;(48):1978. doi:10.3791/1978

14. McCullough LD, Liu F. Middle cerebral artery occlusion model in rodents: Methods and potential pitfalls. *J Biomed Biotechnol*. 2011;2011. doi:10.1155/2011/464701

15. Bogousslavsky J, Van Melle G, Regli F. The Lausanne Stroke Registry: analysis of 1,000 consecutive patients with first stroke. *Stroke*. 1988;19(9):1083-1092. doi:10.1161/01.STR.19.9.1083

16. Kleinschnitz C, Fluri F, Schuhmann M. Animal models of ischemic stroke and their application in clinical research. *Drug Des Devel Ther*. 2015;9:3445. doi:10.2147/DDDT.S56071

17. Liu S, Zhen G, Meloni BP, Campbell K, Winn HR. RODENT STROKE MODEL GUIDELINES FOR PRECLINICAL STROKE TRIALS (1ST EDITION). *J Exp Stroke Transl Med*. 2009;2(2):2-27. doi:10.6030/1939-067x-2.2.2

18. Howells DW, Porritt MJ, Rewell SS, et al. Different Strokes for Different Folks: The Rich Diversity of Animal Models of Focal Cerebral Ischemia. *J Cereb Blood Flow Metab*. 2010;30(8):1412-1431. doi:10.1038/jcbfm.2010.66

19. Sommer CJ. Ischemic stroke: experimental models and reality. *Acta Neuropathol*. 2017;133(2):245-261. doi:10.1007/s00401-017-1667-0

20. Blankenship D, Niemi J, Hilow E, Karl M, Sundararajan S. Oral pioglitazone reduces infarction volume and improves neurologic function following MCAO in rats. In: *Advances in Experimental Medicine and Biology*. Vol 701. Springer New York LLC; 2011:157-162. doi:10.1007/978-1-4419-7756-4_22

21. Martín A, Rojas S, Pérez-Asensio F, Planas AM. Transient benefits but lack of protection by sodium pyruvate after 2-hour middle cerebral artery occlusion in the rat. *Brain Res*. 2009;1272:45-51. doi:10.1016/j.brainres.2009.03.056

22. Wu G, McBride DW, Zhang JH. Axl activation attenuates neuroinflammation by inhibiting the TLR/TRAF/NF-κB pathway after MCAO in rats. *Neurobiol Dis*. 2018;110:59-67. doi:10.1016/j.nbd.2017.11.009

23. Cetinkaya M, Cansev M, Cekmez F, et al. CDP-choline reduces severity of intestinal injury in a neonatal rat model of necrotizing enterocolitis. *J Surg Res*. 2013;183(1):119-128. doi:10.1016/j.jss.2012.11.032

24. Doll DN, Engler-Chiurazzi EB, Lewis SE, et al. Lipopolysaccharide exacerbates infarct size and results in worsened post-stroke behavioral outcomes. *Behav Brain Funct*. 2015;11(1):32. doi:10.1186/s12993-015-0077-5

25. Cunningham CJ, Wong R, Barrington J, Tamburrano S, Pinteaux E, Allan SM. Systemic conditioned medium treatment from interleukin-1 primed mesenchymal stem cells promotes recovery after stroke. *Stem Cell Res Ther*. 2020;11(1):1-12. doi:10.1186/s13287-020-1560-y

26. Saralkar P, Arsiwala T, Geldenhuys WJ. Nanoparticle formulation and *in vitro* efficacy testing of the mitoNEET ligand NL-1 for drug delivery in a brain endothelial model of ischemic reperfusion-injury. *Int J Pharm*. 2020;578:119090. doi:10.1016/j.ijpharm.2020.119090

27. Zhou J, Li J, Rosenbaum DM, et al. The prolyl 4-hydroxylase inhibitor GSK360A decreases post-stroke brain injury and sensory, motor, and cognitive behavioral deficits.

Borlongan C V., ed. *PLoS One*. 2017;12(9):e0184049. doi:10.1371/journal.pone.0184049

28.   Yu J, Moon J, Jang J, et al. Reliability of behavioral tests in the middle cerebral artery

occlusion model of rat. *Lab Anim*. 2019;53(5):478-490. doi:10.1177/0023677218815210

29.   Shen LH, Li Y, Chen J, et al. Intracarotid transplantation of bone marrow stromal cells

increases axon-myelin remodeling after stroke. *Neuroscience*. 2006;137(2):393-399.

doi:10.1016/j.neuroscience.2005.08.092

30.   Chen J, Zhang C, Jiang H, et al. Atorvastatin Induction of VEGF and BDNF Promotes Brain

Plasticity after Stroke in Mice. *J Cereb Blood Flow Metab*. 2005;25(2):281-290.

doi:10.1038/sj.jcbfm.9600034

31.   Ruan J, Yao Y. Behavioral tests in rodent models of stroke. *Brain Hemorrhages*.

September 2020. doi:10.1016/j.hest.2020.09.001

32.   Schaar KL, Brenneman MM, Savitz SI. Functional assessments in the rodent stroke model.

Exp Transl Stroke Med. 2010;2(1):13. doi:10.1186/2040-7378-2-13

33.   Bernard R, Balkaya M, Rex A. Behavioral testing in rodent models of stroke, Part I. In:

Neuromethods. Vol 120. Humana Press Inc.; 2016:199-223. doi:10.1007/978-1-4939-

5620-3_13

34.   Ogay V, Kumasheva V, Li Y, et al. Improvement of Neurological Function in Rats with

Ischemic Stroke by Adipose-derived Pericytes. *Cell Transplant*.

2020;29:096368972095695. doi:10.1177/0963689720956956

35.   Chen H, Guan B, Chen X, et al. Baicalin Attenuates Blood-Brain Barrier Disruption and

Hemorrhagic Transformation and Improves Neurological Outcome in Ischemic Stroke

Rats with Delayed t-PA Treatment: Involvement of ONOO−-MMP-9 Pathway. *Transl*

Stroke Res. 2018;9(5):515-529. doi:10.1007/s12975-017-0598-3

36.   Li X, Zhang D, Bai Y, Xiao J, Jiao H, He R. Ginaton improves neurological function in ischemic stroke rats via inducing autophagy and maintaining mitochondrial homeostasis. *Neuropsychiatr Dis Treat*. 2019;15:1813-1822. doi:10.2147/NDT.S205612

37.   Bederson JB, Pitts LH, Germano SM, Nishimura MC, Davis RL, Bartkowski HM. Evaluation of 2,3,5-triphenyltetrazolium chloride as a stain for detection and quantification of experimental cerebral infarction in rats. *Stroke*. 1986;17(6):1304-1308. doi:10.1161/01.STR.17.6.1304

38.   Türeyen K, Vemuganti R, Sailor KA, Dempsey RJ. Infarct volume quantification in mouse focal cerebral ischemia: A comparison of triphenyltetrazolium chloride and cresyl violet staining techniques. *J Neurosci Methods*. 2004;139(2):203-207. doi:10.1016/j.jneumeth.2004.04.029

39.   Tan Z, Turner RC, Leon RL, et al. Bryostatin improves survival and reduces ischemic brain injury in aged rats after acute ischemic stroke. *Stroke*. 2013;44(12):3490-3497. doi:10.1161/STROKEAHA.113.002411

40.   Yang Y, Shuaib A, Li Q. Quantification of infarct size on focal cerebral ischemia model of rats using a simple and economical method. *J Neurosci Methods*. 1998;84(1-2):9-16. doi:10.1016/S0165-0270(98)00067-3

41.   Wali B, Ishrat T, Atif F, Hua F, Stein DG, Sayeed I. Glibenclamide administration attenuates infarct volume, hemispheric swelling, and functional impairments following permanent focal cerebral ischemia in rats. *Stroke Res Treat*. 2012. doi:10.1155/2012/460909

42.   Muramatsu K, Fukuda A, Togari H, Wada Y, Nishino H. Vulnerability to Cerebral Hypoxic-Ischemic Insult in Neonatal but Not in Adult Rats Is in Parallel With Disruption of the Blood-Brain Barrier. *Stroke*. 1997;28(11):2281-2289. doi:10.1161/01.STR.28.11.2281

43.   Liu P, Zhang Z, Liu Y, et al. TMEM16A Inhibition Preserves Blood–Brain Barrier Integrity After Ischemic Stroke. *Front Cell Neurosci*. 2019;13:360. doi:10.3389/fncel.2019.00360

44.   Yu G, Liang Y, Huang Z, Jones DW, Pritchard KA, Zhang H. Inhibition of myeloperoxidase oxidant production by N-acetyl lysyltyrosylcysteine amide reduces brain damage in a murine model of stroke. *J Neuroinflammation*. 2016;13(1):1-13. doi:10.1186/s12974-016-0583-x

45.   Gliem M, Krammes K, Liaw L, van Rooijen N, Hartung H-P, Jander S. Macrophagederived osteopontin induces reactive astrocyte polarization and promotes re-establishment of the blood brain barrier after ischemic stroke. *Glia*. 2015;63(12):2198-2207. doi:10.1002/glia.22885

46.   Cui X, Chopp M, Zacharek A, Ye X, Roberts C, Chen J. Angiopoietin/Tie2 pathway mediates type 2 diabetes induced vascular damage after cerebral stroke. *Neurobiol Dis*. 2011;43(1):285-292. doi:10.1016/j.nbd.2011.04.005

47.   Kuhn DM, Sakowski SA, Sadidi M, Geddes TJ. Nitrotyrosine as a marker for peroxynitrite-induced neurotoxicity: The beginning or the end of the end of dopamine neurons? *J Neurochem*. 2004;89(3):529-536. doi:10.1111/j.1471-4159.2004.02346.x

48.   Nanetti L, Taffi R, Vignini A, et al. Reactive oxygen species plasmatic levels in ischemic stroke. *Mol Cell Biochem*. 2007;303(1-2):19-25. doi:10.1007/s11010-007-9451-4

49. Xu J, He L, Ahmed SH, Chen S-W, Goldberg MP, Beckman JS. Expression in Cerebral Endothelial Cells Oxygen-Glucose Deprivation Induces Inducible Nitric Oxide Synthase and Nitrotyrosine. 2000. doi:10.1161/01.STR.31.7.1744

50. Adibhatla RM, Hatcher JF. Lipid oxidation and peroxidation in CNS Health and disease: From molecular mechanisms to therapeutic opportunities. *Antioxidants Redox Signal*. 2010;12(1):125-169. doi:10.1089/ars.2009.2668

51. Arnett D, Quillin A, Geldenhuys WJ, Menze MA, Konkle M. 4-Hydroxynonenal and 4-Oxononenal Differentially Bind to the Redox Sensor MitoNEET. *Chem Res Toxicol*. 2019;32(6):977-981. doi:10.1021/acs.chemrestox.9b00166

52. Keller JN, Mark RJ, Bruce AJ, et al. 4-hydroxynonenal, an aldehydic product of membrane lipid peroxidation, impairs glutamate transport and mitochondrial function in synaptosomes. *Neuroscience*. 1997;80(3):685-696. doi:10.1016/S0306-4522(97)00065-1

53. Li W, Suwanwela NC, Patumraj S. Curcumin prevents Reperfusion injury following ischemic stroke in rats via inhibition of NF-κB, ICAM-1, MMP-9 and caspase-3 expression. *Mol Med Rep*. 2017;16(4):4710-4720. doi:10.3892/mmr.2017.7205

54. Sugawara T, Fujimura M, Morita-Fujimura Y, Kawase M, Chan PH. Mitochondrial Release of Cytochrome c Corresponds to the Selective Vulnerability of Hippocampal CA1 Neurons in Rats after Transient Global Cerebral Ischemia. 1999. doi:10.1523/JNEUROSCI.19-22-j0002.1999

55. Tohru Kobayashi, Satoshi Kuroda, Mitsuhiro Tada, Kiyohiro Houkin, Yoshinobu Iwasaki HA. Calcium-induced mitochondrial swelling and cytochrome c release in the brain: its biochemical characteristics and implication in ischemic neuronal injury. *Brain Res*. 2003;960(1-2):62-70. doi:10.1016/s0006-8993(02)03767-8

56.   Pekny M, Wilhelmsson U, Tatlisumak T, Pekna M. Astrocyte activation and reactive

gliosis—A new target in stroke? *Neurosci Lett*. 2019;689:45-55.

doi:10.1016/j.neulet.2018.07.021

57.   Misu T, Fujihara K, Kakita A, et al. Loss of aquaporin 4 in lesions of neuromyelitis optica:

Distinction from multiple sclerosis. *Brain*. 2007;130(5):1224-1234.

doi:10.1093/brain/awm047

58.   Wilson KD, Ochoa LF, Solomon OD, et al. Elimination of intravascular thrombi prevents

early mortality and reduces gliosis in hyper-inflammatory experimental cerebral malaria. *J

Neuroinflammation*. 2018;15(1). doi:10.1186/s12974-018-1207-4

59.   Ito D, Tanaka K, Suzuki S, Dembo T, Fukuuchi Y. Enhanced Expression of Iba1, Ionized

Calcium-Binding Adapter Molecule 1, After Transient Focal Cerebral Ischemia In Rat

Brain. *Stroke*. 2001;32(5):1208-1215. doi:10.1161/01.STR.32.5.1208

60.   Drake C, Boutin H, Jones MS, et al. Brain inflammation is induced by co-morbidities and

risk factors for stroke. *Brain Behav Immun*. 2011;25(6):1113-1122.
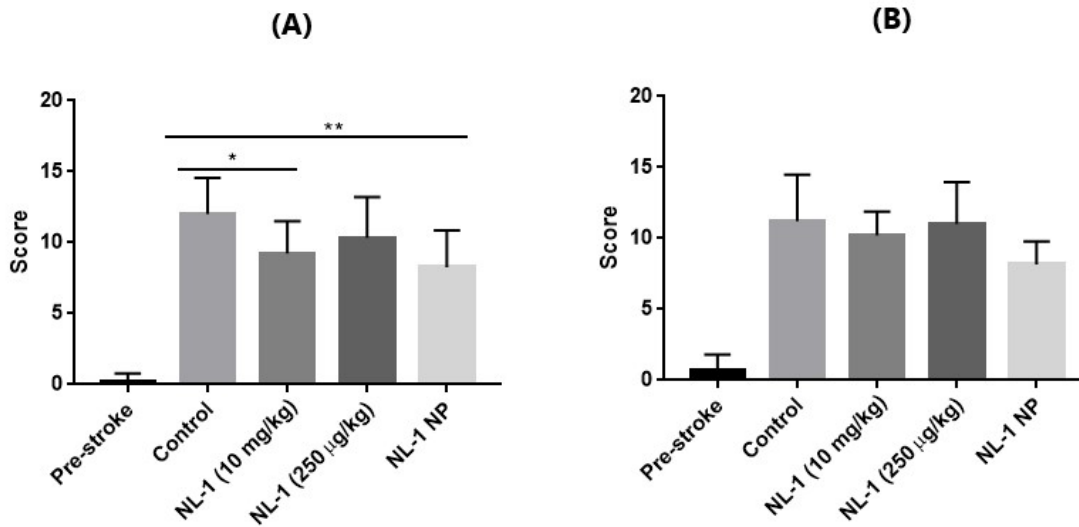
doi:10.1016/j.bbi.2011.02.008

Figure 5.1: Neurological assessment of animals pre-tMCAO and post treatment with control, 10 mg/kg NL-1, 250 µg/kg NL-1 and NL-1 nanoparticles. (A) Health screening and (B) mNSS scoring (*p<0.05, **p<0.01).
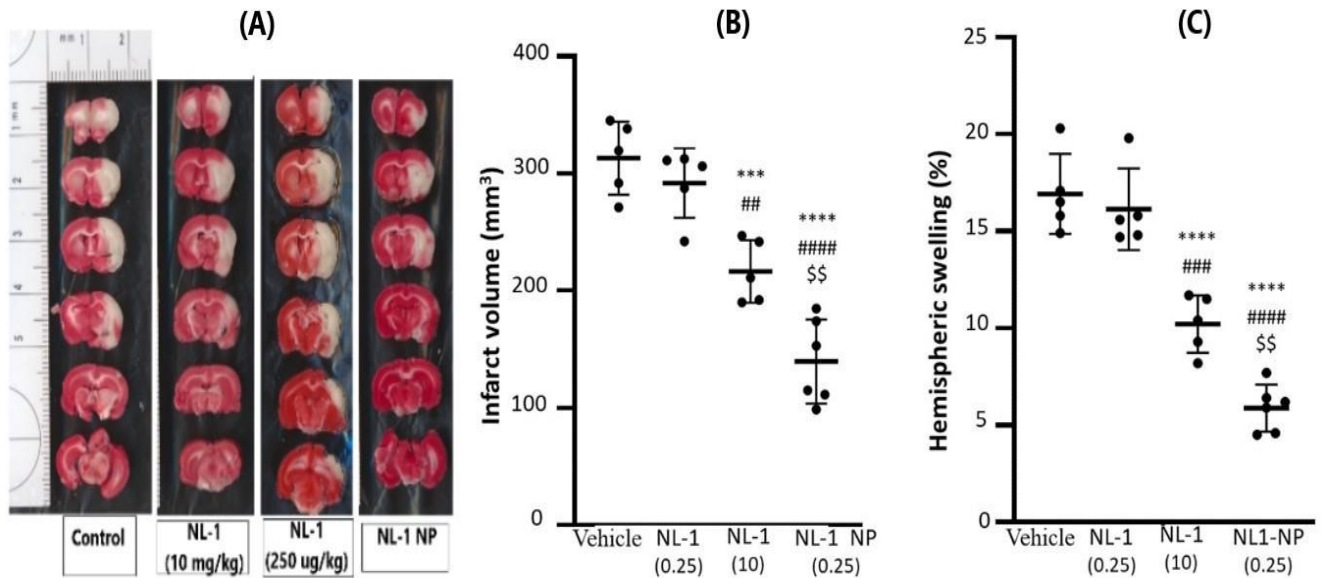

Figure 5.2: Effect of NL-1 therapy on infarct volume and edema (A) Representative TTC stained brain sections for control, 10 mg/kg NL-1, 250 µg/kg NL-1 and NL-1 nanoparticles. Effect of NL-1 and NL-1 nanoparticle treatment on (B) infarct volume and (C) hemispheric swelling after 2 hour tMCAO and 24 hour reperfusion ($_{\$\$, \#\#}$p<0.01, $^{***}, _{\#\#\#}$p<0.001, $^{****}, _{\#\#\#\#}$p<0.0001).
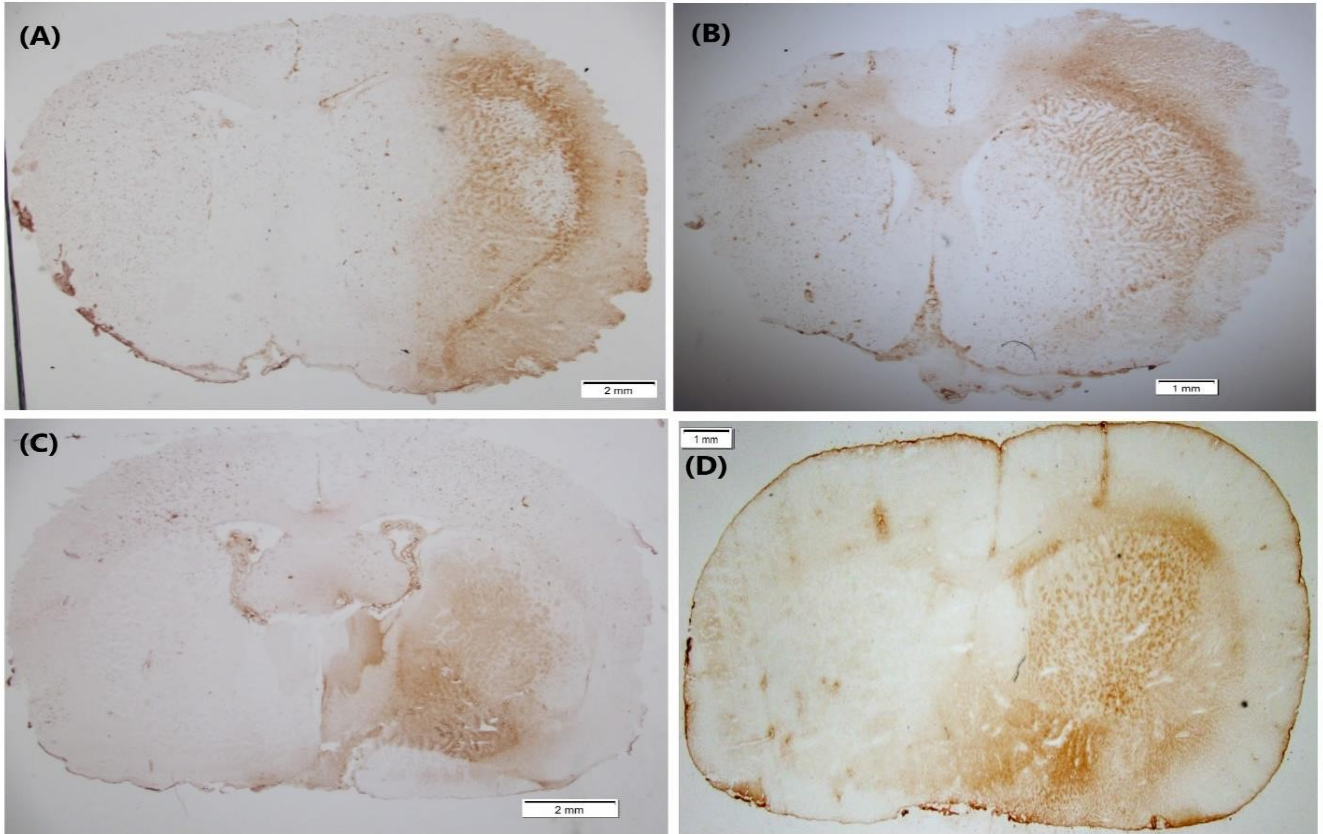
Figure 5.3: Representative sections for IgG extravasation staining for (A) control, (B) 10 mg/kg NL-1 and (C) NL-1 nanoparticles after 2 hour tMCAO and 72 hour reperfusion.
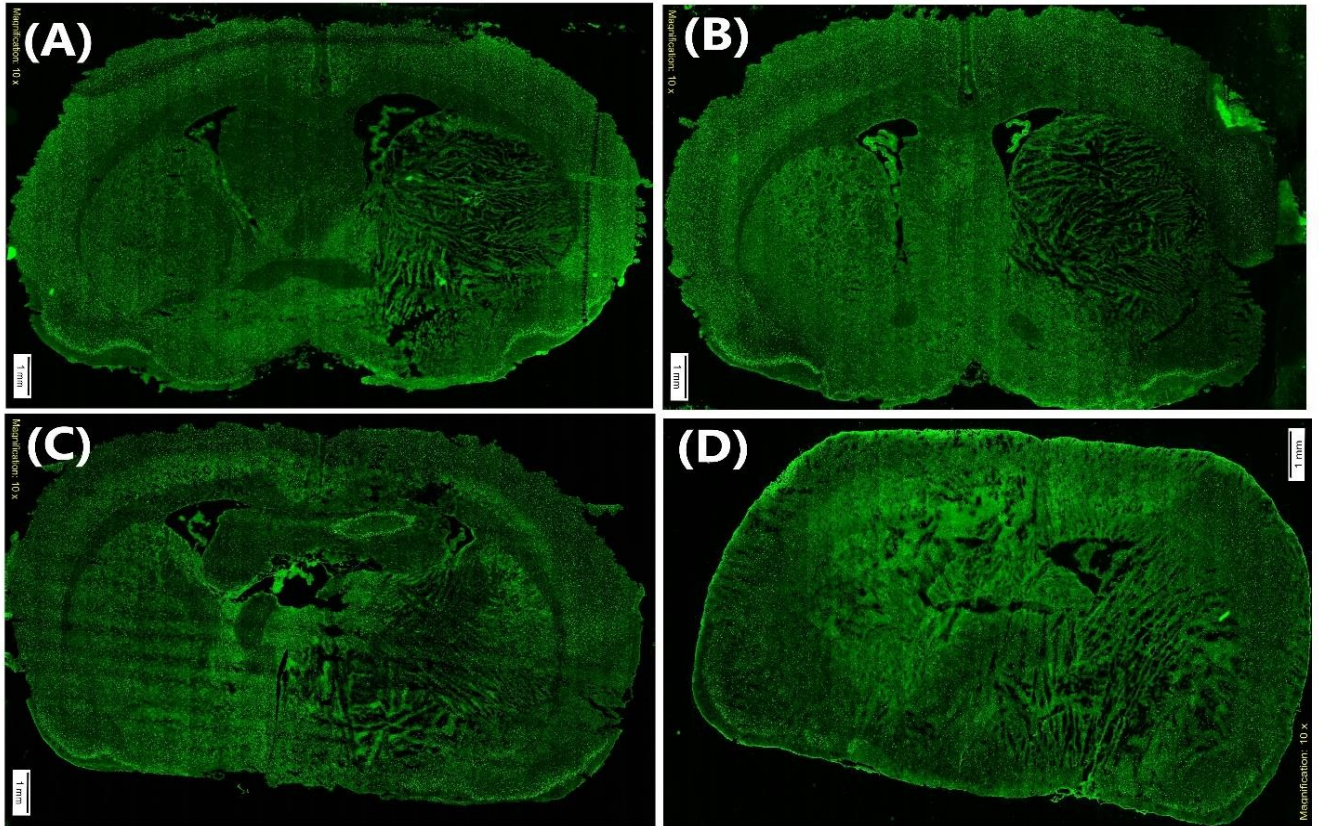
Figure 5.4: Representative sections for mitoNEET immune staining for (A) control, (B) 10 mg/kg NL-1, (C) NL-1 nanoparticles and (D) 250 μg/kg NL-1 after 2 hour tMCAO and 72 hour reperfusion.
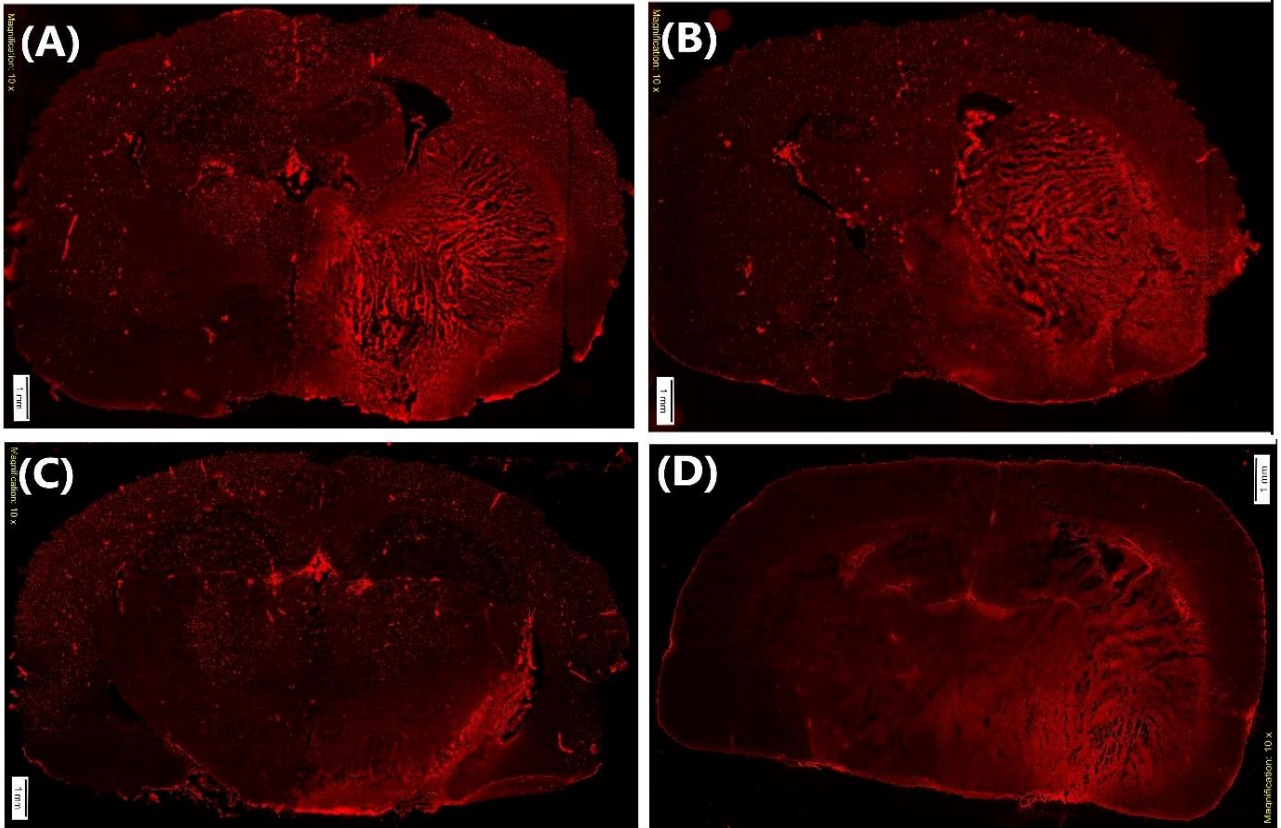
Figure 5.5: Representative sections for nitrotyrosine immune staining for (A) control, (B) 10 mg/kg NL-1, (C) NL-1 nanoparticles and (D) 250 μg/kg NL-1 after 2 hour tMCAO and 72 hour reperfusion.
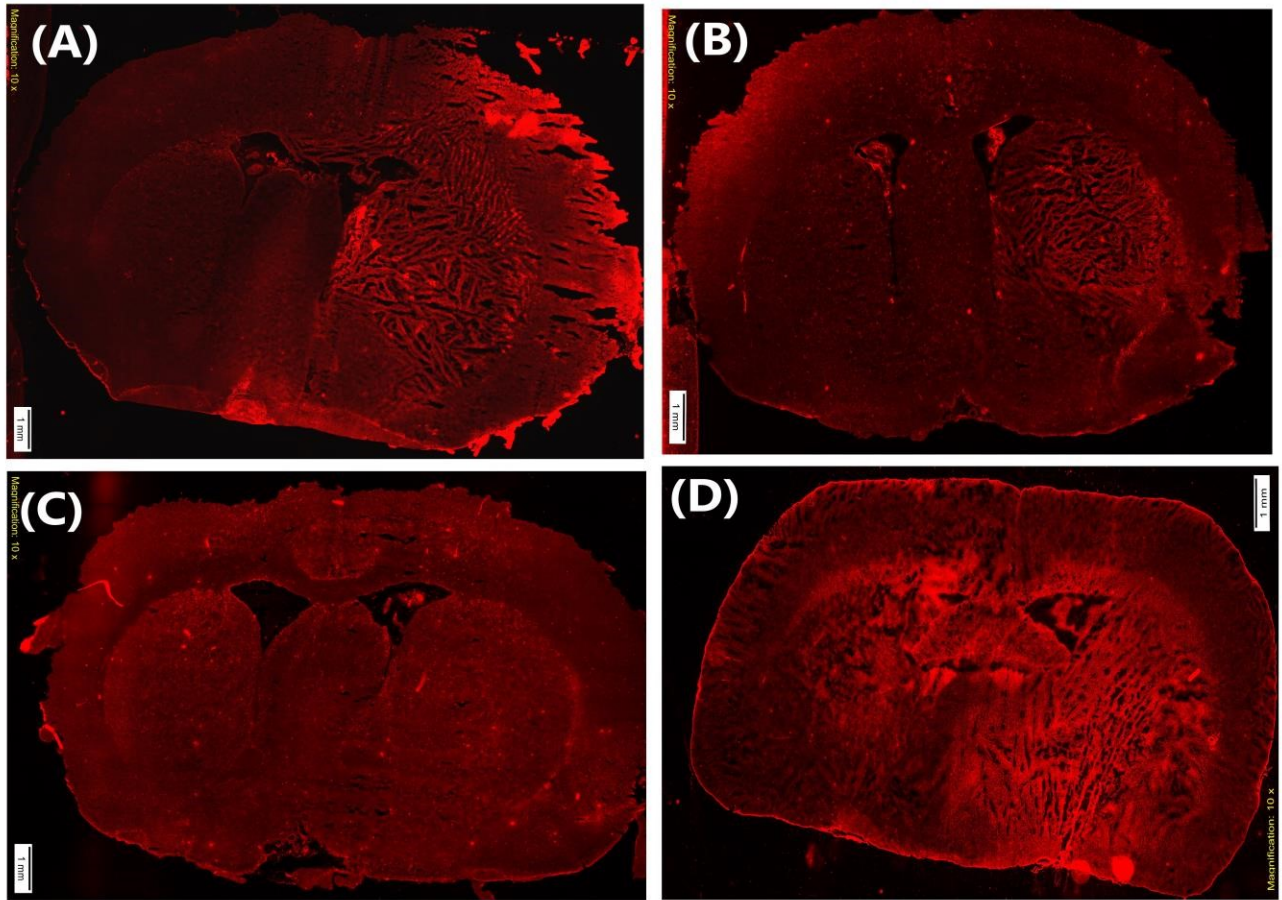
Figure 5.6: Representative sections for 4-hydroxynonenal immune staining for (A) control, (B) 10 mg/kg NL-1, (C) NL-1 nanoparticles and (D) 250 µg/kg NL-1 after 2 hour tMCAO and 72 hour reperfusion.

Figure 5.7: Representative sections for cytochrome c immune staining for (A) control, (B) 10 mg/kg NL-1, (C) NL-1 nanoparticles and (D) 250 µg/kg NL-1 after 2 hour tMCAO and 72 hour reperfusion.

Figure 5.8: Representative sections for caspase-3 immune staining for (A) control, (B) 10 mg/kg NL-1, (C) NL-1 nanoparticles and (D) 250 µg/kg NL-1 after 2 hour tMCAO and 72 hour reperfusion.

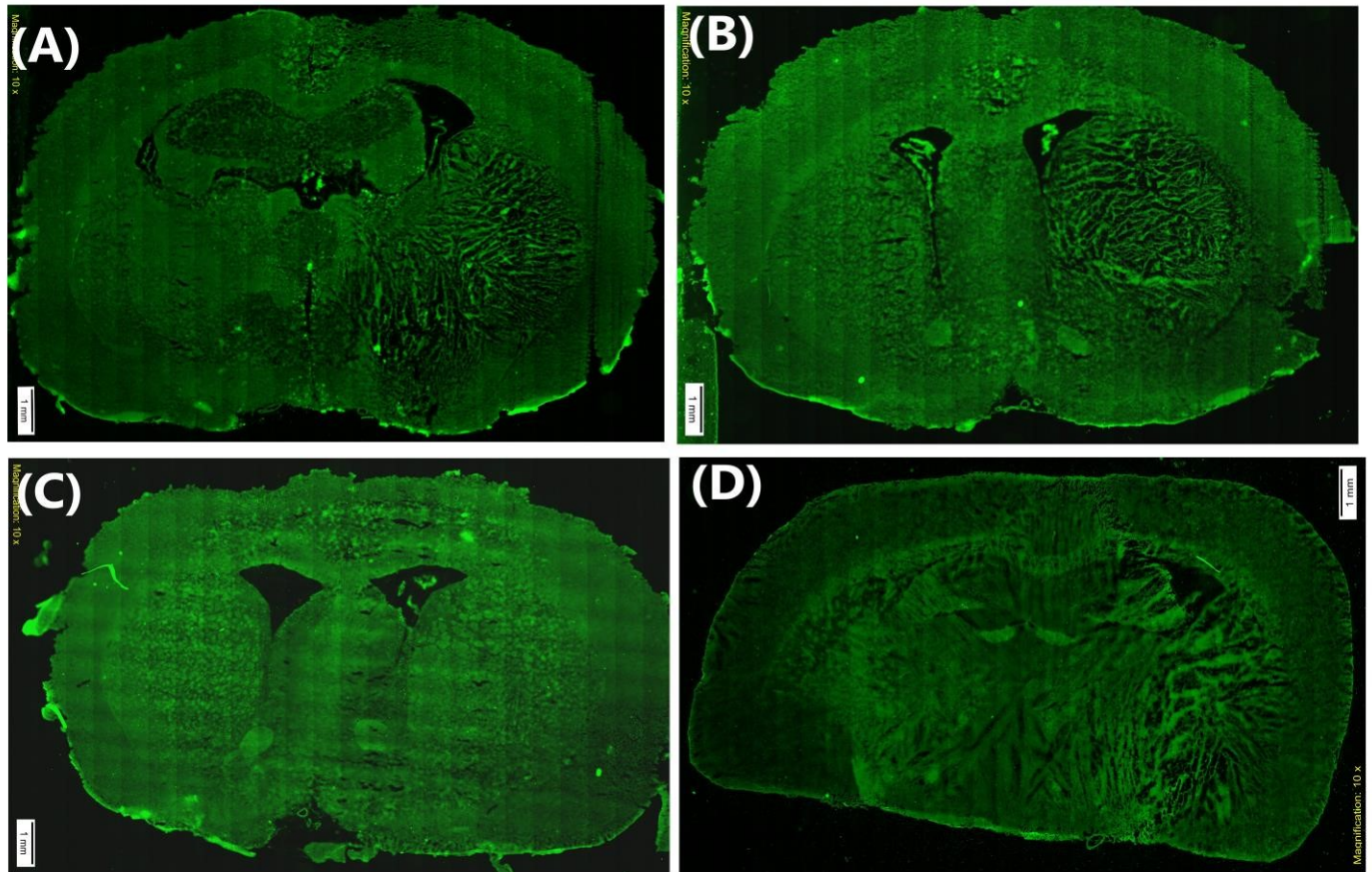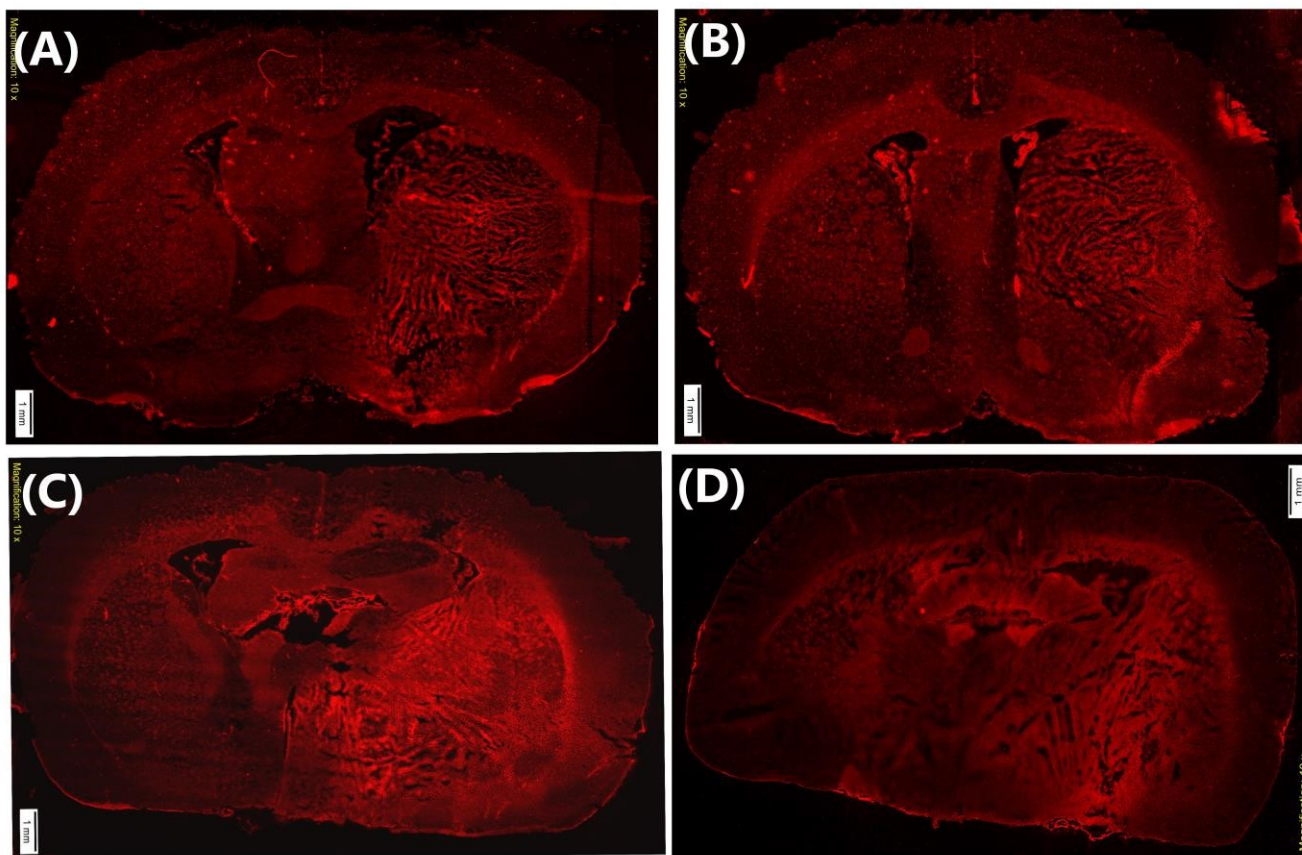**Figure 5.9: Representative sections for GFAP immune staining** for (A) control, (B) 10 mg/kg NL-1, (C) NL-1 nanoparticles and (D) 250 µg/kg NL-1 after 2 hour tMCAO and 72 hour reperfusion.

Figure 5.10: Representative sections for Iba-1 immune staining for (A) control, (B) 10 mg/kg NL-1, (C) NL-1 nanoparticles and (D) 250 µg/kg NL-1 after 2 hour tMCAO and 72 hour reperfusion
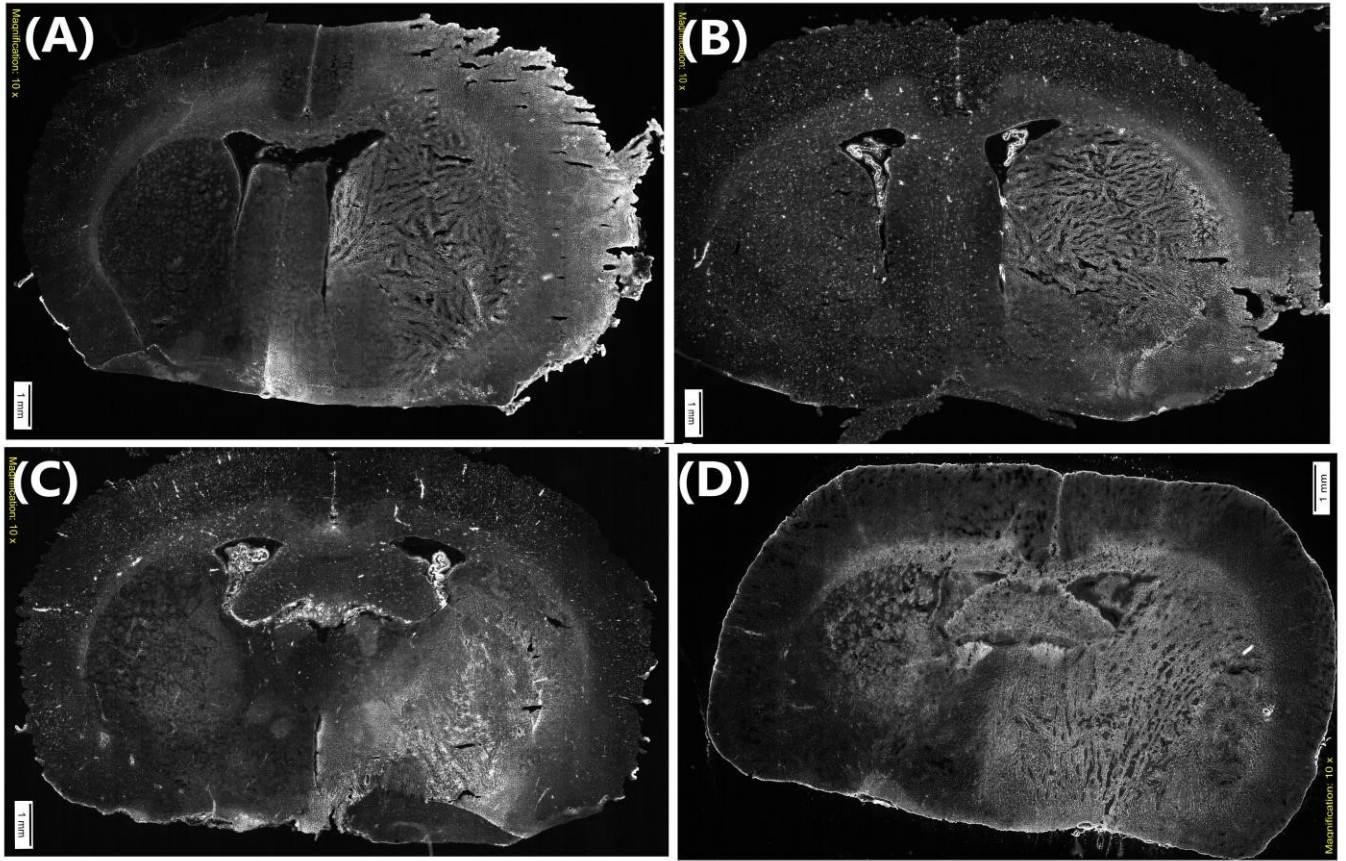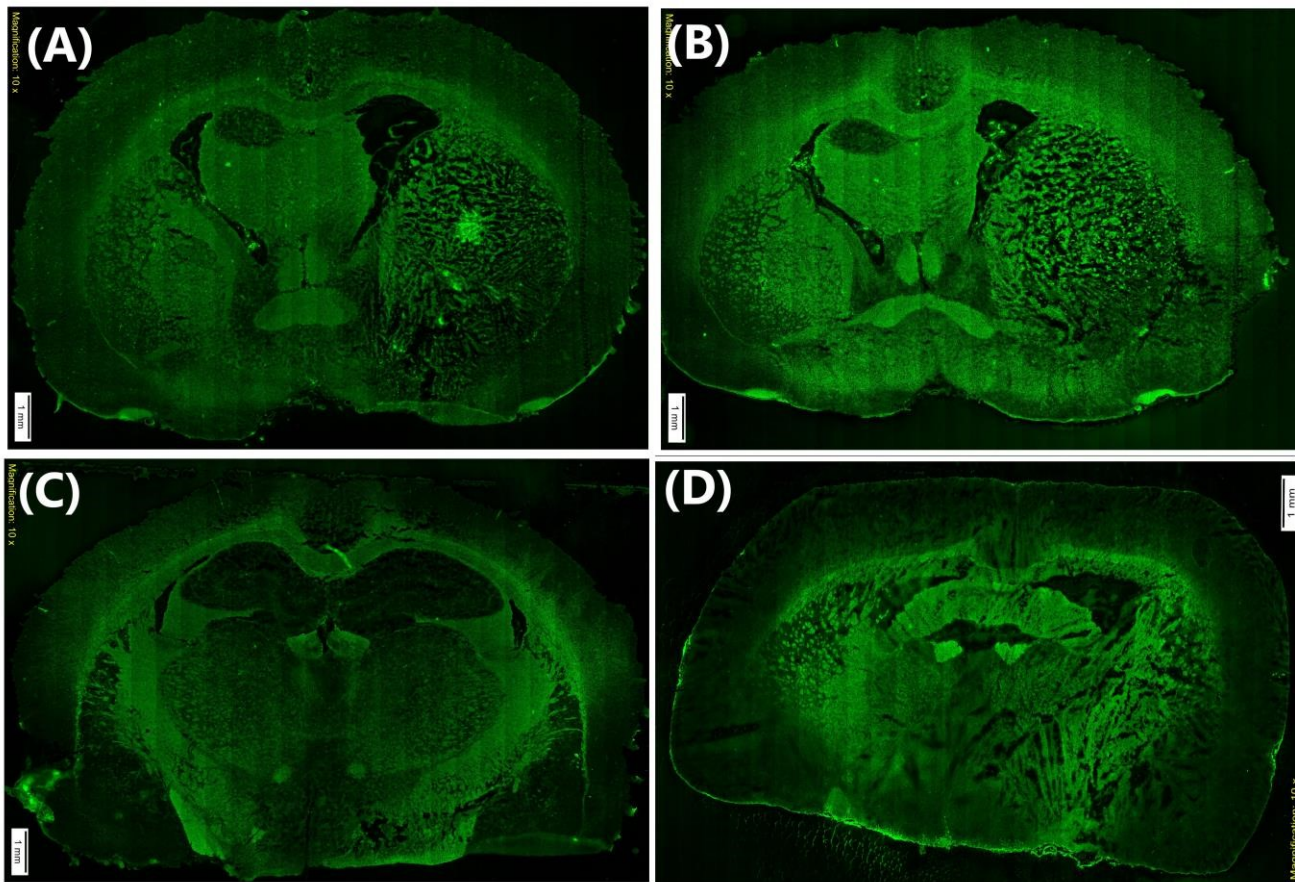
Table 5.1: Health screen scoring table

Parameter	Observation	Score

General Appearance	Normal Groomed, healthy appearing fur, pink mucous membranes and ear lobes	0
	Mild Abnormal Mildly rough/scruffy/dull fur, slightly less well-groomed, light pink mucous membranes/ear lobes, minimal porforin staining, slightly squinted eyes	1
	Moderate Abnormal Rough/scruffy fur, piloerection, poor grooming, pale mucous membranes and ear lobes, squinted eyes	2
	Severe Abnormal Very rough fur, no evidence of grooming, white mucous membranes and ear lobes, substantial porforin staining, severely squinted or closed eyes	3
Posture	Normal	0
	Slight Hunch Spine slightly curved	1
	Moderate Hunch Spine curved, paws slightly under body	2
	Severe Hunch Spine dramatically curved, paws tucked under body, head angled downward	3
Body Condition	Normal	0
	Thin Slight segmentation of vertebrae, dorsal pelvic bones are more prominent, slight dehydration (skin pinch test response is slightly delayed)	1
	Emaciated Prominent vertebrae and skeletal bones that are readily palpable, dehydrated (skin pinch test results in skin remaining tented)	2
Respiration	Normal	0
	Altered Increased rate and/or effort	1
	Abnormal/Distressed Very increased rate or gasping/labored breathing, irregular	2
Body Temperature	Normal/No change	0
	1-4 degree C	1
	5-8 degree C	2
	9-12 degree C	3
Body Weight	0-5% change	0
	5.1-10% change	1
	10.1-15% change	2
	15.1-20% change	3
	> 20.1% change	4
Spontaneous Locomotion/Social Interaction	Normal Active and interacting with cage-mate(s)	0
	Mild Abnormal Still spontaneous activity and some peer interaction but reduced	1
	Moderate Abnormal Lethargic (may need probing via tapping on cage or cage tilt) and minimal peer interaction	2
	Severe Abnormal Immobile and no peer interaction	3

Table 5.2: mNSS screen scoring table

Subtest	Score
1. Reflex test	**3**
Corneal Reflex – lack of eye blink when cornea is touched	1 (0.5/eye)
Pinna Reflex – lack of head shake when pinna is touched	1 (0.5/ear)
Startle – lack of jumping, freezing, moving when loud noise is heard	1
2. Walking test	**3**
Normal	0
Inability to walk straight	1
Circling/falling toward paretic side	2
Immobile (despite probing)	3
3. Placing test	**3**
Visual- lack of placement	1 (0.5/paw)
Tactile – lack of placement	1 (0.5/paw)
Proprioceptive – lack of placement	1 (0.5/paw)
4. Beam balance test	**6**
Balances steadily or traverses beam to clamp	0
Grasps sides of beam but is generally steady	1
Balances unsteadily, hugs beam and/or 1 limb slips/falls down	2
Balances unsteadily, hugs beam, 2 limbs slip/fall down	3
Attempts to balance but very unsteady, falls under beam but recovers	4
Attempts to balance but spins, clings to underside of beam	5
No attempts to balance	6

5. Inverted test		3
	Forelimb flexion or limb not moving to aid with balance	1
	Hindlimb flexion or limb not moving to aid with balance	1
	Head moved more than 10 degrees from vertical center or persistent spin	1
	Total	**18**

CHAPTER 6

Conclusions and Future directions

6.1. Conclusions

In summary, this dissertation describes the journey of establishing the mitoNEET ligand NL-1 as a potential therapeutic for treatment of cerebral ischemia reperfusion injury. Stroke is a condition with a very complex pathophysiology, involving multiple axes resulting in cerebral tissue damage. This is one of the primary reasons for the paucity of effective therapeutic options. Indeed, the thrombolytic t-PA is the only available drug to undo the occlusion to blood flow. However, a t-PA induced resumption of blood supply might not provide any respite, as reperfusion can trigger a cascade of events creating an environment of increased oxidative stress and inflammation. The BBB, responsible for protecting the brain from xenobiotics, undergoes a breakdown with time, leading to fatal edema in the brain.

With the ever looming challenge of developing newer treatment alternatives for this leading cause of permanent disability, we investigated targeting a hitherto relatively unexplored drug target. MitoNEET, is an outer mitochondrial protein that is involved in regulation of cellular bioenergetics. It was discovered due to its binding of the anti-diabetic thiazolidinedione drugs such

as pioglitazone. To date, mitoNEET has no known endogenous ligand, but several reports implicate its involvement in metabolic and redox processes. We previously developed NL-1, a ligand for specific for mitoNEET. The glitazones don't offer a plausible option due to their extraneous hypoglycemic actions. Here, we first reported the specificity of NL-1 for mitoNEET, proving that it had no redundant anti-diabetic effects. We then evaluated our hypothesis that NL1 could be have protective actions in ischemic conditions. Our results indicated that NL-1 could address the elevated oxidative stress and improved cellular respiration in an ischemic environment.

We then proceeded with formulation of NL-1, a drug with poor aqueous solubility, into a polymeric nanoparticle system using the biodegradable polymer PLGA. After a successful formulation with acceptable drug entrapment efficiency, we evaluated the nanoparticle uptake in to the cells. More importantly, we tested our formulation on an *in vitro* model of ischemia and reperfusion injury. Our formulation successfully lowered the peroxide generation and improved cell survival by decreasing the percentage of cells in an apoptotic phase. The successful *in vitro* results helped to establish NL-1 as a potential stroke therapeutic.

However, for any therapeutic to gain substance, it is important that the *in vitro* success can translate into *in vivo* effects. To that effect, we tested NL-1 nanoparticles in an *in vivo* rat tMCAO model, that closely mimics ischemia and reperfusion injury. The NL-1 formulation could show efficacious results *in vivo*, by improving general health of stroke animals. The therapy also reduced the infarct formation in the brains, and significantly decreased the extent of hemispheric swelling, which could lead to hemorrhage, and is a fatal consequence of stroke. Our formulation was able to reduce the dose of NL-1 required to produce these effects, by a possible prolonged drug exposure and effective drug delivery.

This work has helped to lay down a platform for pursing NL-1 as a therapeutic for stroke, which suffers from a dearth of effective clinical translation of therapeutics. We have explored a new drug candidate for a novel target which is the need of the hour for the mitigation of stroke pathophysiology. These promising results could give an impetus for future research into using NL-1 and mitoNEET as neuroprotective agent and target, respectively.

6.2. Future directions

Future studies that can be planned based on this preliminary research include:

1. Firstly, the role of mitoNEET itself could be brought into focus. Future studies should focus on development of vivo models with mitoNEET knockdown and overexpression. The effect of these genetic variations could then be evaluated on the levels of mediators of stroke damage such as ROS, apoptosis and inflammation. This project has opened the possibility of mitoNEET being a factor in more than one of the axes that contribute to neurodegeneration. Such studies would help make mitoNEET a mainstream therapeutic target.

2. The definitive mechanism of action of NL-1, or any mitoNEET ligand in general has not been established yet. This work did not explore the exact molecular pathways involved in the protective effects of NL-1. A well-established mechanism of action would lend substance to NL-1 as a therapeutic. A more extensive evaluation of markers of oxidative stress, apoptosis and neuroinflammation is warranted.

3. Subsequent structure-activity studies on NL-1 could serve as the progenitor molecule to develop more TZD or non-TZD 'me-too' drugs with improved physicochemical properties. Some of the promising analogs that could be evaluated as stroke therapeutics include CI987 and TT01001.

4. Performing a prolonged study for the neurological deficits would help to determine long term effects of NL-1 treatment. A robust study with periodical assessment of neurological scores and survival over 30 days can be performed.

5. Lastly, many neurodegenerative diseases tend to share some common features in their pathophysiology. It would be worthwhile to investigate NL-1 as a global neuroprotective agent, in conditions such as traumatic brain injury or Alzheimer's disease.